

# **In vitro and In vivo Caspase-3 Knock down by Poly (butyl Cyanoacrylate) Nanoparticle-Based RNA Interference**

## **Dissertation**

zur Erlangung des akademischen Grades

**Doktoringenieurin / Doktoringenieur**

**(Dr.-Ing.)**

von M.Sc. Xiwei Zhang

geb. am 01.06.1988 in Henan (China)

genehmigt durch die Fakultät für Verfahrens- und Systemtechnik  
der Otto-von-Guericke-Universität Magdeburg

Promotionskommission: Jun.-Prof. Dr.-Ing. Benoît Fond (Vorsitz)  
Prof. Berend van Wachem (Gutachter)  
Prof. Dr. Ph.D. Bernhard Sabel (Gutachter)  
Prof. Dr. Hans-Joachim Galla (Mitglied)

eingereicht am: 03.09.2018

Promotionskolloquium am: 22.11.2018

# Abstract

Apoptosis is one of the main mechanisms leading to neuronal death after central nervous system (CNS) damage. The aim of the current work is to design a nanoparticle-based delivery system to bring caspase-3 small interfering RNA (siRNA) to the retina, which comprises of CNS tissue, to prevent the deleterious apoptotic pathophysiology after traumatic injury.

The retina is of great importance to humans and animals, for interacting with the environment. Most patients who have vision loss caused by trauma, glaucoma, optic neuropathy, *etc.* suffer from the gradual deterioration of their vision because of optic nerve and retinal ganglion cell programmed cell death, called apoptosis. This is particularly problematic because of the following crucial disadvantages of the affected cells: high vulnerability, non-regeneration, post-mitotic, an irreversible apoptosis induced neuronal damage. Therefore, an important goal is to prevent or stop the apoptosis process so to protect the nerve cells in the retina from dying. Otherwise it would be difficult to recover their vision once the nerve cells are dead. Caspase-3 has drawn wide attention because of its unique role in the apoptosis process. Therefore, it would be desirable to find means to antagonize apoptosis. In this study, I designed a water-in-oil mini-emulsion polymerization system to produce poly (butyl cyanoacrylate) nanoparticles (PBCA NPs) as nanocapsules, with the goal to protect siRNA from biodegradation, deliver it into target organs and cells, and finally, to down-regulate caspase-3 expression (“knock-down”).

To this end, siRNA encapsulated in PBCA NPs was produced with a median diameter ( $d_{50,3}$ ) of 259.8 nm and a Polydispersity Index (PDI) of 0.233. Specification of blank PBCA NPs was 195 nm in  $d_{50,3}$  and 0.227 in PDI. Different factors, including water/oil rate, surfactants/oil rate, butylcyanoacrylate monomer/oil rate, and surfactant types, were investigated to optimize the PBCA NPs.

The knock-down effect was documented by using western blot analysis *in vitro*. A down-regulation of caspase-3 gene appeared after the treatment with caspase-3 siRNA-PBCA NPs. For control purposes, caspase-3 siRNA-calcium particles and the casp3 & NPs were tested as well. In the C6 cells, they lead a significant decrease in caspase-3 expression compared to the treatment with phosphate buffered saline (PBS), but still have higher caspase-3 expression compared to the treatment with caspase-3 siRNA-PBCA NPs.

To test the effects *in vivo*, a rat optic nerve crush (ONC) model was employed in this study. Lesioned and naive eyes of the rats were treated with caspase-3 siRNA-PBCA NPs, negative siRNA-PBCA NPs, blank PBCA NPs or caspase-3 siRNA which were delivered into the eye by intravitreal injection. The immunofluorescence technique was used to detect caspase-3 in the retina. A reduction of caspase-3 expression was found in the post ONC retina only when rats were treated with caspase-3 siRNA-PBCA NPs. Here, the concentration of caspase-3 in the retina decreased to the near-normal concentration of the naive retina. The control treatments using negative siRNA-PBCA NPs, blank PBCA NPs and caspase-3 siRNA-calcium particles did not result in the decrease of the elevated caspase-3 concentrations post ONC.

In addition to the local application of the PBCA NPs, the passage across the blood brain barriers was investigated using an *in vivo* confocal neuroimaging (ICON) system in living rats. Rhodamine 123 labelled PBCA NPs were detected in the retinal tissue within 1 min after intravenous injection into the tail vein. This signal persisted for 2 hrs in the retina as monitored by ICON. It confirmed the value of PBCA NPs as a carrier to pass the blood brain barrier and its potential to release drugs into retina tissues.

In summary, the results of the present thesis suggest that siRNA-PBCA NPs can serve as a potential therapeutic tool to reduce retinal ganglion cell death, but this requires further pre-clinical and clinical studies.

**Key words:** PBCA nanoparticles; siRNA; caspase-3; retina, optic nerve crush.

# Zusammenfassung

Apoptose ist einer der wesentlichen Mechanismen, der zum neuronalen Tod nach einer Schädigung des zentralen Nervensystems (ZNS) führt. Das Ziel der vorliegenden Arbeit war es, ein Nanopartikel-basiertes Transportsystem zu entwickeln, welches eine Behandlung der Netzhaut (Retina) mit „Caspase-3 small interference RNA“ (Caspase-3 siRNA) ermöglicht. Dies soll die Retina, die eine Struktur des ZNS ist, vor der schädigenden apoptotischen Pathophysiologie nach traumatischen Verletzungen schützen.

Die Netzhaut ist für Mensch und Tier bei der Interaktion mit der Umwelt von großer Bedeutung. Die meisten Patienten mit zerebralen und ophthalmologischen Erkrankungen sind durch den Verlust der Sehkraft, verursacht durch Trauma, grünem Star oder Optikusneuropathien etc., stark beeinträchtigt. Denn entscheidende Probleme der retinalen Nervenzellen sind folgende: eine hohe Vulnerabilität, keine Regenerationskapazität, ihr post-mitotischer Zustand sowie die durch neuronale Schäden induzierte Apoptose. Aufgrund dessen ist das Abschalten des Apoptose-Prozesses ein geeigneter Weg, um die Nervenzellen der Retina zu schützen. Ansonsten ist es schwierig, den Sehverlust zu behandeln, wenn die Zellen bereits abgestorben sind.

Das Caspase-3 hat aufgrund seiner einzigartigen Funktion im Prozess der Apoptose große Aufmerksamkeit auf sich gezogen. In der vorliegenden Arbeit wurde ein Polymerisationsprozess auf Grundlage einer Wasser-in-Öl-Miniemulsion entwickelt, um Poly(butylcyanoacrylat)-Nanopartikel (PBCA-NP) in Form von Nanokapseln herzustellen, welche die siRNA vor dem Abbau schützen und sie in die Zielorgane und Zellen transportieren, wo sie letztendlich die Expression der Caspase-3 herunterregulieren („knock-down“).

Es wurden PBCA-NP mit inkorporierter siRNA mit folgenden granulometrischen Eigenschaften hergestellt. Die Partikel hatten einem mittleren Durchmesser ( $d_{50,3}$ ) von 259,8 nm und einem Polydispersitäts-Index (PDI) von 0,233. Die PBCA-NP ohne inkorporierter siRNA wiesen einen Durchmesser von 195nm und einen PDI von 0,227 auf. Verschiedene Prozessfaktoren, einschließlich Wasser/Öl-Verhältnis, Tensid/Öl-Verhältnis, Monomer/Öl-Verhältnis sowie Tensidtyp wurden untersucht, um die PBCA-NP zu optimieren.

Der Knock-down-Effekt wurde *in vitro* durch die Western-Blot-Methode untersucht. Die Ergebnisse zeigten eine Herabregulierung der Caspase-3-Expression nach Behandlung mit Caspase-3 siRNA-PBCA-NP. Als Kontrolle wurden sowohl Caspase-3 siRNA-Kalzium-Partikel als auch eine Mischung aus unbeladenen NP und Caspase-3 siRNA getestet, welche im Gegensatz zur Behandlung mit Phosphat gepufferter Kochsalzlösung (PBS) ebenfalls einen signifikanten Rückgang zeigten. Die Expression der Caspase-3 war jedoch in Vergleich zu den Caspase-3 siRNA-PBCA-NPs immer noch höher.

In der vorliegenden Arbeit wurde auch für die *in vivo*-Prüfung der siRNA-PBCA-NP das Modell der Sehnerv-Quetschung (optic nerve crush/ONC) in Ratten verwendet. Geschädigte und naive (ungeschädigte) Augen der Ratten wurden durch intravitreale Injektion mit Caspase-3 siRNA-PBCA-NP, negativer siRNA-PBCA-NP, unbeladenen PBCA-NPs bzw. Caspase-3 siRNA-Kalzium-Partikel behandelt, und das Caspase-3 durch Immunfluoreszenzfärbung in der Retina detektiert. Hierbei zeigte sich eine Reduktion der Caspase-3-Expression nur in der post-ONC-Retina, welche mit Caspase-3 siRNA-PBCA-NP soweit verringert werden konnte, dass vergleichbare Konzentrationen wie in der naiven Netzhaut erzielt werden konnten. Die Kontroll-Behandlungen mit negativen siRNA-PBCA-NP, unbeladenen PBCA-NP und Caspase-3 siRNA-Kalzium-Partikeln hingegen reduzierte die hohe Konzentration des Caspase-3 post-ONC nicht.

Neben der lokalen Anwendung von PBCA-NP wurde die Überwindung der Blut-Hirn-Schranke *in vivo* mittels konfokalem Neuroimaging (ICON) untersucht. Mit Rhodamin 123 markierte PBCA-NP wurden im Gewebe der Netzhaut innerhalb von einer Minute nach intravenöser Injektion über die Schwanzvene sichtbar. In den nachfolgenden zwei Stunden blieb das Signal in der Netzhaut bestehen, was mittels ICON beobachtet werden konnte. Das Ergebnis weist darauf hin, dass PBCA-NP als Trägersubstanz die Blut-Hirn-Schranke überwinden können und somit Medikamente in das Netzhautgewebe freisetzen könnten.

Zusammenfassend zeigen die Ergebnisse der vorliegenden Studie, dass siRNA-PBCA-NP ein neuer therapeutischer Weg sein könnte, den Tod von retinalen Ganglienzellen zu verhindern. Dies bedarf aber weiterführender präklinischer und klinischer Studien.

**Schlüsselwörter:** PBCA Nanopartikel; siRNA; Caspase-3, Netzhaut, Sehnerv Quetschung.

## List of abbreviations

Abbreviations	Full names	Abbreviations	Full names
apop	apoptosome	LDV	Laser Doppler Velocimetry
BAR	bifunctional apoptosis inhibitor	LD50	median lethal dose
BBB	blood-brain barrier	mRNA	messenger RNA
casp3	caspase-3	BCA	<i>n</i> -Butyl-2-cyanoacrylate
casp3 & NPs	the mixture of caspase-3 siRNA and blank poly (butyl cyanoacrylate) nanoparticles	PBCA NPs	poly (butyl cyanoacrylate) nanoparticles
casp3 PBCA NPs	the caspase-3 siRNA loaded poly (butyl cyanoacrylate) nanoparticles	neg NPs	the negative silence control siRNA loaded poly (butyl cyanoacrylate) nanoparticles
casp8	caspase-8	ONC	optic nerve crush
casp9	caspase-9	O/W	oil-in-water
CNS	central nervous system	NPs	nanoparticles
Cyt c	cytochrome c	PBS	phosphate-buffered saline
d <sub>50,3</sub>	Median diameter	PDI	Polydispersity Index
DISC	death-inducing signalling complex	C6	Rat glioma cells
DMSO	dimethyl sulfoxide	NADH	nicotinamide adenine dinucleotide
DNA	deoxyribonucleic acid	RNA	Ribonucleic acid
dsRNA	double-stranded RNA	RISC	RNA-induced silencing complex
FasL	first apoptosis signal ligand	rRNA	ribosomal RNA
FasR	first apoptosis signal receptor	Smac	second mitochondria-derived activator of caspases
HLB	hydrophilic-lipophilic balance	siRNA	small interfering RNA

HRP	horseradish peroxidase	Stau	Staurosporine
<i>i.v.</i> injection	Intravenous injection	tRNA	transfer RNA
ICON	<i>in vivo</i> confocal neuroimaging	SDS-PAGE	Sodium Dodecyl Sulfate- Poly Acrylamide Gel Electrophoresis
IOD	integrated optical density	SDS	sodium dodecyl sulphate
W/O	water-in-oil	MTT	Thiazolyl Blue Tetrazolium Bromide
XIAP	X-linked inhibitor of apoptosis protein		

# Contents

1. Introduction.....	1
2. Technology state of the art.....	3
2.1. RNA Interference .....	3
2.1.1. Ribonucleic Acid.....	3
2.1.2. RNA Interference .....	4
2.2. Apoptosis.....	5
2.3. Drug Carrier.....	7
2.3.1. Liposome.....	7
2.3.2. Micelles .....	8
2.3.3. Inorganic nanoparticles .....	9
2.3.4. Polymeric nanoparticle.....	9
2.4. Poly (Butyl Cyanoacrylate) Nanoparticles .....	10
2.4.1. Polymerization of <i>n</i> -Butyl-2-Cyanoacrylate .....	11
2.4.2. Synthesis in Water-in-Oil Mini-emulsion.....	12
2.5. Characterization of Nanoparticles .....	13
2.5.1. Size.....	14
2.5.2. Zeta Potential.....	15
2.5.3. Polydispersity Index .....	16
2.6. Cytotoxicity .....	16
2.7. Protein Immunoblot.....	17
2.7.1. Gel Electrophoresis .....	17
2.7.2. Transference .....	18
2.7.3. Antibody Probing .....	19



2.8.	Paraffin section & immunofluorescence .....	19
2.8.1.	Fixation.....	19
2.8.2.	Dehydration & Embedding .....	20
2.8.3.	Slicing.....	20
2.8.4.	Hydration.....	20
2.8.5.	Epitope Retrieval.....	21
2.8.6.	Fluorescence Imaging .....	21
2.9.	<i>In Vivo</i> Confocal Neuroimaging.....	22
2.10.	Retina .....	23
3.	Methods.....	25
3.1.	Preparation of Poly (Butyl Cyanoacrylate) Nanoparticles .....	25
3.2.	Characterization of Nanoparticles .....	25
3.3.	Cell Culture.....	26
3.4.	Cytotoxicity .....	27
3.5.	Protein Samples Preparation, SDS-PAGE and Immunoblotting.....	28
3.6.	Optic Nerve Crush Surgery & Intravitreal Injection .....	30
3.7.	Paraffin Section & Immuno-Fluorescence .....	31
3.8.	<i>In Vivo</i> Confocal Neuroimaging.....	33
4.	Results.....	35
4.1.	Characterization and Optimization of PBCA NPs .....	35
4.1.1.	Surfactants .....	35
4.1.2.	Water Phase.....	41
4.1.3.	<i>n</i> -Butyl-2-Cyanoacrylate .....	44
4.2.	Cytotoxicity of PBCA NPs.....	48
4.3.	Immunoblotting of Caspase-3 expression .....	51
4.3.1.	Caspase-3 Silencing by siRNA-PBCA NPs.....	51
4.3.2.	siRNA Transfection by Different Delivery Strategies .....	52
4.3.3.	Transfection Efficiency of Caspase-3 siRNA-PBCA NPs.....	56

4.4.	Immunofluorescence of Retina.....	60
4.4.1.	Caspase-3 siRNA-PBCA NPs.....	60
4.4.2.	Control Treatments.....	65
4.4.3.	Mean IOD Analysis.....	70
4.5.	<i>In Vivo</i> Confocal Neuroimaging of PBCA NPs .....	71
5.	Conclusions.....	74
6.	Acknowledgments.....	77
7.	Bibliography .....	78
8.	Appendix.....	89
8.1.	Support Information: Instruments .....	89
8.2.	Support Information: Materials .....	91
8.3.	Ingredient List of the Cell Medium .....	94

# 1. Introduction

Because of the promotion of gene detection and modification techniques, a variety of gene editing methods have been developed with a therapeutic purpose. Gene editing tools, which are usually nucleic acids, are aimed to be delivered into cells (as drugs) to repair, replace, or regulate genes in order to prevent or treat diseases. This method is identified as gene therapy [1]. In this way, inherited diseases and disorders may be cured, which may be associated with pathological gene expression, such as severe combined immunodeficiency [2], Alzheimer's disease [3], and cancer [4]. But, on the other hand, the disadvantages of gene therapy are: risks of unpredicted gene expression, poor therapy efficiency [5], and the immune response when a virus is used as a transport vector. In order to reduce the effects of these negative factors, several strategies have been put forward to improve gene therapy [4, 6]. One of them is to use drug carriers, which are able to protect drugs from biodegradation and to be modified with different functions, such as targeting system [7, 8]. So, drug carriers system can be designed to transfer nucleic acid into cells. Until now, it has been reported that both DNA and RNA are able to be delivered by nanoscale drug systems and transfect cells [9-11], but they are, so-far, rarely used on humans or animals [121].

Poly (butyl cyanoacrylate) nanoparticles (PBCA NPs) are well known for their non-toxicity [12, 13], their excellent ability to penetrate cell membrane and the blood-brain barrier (BBB) [14, 15]. The particles are usually synthesized via polymerization in a mini-emulsion. In the emulsion, which is mainly composed of a water phase and oil phase, a variety of drugs can be incorporated into the NPs according to the charge, reactivity, or/and solubility of these drugs [16, 17]. Meanwhile, the surface modification of NPs is usually used to label the particles with fluorescence chemicals, by which NPs can be tracked in cells *in vitro* and *in vivo* [18]. Thus, it is very promising to use PBCA NPs as a DNA or RNA carrier as delivery systems for gene therapy in cells [19-22]. However, so-far, these NPs were rarely found in therapeutic treatments for retina damage, because retina cells are extremely vulnerable and sensitive to the components used for the design of PBCA NPs, such as SDS.

Apoptosis is also known as "Programmed Cell Death", which is a process under the regulation of the gene [23]. There are lots of incidences which can initiate apoptosis [24, 25],

such as aging, trauma, diseases, *etc.* All of these reasons reflect on two initiation pathways: intrinsic and extrinsic pathways (see Figure 2.3). Due to these pathways, apoptosis plays a crucial role in the structural balance of mammalian organisms, especially during its development stage [26]. But, lots of diseases are mediated via an imbalance in apoptotic pathways, such as cancer [27], systemic lupus erythematosus [28], and Alzheimer's disease [29]. Sometimes, apoptosis is also the culprit of disease deterioration. For example, an optic nerve injury may lead to apoptotic death of retinal ganglion cells (RGCs), and patients suffer not only from the damage-induced vision loss in the beginning but from permanent vision impairment due to apoptotic cell death [30]. Moreover, the optic nerve as a part of the central nervous system is unable to regenerate and therefore the vision loss can hardly recover [31]. In this situation, patients will benefit from anti-apoptosis treatment. siRNA, a gene therapeutic tool, might be able to solve this problem due to its highly efficient and specific gene silencing.

RNA interference was discovered at the end of the 20<sup>th</sup> century. Until now, numerous siRNA products have been synthesized and applied in gene therapy [32-34]. Different strategies are applied for efficient and specific delivery of siRNA into cells and tissues [21, 35, 36]. But PBCA NPs as nanoscale drug carriers are rarely used to deliver siRNA in the gene interference. In this study, PBCA NPs were employed to deliver caspase-3 siRNA, and the possibility of PBCA NPs-mediated caspase-3 silencing, both *in vitro* and *in vivo*, was investigated.

As the following section shows, the study builds upon a large body of prior technological state of the art, the elements of which are now discussed.

## 2. Technology state of the art

### 2.1. RNA Interference

#### 2.1.1. Ribonucleic Acid

Ribonucleic acids (RNA) as well as deoxyribonucleic acids (DNA) are carriers of genetic information. Ribonucleotide is the basic unit of RNA, which is composed of a ribose, a nitrogenous base, and a phosphate group. Ribonucleotides polymerize each other via phosphodiester bond into a RNA strand (see Figure 2.1).

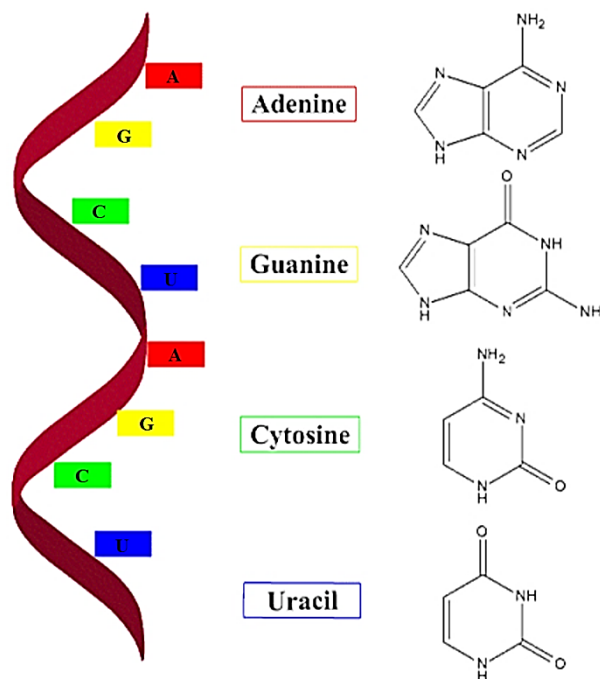


Figure 2.1: the schematic structure of RNA. There are 4 types of nitrogenous base for ribonucleotide: adenine (A), guanine (G), cytosine (C) and uracil (U); and their molecular formulas are shown on the right.

Different from other bio-macromolecules, such as lipids, proteins, and carbohydrates, RNA has the ability to store genetic information because of the different nitrogenous bases: A, G, C,

and U in each ribonucleotide. Following the principle of base pair complementarity, these different ribonucleotides are connected together according to their DNA template. Genetic information from their DNA template then can be recorded by the coding sequence of these nitrogenous bases. This process that synthesizes RNA using a DNA template in nucleus is also known as “transcription”. After that, the produced RNA with the genetic information is named as messenger RNA (mRNA) and delivered from nucleus to ribosome, which is the site of protein synthesis in the cytoplasm. The process that synthesizes protein using its mRNA is known as “translation”. The whole process that produces protein according to its DNA template is called “expression” or “gene expression”.

In nature, RNA is indispensable for protein synthesis. It is not only a carrier of genetic information mentioned above, but also a manager during the whole process of gene expression [37]. For example, transfer RNA (tRNA) containing an anticodon that delivers amino acid to ribosome, and the ribosome is also mainly constructed by RNA (ribosomal RNA, rRNA). But different from mRNA, this regulating RNA is usually very short and copied from intron of a gene. These RNA control protein expression happens at all stages after transcription, such as mRNA modification, initiation of translation, *etc.*

### **2.1.2. RNA Interference**

During a protein generation process, a regulation at post-transcription level is possible because the mRNA can be interfered before binding to ribosomes in the cytoplasm, and this effect was identified as RNA interference by Fire and Mello in 1998 [38]. These authors succeeded in silencing the *par-1* gene expression using double-stranded RNA (ds RNA). Furthermore, Elbashir and Tuschl demonstrated that it was possible to target the silencing of a specific fragment of gene using small interfering RNA (siRNA) [39]. Since then, many variations of siRNA have been designed for a variety of targets protein and purposes.

Nowadays, RNA interference is well understood. SiRNA are an endogenous product to control gene expression. Currently, however, it is popular as a product of life-science technology and used as an exogenous reagent. The interference process is initiated from the binding of RNA-induced silencing complex (RISC) and siRNA which is obtained from spontaneous hydrolysis of dsRNA in the cytoplasm [40-42], and this connection is controlled by RISC component argonaute enzymes [43]. After that, siRNA helps RISC to recognize the target mRNA, based on the principle of complementary base pairing, and cleave the target mRNA into short fragments. These short fragments of mRNA are unable to act as the

translation template for protein expression. As a result, the target protein cannot be yielded anymore, although the gene still exists (see Figure 2.2).

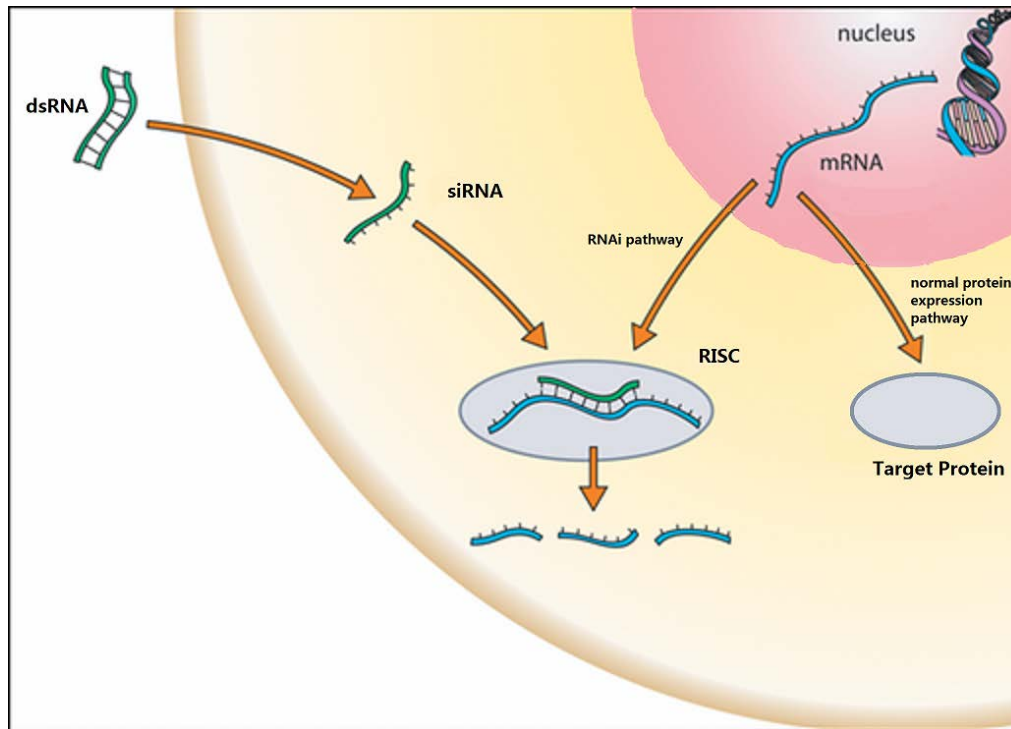


Figure 2.2: Schematic diagram of RNA interference. Normally, DNA is transcribed to mRNA in nucleus, mRNA then is sent to the cytoplasm and translated to protein. But if siRNA exist, the siRNA binds to the mRNA and cut it into pieces. As a result, protein expression is terminated [44].

## 2.2. Apoptosis

Apoptosis is considered as a distinctive and important mode of “Programmed Cell Death” since 1972, although its relative components were reported earlier [45, 46]. Apoptosis occurs naturally during developing and aging as a homeostatic mechanism to maintain cell populations in tissues and organs [23]. It also plays a role as the defence mechanism in immune reactions or damaged cells under diseases [47]. There are varieties of stimuli and conditions that can trigger apoptosis. For example, irradiation and drugs used for cancer chemotherapy cause DNA damage in cells, which can activate apoptotic death [48, 49]. Besides, hormones are also related to the apoptotic death, such as corticosteroids to thymocyte [50].

Regarding morphology, apoptosis has its unique features compared to necrosis. In the early stage of apoptosis, cell shrinkage and pyknosis can be observed. The cells are smaller, the

cytoplasm is dense, and the organelles are more tightly packed [23]. With the progress of apoptosis, the plasma membrane starts to blister and karyorrhexis appears, although the plasma membrane is still intact, which is an important difference from necrosis. Finally, macrophages or parenchymal cells degrade these apoptotic cells to complete the apoptosis process. During the whole process, no inflammatory reaction occurs, which is another features differing from necrosis.

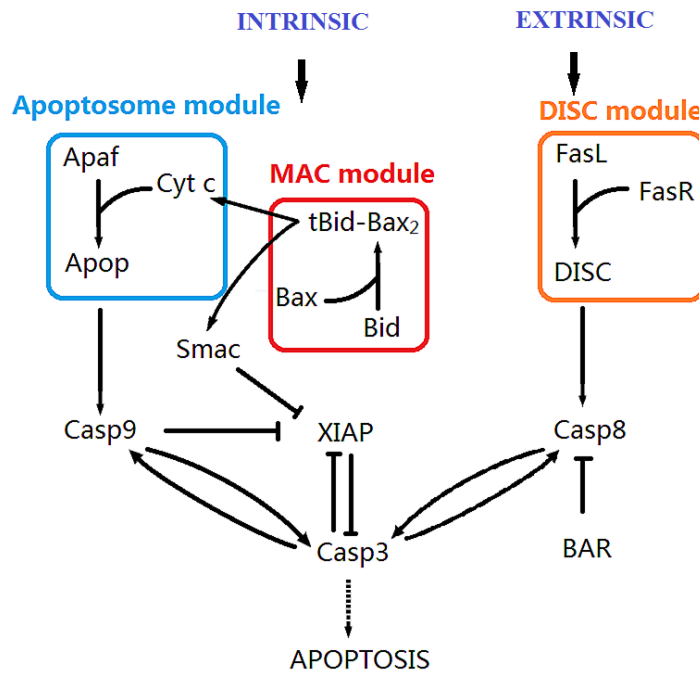


Figure 2.3: Proteins interactions of the apoptosis activation. Apoptosis can be initiated by both intrinsic and extrinsic pathways. Many variations of proteins are interacting in these two pathways. But, whatever the pathway is, caspase-3 dominates the last and irreplaceable switch to apoptosis.

Apoptosis is a highly regulated and complex process under the control of genes. According to the different stimuli and conditions, there are two main pathways: extrinsic pathway (death receptor pathway) and intrinsic pathway (mitochondrial pathway) to initiate apoptosis (see Figure 2.3). In extrinsic pathway, the process starts with the binding of first apoptosis signal receptor (FasR) and first apoptosis signal ligand (FasL) [51], and a death-inducing signalling complex (DISC) is formed which catalyses the activation of caspase-8 (casp8) [52]. Compared to extrinsic, the intrinsic pathway is a non-receptor-mediated stimuli action. The inner mitochondrial membrane is changed by stimuli resulting in the release of cytochrome c (Cyt c) from mitochondria to the cytoplasm [53]. Thus, cytosolic Cyt c activates Apaf-1 and



forms the apoptosome (apop) where caspase-9 (casp9) is activated [54-56]. Finally, apoptosis starts due to an accumulation of caspase-3 (casp3) which is produced via the catalytic reaction of casp8 and casp9. Besides that, regulators are included to control the activation process, such as bifunctional apoptosis inhibitor (BAR), X-linked inhibitor of apoptosis protein (XIAP) and second mitochondria-derived activator of caspases (Smac) [57-60].

In summary, apoptosis is an essential process during animal and human growth. On the one hand, this important process is closely monitored and controlled, and many enzymes and regulators are involved in apoptosis. But on the other hand, damage and diseases also often induce apoptosis and worsen the condition which is therefore hard to cure.

## **2.3. Drug Carrier**

A drug carrier has the function of purpose-designed drug distribution, controllable release and/or target delivery [61]. Viruses are natural drug carriers, which capture specific target cells and inject its DNA/RNA into the cells. This process that delivers DNA/RNA product into a cell is called “transfection”. According to the mechanism of transfection, viral carriers can be changed by replacing viruses’ DNA/RNA with drugs, and transfect target cells [62]. But because viral carriers have the risk of provoking illness, non-viral carriers are widely favoured, and thousands of non-viral carriers have been designed and produced. There are mainly four types of non-viral carriers: liposome, micelle, inorganic NPs, and polymeric NPs.

### **2.3.1. Liposome**

A sphere formed by lipid bilayer is termed “liposome” (see Figure 2.4). Cells have a similar structure as they are formed by phospholipid bilayer, albeit in general at another scale (micrometer). When applied in therapy, liposomes have the abilities to improve bio-distribution of compounds in target sites and stabilize therapeutic chemicals *in vivo* [63]. As the lipid skeleton structure is very similar to the cell membrane (phospholipid bilayer), the obstacle of cellular and tissue uptake can be easily overcome due to the good compatibility and solubility between lipids [64]. But liposomes have a poor ability for permeation, as they dissolve in the cell membrane during uptake, considering that tissues and organisms usually have several cell layers. The functionalized agents on the surface of liposomes will also be inserted into the cellular membrane and offer new “receptors”, which may, for example, lead to cells being attacked by the immune system. In addition, the lipid bilayer structure is formed

by a hydrophobic force, so liposomes are in general instable in a complex biological environment, such as blood and tissue fluid.

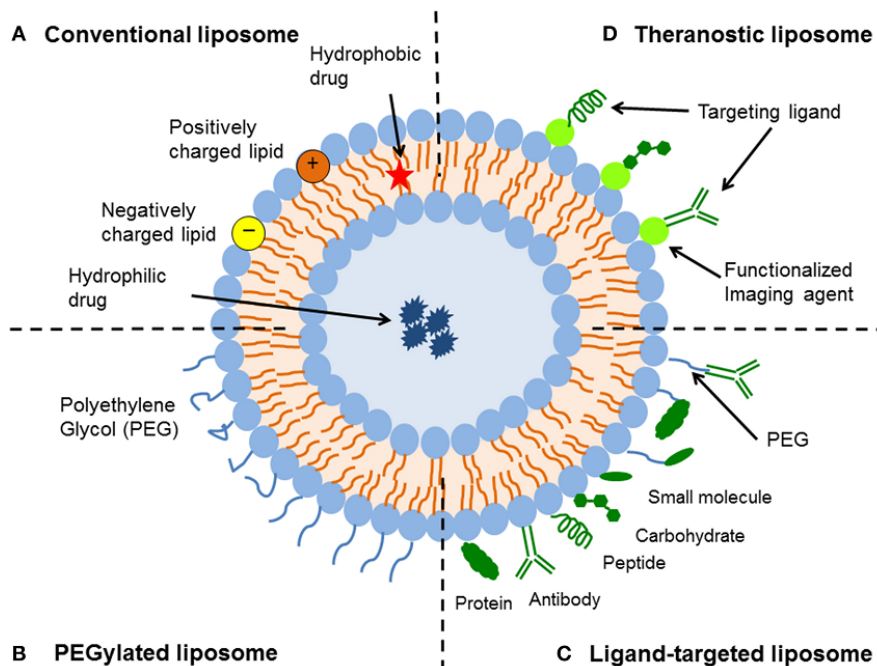


Figure 2.4: Schematic representation of the different types of liposomal drug delivery systems [taken from reference 63].

### 2.3.2. Micelles

A micelle has a similar but much simpler structure than a liposome. It is built from a layer of surfactant molecules. Surfactants have a hydrophilic head and a lipophilic tail, and the structure of a micelle is stabilized by a hydrophobic force. According to the different tails of surfactants, there are two types of micelle formation: micelles and reverse micelles, which are composed of cone sharp surfactants and inverted cone sharp surfactants, respectively (see Figure 2.5) [65]. Therefore, both water-soluble and fat-soluble drugs can be wrapped in micelles. But their size (usually 5-30 nm) limits the loading capacity, and their stability is concentration dependent [66], so it is still difficult to use micelles in the complex conditions in human and animal organisms.

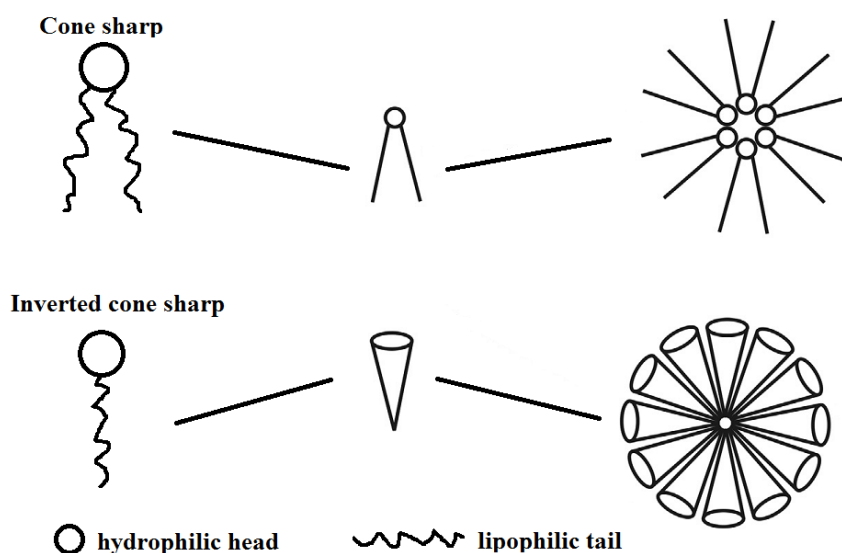


Figure 2.5: Schematic of two types of micelle: cone sharp and inverted cone sharp [taken from reference 65].

### 2.3.3. Inorganic nanoparticles

Distinct from the other types of drug carriers, inorganic NPs have a very simple structure: an inorganic core and/or functionalized coating [67]. Lots of inorganic NPs have been reported, for example, magnetic NPs [68], gold NPs [69], silica NPs [70], *etc.* Each of these particles inhibits a unique function and can be used for bio-applications [71]. Their advantages have been widely used in drug delivery, such as magnetic targeting, magnetic resonance imaging, large absorption coefficients, and low cytotoxicity [6]. However, the disadvantage is that drugs are usually loaded on the surface of inorganic NPs and by this exposed to external environment directly. This requires many and complex surface modifications to protect the drugs. In addition, these inorganic elements can accumulate easily in animals' and humans' organs, which may lead to diseases.

### 2.3.4. Polymeric nanoparticle

A polymeric NP has a similar structure as a micelle. It is formed by a surfactant layer in combination with a surrounding layer of polymer. Polymeric NPs are submicron-sized solid colloidal particles consisting of a polymer or co-polymer. There are a variety of polymeric materials used for drug carrier systems, such as lactic acid [72], glycolic acid [73], ethylenimines [74], and butylcyanoacrylate [75]. It is remarkable that the biodegradation of polymeric NPs is controllable according to the type and concentrations of polymer as well as surface modifications [76, 77]. Both fast- and slow-release polymeric NPs are designed for

different requirements [76, 78, 79]. The excellent kinetic characteristics of polymeric NPs have been applied to deliver drugs into the brain [13, 14]. But, similar to inorganic NPs, the accumulation of polymeric material in animals' and humans' organs may cause diseases [13]. Furthermore, some stabilizers, such as sodium dodecyl sulphate (SDS), are toxic for cells but important to produce polymeric NPs.

Biocompatibility is an essential characteristic for all the carriers which are designed for human and animal applications. The carriers shall be biodegradable or excretable by the urinary or biliary system to avoid accumulation in body. As a result, poly (butyl cyanoacrylate) NPs stand out, because of their excellent biodegradation and non-toxic properties [12]. Therefore, in this study, poly (butyl cyanoacrylate) NPs are employed to deliver siRNA into cells and tissues.

## **2.4. Poly (Butyl Cyanoacrylate) Nanoparticles**

Poly (butyl cyanoacrylate) nanoparticles (PBCA NPs) are one type of polymeric NPs. Surfactant is used to stabilize NPs in solvent. According to the property of their cores, PBCA NPs can be clarified in three different types: oil core [80], water core [9] and bubble [81]. In the mini-emulsion process, NPs with oil core or water core can be prepared via oil-in-water (O/W) mini-emulsion or water-in-oil (W/O) mini-emulsion, respectively, and then polymerization occurs at the interface of water and oil. So then, both water and oil soluble chemicals can be encapsulated in NPs. For bubble NPs, the polymerization occurs at the interface of air and water, then the air is encapsulated by polymeric microbubbles and drugs are incorporated into the bubbles. Because of the air core, they are usually used for imaging [82].

In this project, siRNA are encapsulated in PBCA NPs (see Figure 2.6). The core of the PBCA NPs is water, where RNA or fluorescence dye is dissolved and protected by a layer of *n*-butyl-2-cyanoacrylate (BCA) polymer, which can be degraded in endosome or lysosome after uptake. As a result, the encapsulated RNA or fluorescent dye can be released into the cytoplasm. Moreover, surfactants are used to stabilize nano-drops and initiate polymerization in mini-emulsion and enhance cellular uptake of PBCA NPs [14, 83]. Non-toxicity and good permeability are very important features of PBCA NPs as drug carriers, which have been demonstrated [12, 13, 84]. In this work, PBCA NPs are used to deliver siRNA into neural cells in the retina.

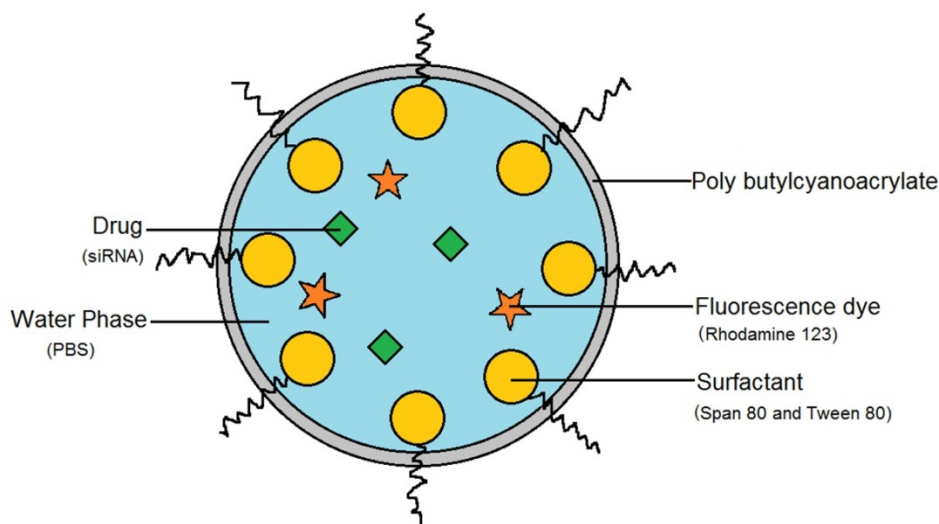


Figure 2.6: Ideal structure model of PBCA NPs. The water core contains drug and/or fluorescence dye is covered by BCA polymer and surfactants help to stabilize the particle [taken from reference 116].

The DNA loading capability of PBCA NPs has been previously investigated [9, 20]. RNA, which has a highly similar structure to DNA, can be incorporated into PBCA NPs. Because of the vulnerable structure of RNA there are lots of obstacles that affect the integrity and function of RNA during the production, delivery and transfection. The possibility of PBCA NP-mediated RNA interference is still unknown. So in this project, the possibility of PBCA NP-induced RNA interference has been investigated.

#### 2.4.1. Polymerization of *n*-Butyl-2-Cyanoacrylate

*n*-Butyl-2-cyanoacrylate (BCA), a monomer, is commonly used as the main component of medical glues [85]. Also, it is famous for its rapid polymerization, which is a process where an unsaturated monomer reacts with another monomer and forms a polymer. It benefits from excellent stability of polymerized form. BCA is used to produce the PBCA NPs used in this study. There are three steps for the polymerization of BCA (see Figure 2.7). Initiation is where an anionic hydroxide initiates the reaction at the site of the double carbon-carbon bond in the BCA monomer. In the second step, the BCA becomes negatively charged, and is able to initiate the reaction with another BCA monomer. In this way, more and more BCA monomers connect to each other, and at last, the BCA polymer is formed [86].

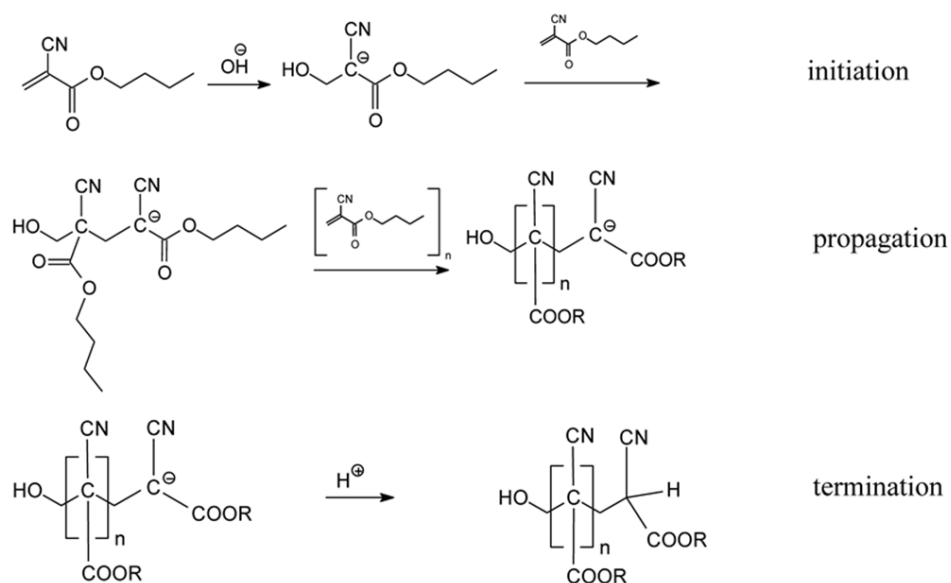


Figure 2.7: Polymerization of BCA monomers. The initiation of the reaction is the contact of a BCA monomer with a negatively charged ion, and then monomers connect to each other to form a polymer. The reaction stops when a positive charged ion is added [taken from reference 116].

## 2.4.2. Synthesis in Water-in-Oil Mini-emulsion

After mini-emulsion polymerization was discovered, it became one of the most common approaches to synthesize polymeric NPs [87]. Initially, the NPs with oil cores were primarily produced because of the easily available O/W mini-emulsion, which implies that only lipid-soluble drugs can be encapsulated in NPs. Due to the requirement of water-soluble drug delivery, a W/O mini-emulsion is designed and used to produce PBCA NPs containing an aqueous core (see Figure 2.8) [83].

To prepare PBCA NPs with an aqueous core, an oil phase and a water phase are mixed together to form a W/O mini-emulsion. In the emulsion, plenty of water droplets containing drugs are suspended in oil. Because of the lack of ions in the oil phase, the polymerization will mainly occur at the interface of water and oil, where BCA monomers attach to the aqueous phase. Therefore, it is expected that the size of the droplets is strongly coupled to the size of the NPs. To achieve small droplets, ultra-sonication is used to minimize and homogenize the water droplets [88, 89].

Surfactants are frequently utilized in mini-emulsion to stabilize water droplets. They also have a great influence on the size distribution and stability of NPs. In mini-emulsion system, their hydrophilic heads hold the water droplets and lipophilic tails insert into oil to avoid the integration of water droplets. The hydrophilic-lipophilic balance (HLB) value, which describes the degree of hydrophilicity or lipophilicity for surfactants, is a standard to evaluate the capacity to stabilize the mini-emulsion [90].

After homogenization, the BCA monomer is added into the W/O mini-emulsion immediately, and polymerization is initiated by the hydroxyl ions by the water molecules at the interface between water and oil phase. Because of the low percentage of water in the W/O mini-emulsion, the reaction requires much longer time than in a O/W mini-emulsion, and the reaction time also depends on the specific surface area of the colloid. When polymerization is completed, the water droplets are surrounded by the BCA polymer, but are suspended in oil, which is inappropriate to cell culture and animal tests. Therefore, it is necessary to separate NPs from the oil phase by using centrifugation, and finally, these particles are re-dispersed in water [91].

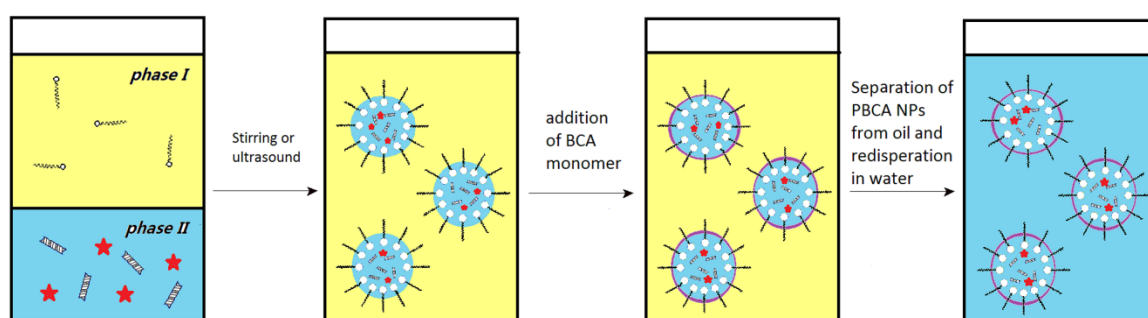


Figure 2.8: A water-in-oil mini-emulsion process to produce PBCA NPs. Oil and surfactants as phase I (yellow) as well as PBS, siRNA or rhodamine-123 as phase II (blue) are mixed and ultra-sonicated. After the formation of a mini-emulsion, BCA (purple) is added and the polymerization is activated. Finally, PBCA NPs are separated from oil by centrifugation and the wet pellets are re-dispersed in water [taken from reference 116].

## 2.5. Characterization of Nanoparticles

In order to produce NPs, there are two important factors that need to be determined: size and Zeta potential of the particles. The particle size is a parameter to describe the dimensions of a particle. It involves a solid sphere and parts of electrochemical layers. The Zeta potential reflects the strength of electrochemical layers of a NP in a solution [92].

### 2.5.1. Size

The particle size not only determines the loading efficiency of drugs, but also influences the passage into cells and tissues. However, NPs are too small to be observed by the naked eye, therefore, the diameter is evaluated by measuring the Brownian motion of the particles, using dynamic light scattering [93]. This technique is based on the fact that a particle scatters the laser into all directions when it is illuminated, and the scattered light can be detected (see Figure 2.9). In addition, particles are never stationary in a liquid. According to Brownian motion theory, the smaller particles are moving faster and the relationship between size of particle and its speed is related to the diffusion coefficient which can be converted into the particle radius by the Stokes-Einstein equation [94]:

$$D = \frac{k T}{6 \pi \eta r}$$

$D$ : diffusion constant;  $k$ : Boltzmann constant;

$T$ : absolute temperature;  $\eta$ : dynamic viscosity;

$r$ : radius of the spherical particle

As a result, the diameter of the NPs (related to  $r$  in equation) can be calculated via the speed of the NPs, taking into account the dynamic viscosity of the liquid, while the other parameters are kept constant.

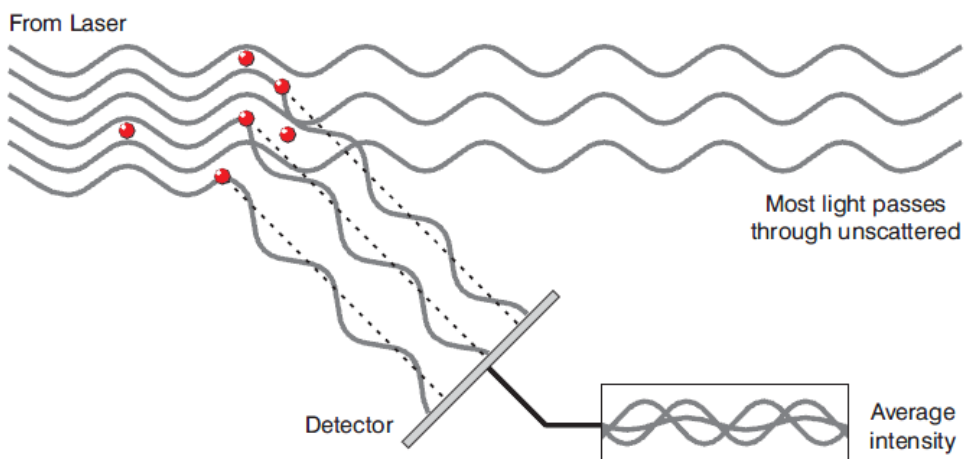


Figure 2.9: The laser is scattered by the NPs. the scattered light falling on the detector [taken from reference 95]. The average intensity is used to evaluate the dynamic viscosity of particles, and calculate the diameter of particles.



## 2.5.2. Zeta Potential

The net electrical charge at the particle surface influences the distribution of ions in the surrounding interfacial region. As a result, a higher concentration of opposite charged ions from the solution is accumulated close to the particle surface. Thus, an electrical double layer exists around each particle. In a liquid, the electrical double layer of a particle consists of two parts: the Stern layer and the diffuse layer. The Stern layer is an inner layer and the ions are strongly bound to the particle surface. The diffuse layer disperses in outer region, where they are less firmly attached. In the diffuse layer, a conceptual boundary is identified where the ions and particles form a stable entity. In other words, when a particle is moving, ions within this boundary are moving together, but any ions beyond this boundary detach from the particle. This boundary is called shear plane. The electrical potential that exists at this boundary is known as the Zeta Potential [96].

The Zeta potential is an important measure to determine the stability of NPs, as it shows the degree of electrostatic repulsion force. The NPs with a high Zeta potential are difficult to aggregate together due to the strong repulsion force. A colloid dispersion is more stable.

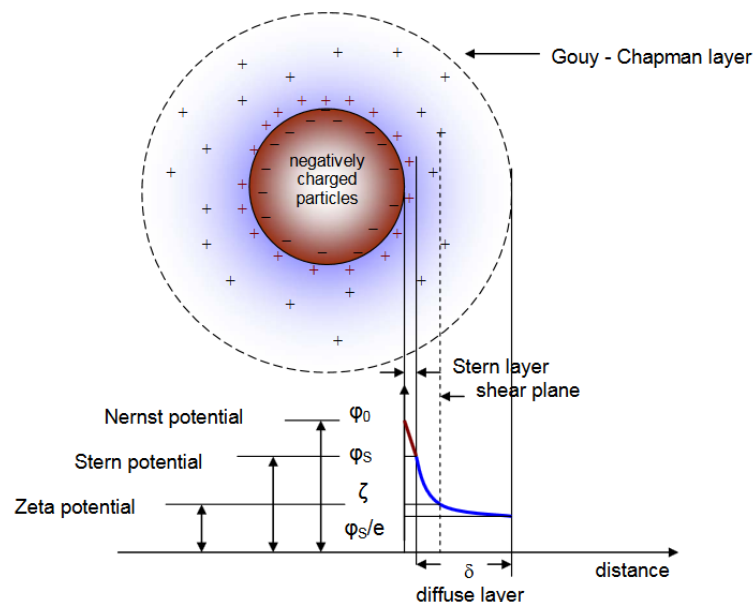


Figure 2.10: Electrochemical double layer model and the Zeta potential for particles. The shear plane is a conceptual layer that the ions and particles form a stable entity. The potential that exists at the boundary of shear plane is named as Zeta Potential [from reference 117].

The Zeta potential is measured using a Laser Doppler Electrophoresis technique, which is a combination of electrophoresis and Laser Doppler Velocimetry (LDV) [97]. Basically, the velocity of a particle under an electric field can be described as:

$$U_E = \frac{2\zeta \varepsilon f(Ka)}{3\eta}$$

$U_E$ : electrophoretic mobility;  $\varepsilon$ : dielectric constant;  
 $\zeta$ : Zeta potential;  $f(Ka)$ : Henrys function;  $\eta$ : viscosity

In the same solvent,  $f(Ka)$  and  $\eta$  are constants, so the Zeta potential can be evaluated from the velocity of the particles. Therefore, LDV is used to measure the velocity of the moving particles and subsequently the Zeta potential of the particles can be determined.

### 2.5.3. Polydispersity Index

The polydispersity index (PDI) is a term used to describe the degree of “non-uniformity” of the particle size. Ideally, if the particles have the same size, shape, or mass; they are called uniform and the PDI is zero. In general, the PDI value ranges from 0 to 1. A monodisperse sample has a PDI value smaller than 0.1, the PDI of polydisperse sample is usually between 0.1 and 0.3, and a PDI value above 0.3 indicates a broad distribution of the particle size. In this study, the PDI of PBCA NPs is measured by a Zetasizer (see Section 8.1 support information: Instruments), which obtains the value from the correlation function of the intensity fluctuation of the scattered light according to:

$$\log[G1] = a + bt + ct^2 + dt^3 + \dots$$

$G1$ : correlation function;  $t$ : time.  
 $b$ : the second order cumulant  
 $c$ : the third order cumulant

$$PDI = \frac{2c}{b}$$

The definition of the PDI is based on the cumulants analysis of the log of correlation function.

## 2.6. Cytotoxicity

Toxicity effects of chemicals are not only caused by chemical reactions disturbing cell metabolism, but also by the physical damage of the cell structure. Too high a concentration of drugs can lacerate the cell membrane because of high osmotic pressure [98]. Furthermore, different types of cells have different sensitivity to the same drug. Hence, to apply PBCA NPs to C6 cells, a cytotoxicity assay is necessary to find out a proper range of concentration for cells.

The MTT (Thiazolyl Blue Tetrazolium Bromide) assay has been a very popular method to measure the cell survival, ever since it was published in 1983 [99]. In principle, the yellow MTT is reduced by nicotinamide adenine dinucleotide (NADH) in the mitochondrion of a cell; and its product, formazan, is purple in colour (see Figure 2.11). This reaction happens only in living cells, because it consumes energy and depends on a NADH-based redox-reaction, which is one of the key indicators for cell activity. Besides that, formazan is insoluble in water, so it can be easily separated from MTT solutions, and then dissolves in dimethyl sulfoxide (DMSO); the cell survival can be evaluated by measuring the absorbance of formazan solution.

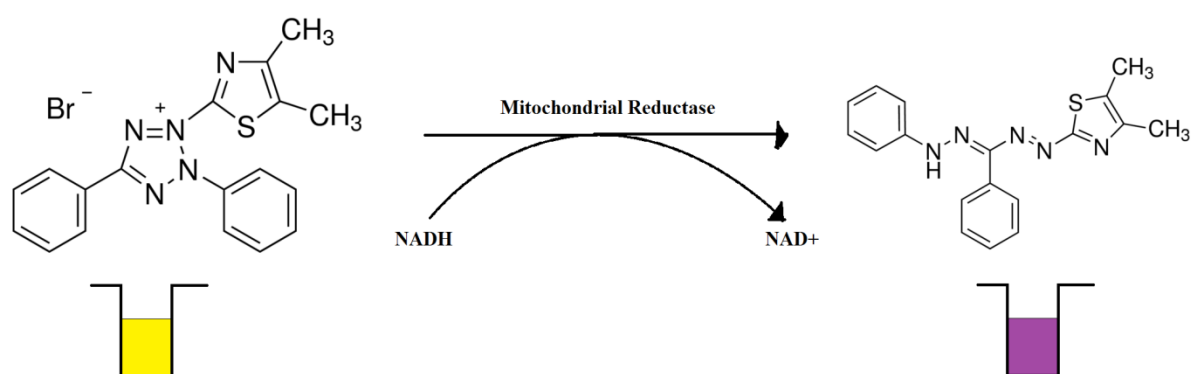


Figure 2.11: Reaction of MTT to formazan. The reaction occurs in mitochondrion and NADH provides ions and energy. The original yellow solution turns to purple in colour.

## 2.7. Protein Immunoblot

Protein immunoblot was originally established by Towbin et al. (1979) [100] and named as “Western Blot” to distinguish from “Southern Blot” and “Northern Blot” as RNA and DNA detection methods [101]. It is commonly used as an analytic technique for qualitative or semi-quantitative detection of proteins in molecular biology, genetics and biochemistry. Western blot analysis is able to not only detect a pure protein sample, but also picks out target protein from a mixture, such as a tissue extract. A protein sample is segregated by gel electrophoresis, and then transferred onto a nitrocellulose membrane. The membrane is continuously washed with the antibody buffer. As a result, the target protein can be differentiated from the other protein (see Figure 2.12).

### 2.7.1. Gel Electrophoresis

For a complex protein sample, each type of protein needs to be segregated and purified, in order to avoid a false positive detection. Sodium Dodecyl Sulfate- Poly Acrylamide Gel Electrophoresis (SDS-PAGE) is used to separate proteins according to their size. SDS, which has a great high negative charge, binds with the proteins and adjusts the charge of the proteins corresponding to their molecular weight, so in a SDS-gel, the running speed of a protein only depends on its size during electrophoresis; as a result, proteins are separated according to their size [102].

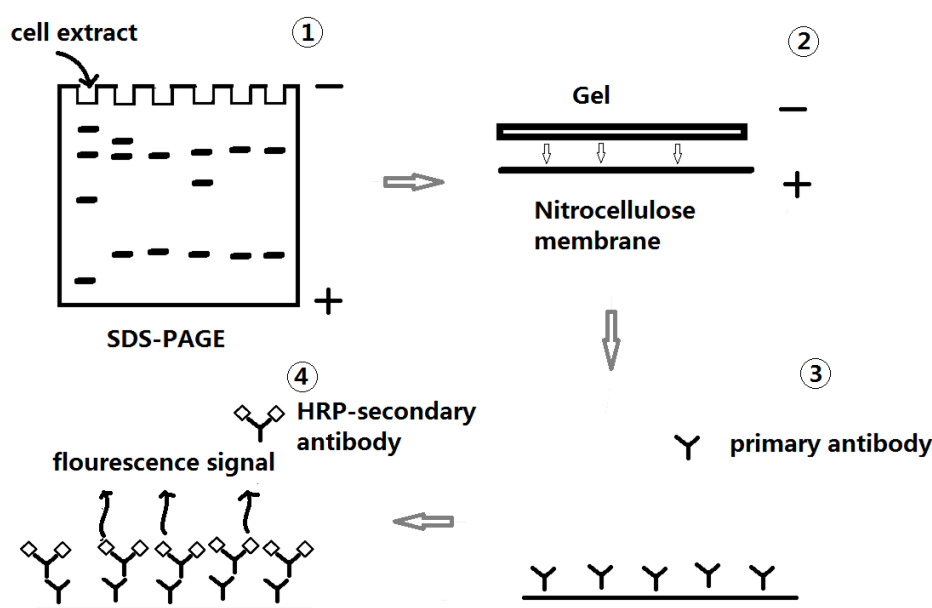


Figure 2.12: Scheme of the western blot process. First, a cell extract is loaded on a SDS-polyacrylamide gel to separate proteins by size. Second, these proteins are transferred on a nitrocellulose membrane. Third, the membrane containing target protein is washed with primary antibody; the antibody recognizes and binds to target protein. Fourth, luminous group (Horse radish peroxidase, HRP) linked secondary antibody is used to bind to primary antibody. As a result, the target protein is detected.

### 2.7.2. Transference

Due to the tight structure of polyacrylamide gel, a further detection with antibody incubation will hardly be successful. Hence, after electrophoresis, proteins are transferred onto a 0.8 mm thick nitrocellulose (NC) membrane<sup>1</sup>, which has high protein-binding affinity, compatibility with a variety of detection methods, and the ability to immobilize proteins. As shown in Figure 2.12, transferring is performed under an electric field. The gel acts as a negative

<sup>1</sup> Polyvinylidene difluoride membrane is also possible to western blot analysis, but not used in this study.

electrode while the NC membrane is positive. As a consequence, the negatively charged proteins are transferred from gel onto NC membrane and are immobilized there. Therefore, proteins are available for the antibody detection.

### **2.7.3. Antibody Probing**

An antibody is a Y-shaped protein which is physiologically produced by the plasma cells. For applications in molecular biology, antibodies are designed and generated to detect a specific target protein. In western blot analysis, the selected antibodies are used to probe the target proteins on the membrane. In the beginning of the antibody probing, the membrane is blocked after transference to prevent a non-specific binding of the antibody to the membrane. Afterwards, a primary antibody starts to bind to target proteins. Thereafter, the primary antibody is probed by a secondary antibody, which has a luminescence group, such as horseradish peroxidase (HRP), or Alexa Fluor<sup>®</sup> 647. According to the light signal from the secondary antibody, the target proteins can be specifically detected.

## **2.8. Paraffin section & immunofluorescence**

A paraffin section is a very thin slice of a tissue that has been infiltrated with paraffin (see Figure 2.13). The preparation of paraffin sections is a common and useful technique in histology. It is used not only to observe the morphological structure of cells and tissues, but also to diagnose diseases and determine therapeutics [103, 104]. The cells and tissues embedded in paraffin can be stored for a long time because of the dehydrated state, and they are also suitable for immunohistochemistry after hydration and antigen retrieval. Moreover, the paraffin sections enable the observation of cell and tissue morphologically under a microscope, because the tissues are cut into thin slices (around 5-10  $\mu\text{m}$ ) containing only one or two layers of the cells. The detailed protocol of preparing paraffin sections and immune-detection is introduced below.

### **2.8.1. Fixation**

Fixation is the first step to prepare a paraffin section. In this process, the target tissue is protected from autolysis or putrefaction and all the ongoing biochemical reactions are terminated. Furthermore, the fixative, the agent used in fixating, enhances the tissues' mechanical strength and stability by denaturing proteins, but preserves the main structures of these proteins in cells and tissues. Moreover, the fixative induced protein denaturation is

reversible, and the retrieved proteins can be recognized by antibodies. Four percent of formaldehyde in phosphate-buffered saline (PBS) is the most popular fixative for preparing a paraffin section [105].

### 2.8.2. Dehydration & Embedding

The purpose of dehydration and embedding is to prepare a solidified sample to be cut. After the fixation, the tissue is still too soft, and is hardly cut into thin slices. To obtain a high quality tissue slice, it is necessary to replace the water in the tissue with paraffin, which is a clear substance used to solidify. The dehydration process starts with progressively increasing the ethanol concentrations to remove the water. Thereafter, the ethanol is removed by a hydrophobic clearing medium, such as xylene. Finally, molten paraffin wax replaces the clearing medium. After the dehydration, the tissue is embedded in a paraffin cube. The molten paraffin wax, which immerses the whole tissue, is hardened by cooling, and provides a sufficiently hard matrix for slicing.

### 2.8.3. Slicing

To observe the tissue's structure under a microscope, the samples shall be cut to very thin slices. After embedding, the samples are already infiltrated by paraffin; so they are sufficiently hard to be cut. The paraffin cube containing the tissues is immobilized on a plate, and a steel blade is used to cut the paraffin cube as well as the tissue inside. Thereafter, the slices are stretched on warm water, which slightly softens paraffin wax and straightens the slices by the surface tension of water and air. Then the slices are placed on microscope slides, thin flat pieces of glass, and warmed up, to remove water (see Figure 2.13).

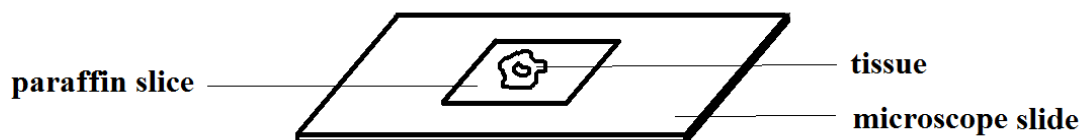


Figure 2.13: Scheme of a paraffin section. The paraffin section is composed of a paraffin slice with a piece of the tissue, and a microscope slide.

### 2.8.4. Hydration

Although the slices can be imaged under a microscope directly, immunofluorescence imaging is a much more specific and sensitive method. However, the proteins in the tissues are surrounded by paraffin and are impossible to be captured by antibodies, so the hydration process is used to replace the paraffin with water. It is a reverse process to dehydration. In the beginning, the slices are immersed in xylene to remove the paraffin, and then washed by gradually decreasing concentration of ethanol to exclude the xylene. Finally, the ethanol is replaced by water, to refill the tissues with water.

### **2.8.5. Epitope Retrieval**

An epitope, as a part of antigen, is the site of recognition for an antibody. Due to the fixation process, the proteins and their epitopes in the slices are denatured even after hydration. Samples cannot perform any immune reaction. Hence, the detection by the antibody-based fluorescence detection is impossible. So, the aim of this process is to retrieve these epitopes in the tissue samples. The principle is that the aldehyde of formaldehyde-protein bonds are broken in a sufficiently high temperature, and the structure of proteins are recovered during cooling down [106]. As a result, the proteins transform to their natural structure and regain the ability of an immune response. Citrate buffer is one of the most popular retrieval reagents for immunohistochemistry and was also used in this study.

### **2.8.6. Fluorescence Imaging**

Fluorescence imaging is performed to detect antibodies which are linked with fluorescent groups. The principle is similar to the antibody probing of western blot analysis (see section 2.6.3.). But, there are some different features for a sliced tissue sample on a slide. First, both methods enable a semi-quantitative evaluation of the concentration of the target protein, but the fluorescence imaging of the paraffin section also allows observing the location and distribution of the target protein in the tissue. Second, a multi-labelling technique can be applied in the immunofluorescence protocol, which uses two or more types of antibodies for different kinds of proteins, and distinguish them in different wavelengths of luminescent light. Finally, the immunofluorescence is much more sensitive and specific than western blot. The tissue slices are incubated in a primary antibody solution, and subsequently in the fluorescent-labelled secondary antibody solution. Under a confocal microscope, the fluorescent signal reveals the position of the target protein, and its concentration can be semi-quantitatively evaluated according to the intensity of the signal of the target protein (see Figure 2.14).

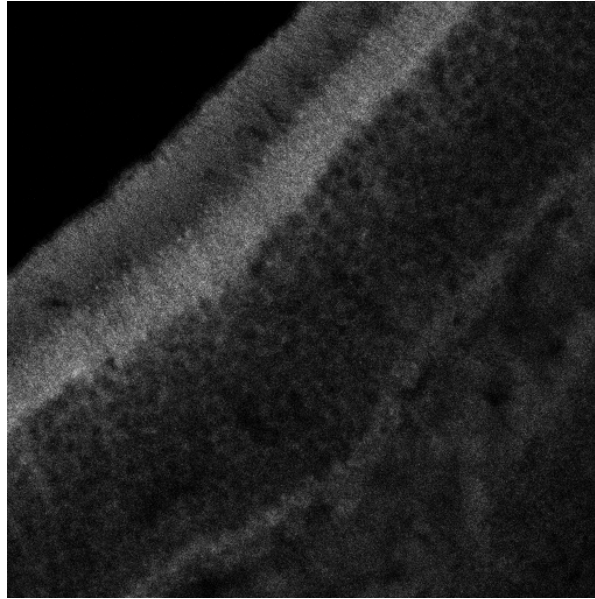


Figure 2.14: An immunofluorescence image of the retina. The target protein is caspase-3, which is detected in almost the entire retina.

## 2.9. *In Vivo* Confocal Neuroimaging

The PBCA NPs distribution in the retina after the intravenous (*i.v.*) injection has been investigated by the *In vivo* Confocal Neuroimaging (ICON) technique [18, 107]. This is a non-invasive imaging technique to trace fluorescent signal in the retina. To detect a fluorescent signal, such as a labelled NP, a laser with an appropriate wavelength is sent into the eye, and the fluorescent groups on the NP are excited and emit a fluorescent light which is captured by a detector (see Figure 2.15). As a result, the signals of the NPs can be detected in the retinal structures (see Figure 2.16). Moreover, PBCA NPs crossing the blood-retina barrier, which is virtually the same as the blood-brain barrier, can be also demonstrated. If the passage of the blood-retinal barrier is confirmed, it is assumed that the PBCA NPs have the ability to cross the blood-brain barrier [14].



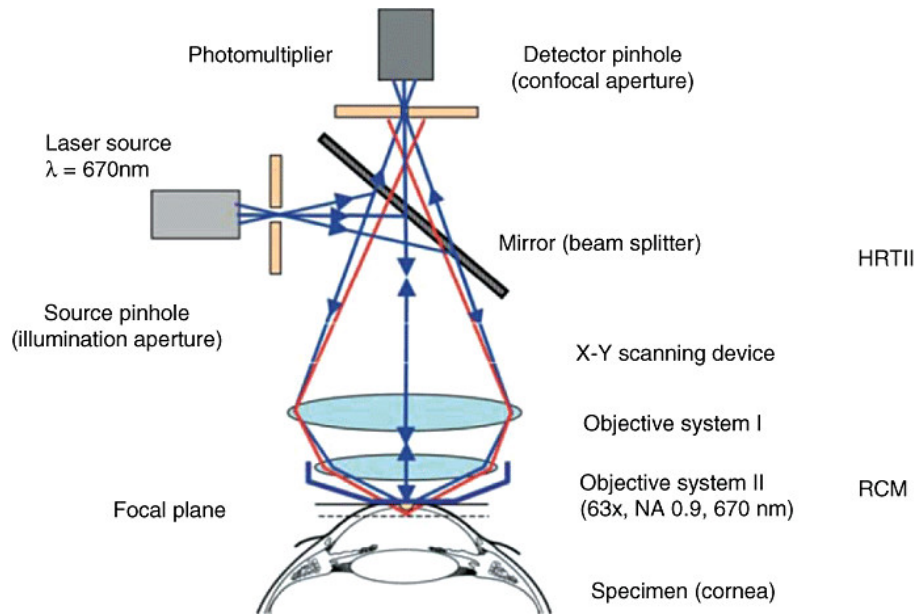


Figure 2.15: Schematic of an *in vivo* confocal microscope [108]. In the current experiments, the system is adapted insofar as a plan-concave lens is placed on the cornea, which guides the laser beam to the retina.

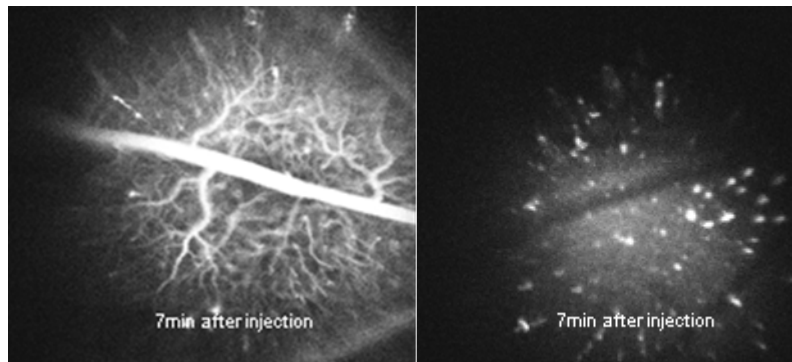


Figure 2.16: The images of *In vivo* Confocal Neuroimaging. The fluorescent dye is injected intravenously and the signal is detected in blood vessel only (left), but the passage of the blood-retinal barrier with PBCA NPs is demonstrated after *i.v.* injection of the fluorescence-labelled PBCA NPs (right), as signal dots are localized outside of blood vessels [14].

## 2.10. Retina

The retina is a light-sensitive tissue, which transforms light signals into electro-chemical signals. It includes cells of different types, locations, and morphological shapes. The retina is usually subdivided in 7 layers of tissues (see Figure 2.17): 1) a retinal ganglion layer, 2) an inner plexiform layer, 3) an inner nuclear layer, 4) an outer plexiform layer, 5) an outer nuclear layer, 6) a photoreceptor layer, and 7) a pigment epithelium [109]. Each layer has its

unique structure and function, for instance the photoreceptor layer can receive light signals by rods and cones, but the nuclei of these rods and cones are in the outer nuclear layer.

The delicate retina parenchyma is protected by the blood-retina barrier, which is a special and tight insulation of the blood vessel. Its function and structure are highly similar to the blood-brain barrier, and most of drugs and compounds fail to go through this barrier. Therefore, it is a challenge for siRNA-PBCA NPs to reach the retina parenchyma and deliver the siRNA into retinal cells after *i.v.* injection.

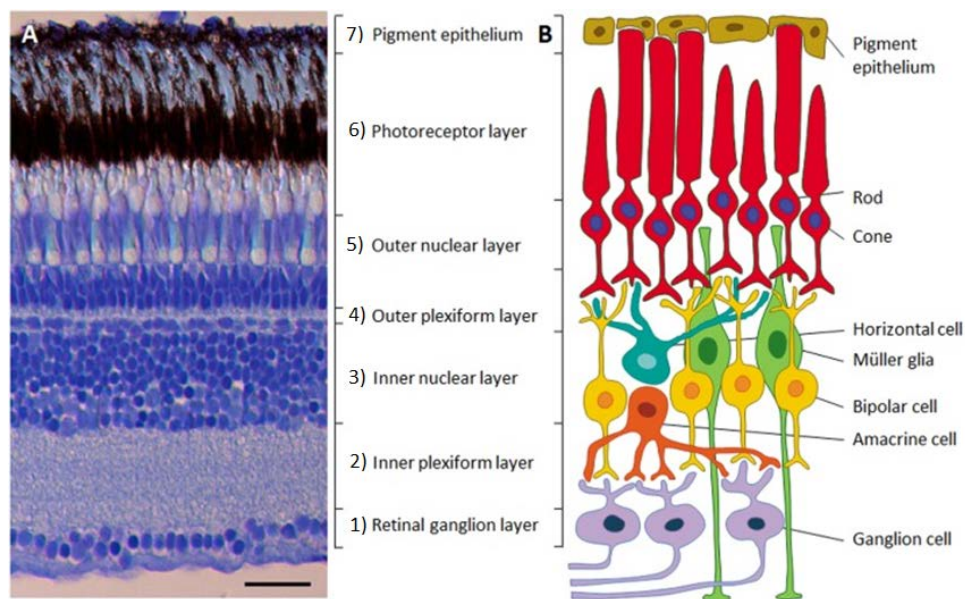


Figure 2.17: the structure of the retina. A: Microphotograph of a cross-section through the retina of an adult zebrafish, showing the different cellular and synaptic retinal layers. In A, the scale bar = 25  $\mu\text{m}$ . B: Diagram of the neural circuit of the retina, showing the six neuronal cell types and the two supporting cell types [109].

In this study, we used target protein caspase-3, which mainly exists in the cytoplasm. It is, therefore, expected that the signal can be observed in the inner and the outer plexiform layer, which are composed of the cytoplasm. Furthermore, the inner and outer nuclear layers, which are full of nuclei, are labelled by the nuclei staining dye “Hoechst 33342”. The passage of blood-retina barrier with PBCA NPs was also investigated to find out a proper method for PBCA NPs delivery targeting retina in this study.

## **3. Methods**

### **3.1. Preparation of Poly (Butyl Cyanoacrylate) Nanoparticles**

PBCA NPs were produced via the W/O mini-emulsion method [9]. The synthesis process was as follows: a mixture of Span® 80 and Tween® 80 was added into an oil phase of Migyol® 812N, by stirring for 10 min. Then, the water phase, containing siRNA or Rhodamine 123, was added drop-wise into the oil phase under stirring. After 30 min, the mini-emulsion was obtained by using a homogenizer with 50 % amplitude for 60 s. The polymerization was activated by the addition of the BCA monomer into the mini-emulsion. The NPs were formed in the oil, after stirring for 4 hrs. Then, a centrifugation of 8000 g for 5 min was performed, to separate the wet pellets from the oil. Finally, these pellets were re-dispersed in water. The NPs were ready to the following experiments.

### **3.2. Characterization of Nanoparticles**

The particle size and the Zeta potential of the PBCA NPs were measured by a Zetasizer [95, 96, 117]. 50 µL of the PBCA NPs solution was diluted in 950 µL of double distilled water. For the particle size measurement, the diluted NP solution was filled into a polystyrene cuvette (see Figure 3.1), and then the cuvette was inserted in the sample cell slot of the Zetasizer. For the Zeta potential measurement, the probe was gently inserted into the cuvette containing the diluted NP solution (see Figure 3.1), and then the module was mounted in the machine. In the Zetasizer program, the measurement parameters for the particle size and the Zeta potential were set up according to the value given in Table 3.1.



Figure 3.1: the polystyrene cuvettes for the particle size measurement (left) and a Dip Cell Kit for the Zeta potential measurement (right)

The solid content was obtained by weighing the solid powder of PBCA NPs after baking. Briefly, the weight of the glass dish was measured and recorded as  $M_d$ . A constant volume ( $V$ ) of the PBCA NPs was spread on the glass dish. The sample was baked at  $80^\circ\text{C}$  overnight, and the weight of the sample and dish was measured as  $M$ . The solid content was calculated according to:

$$\text{Solid Content} = \frac{M - M_d}{V} \left( \frac{g}{mL} \right)$$

Table 3.1: The measurement parameters for the Particle Size and the Zeta potential in the program of the Zetasiser. All the PBCA NPs were measured in the same setting.

Parameters	Particle Size	Zeta potential
Measurement Type	Size	Zeta potential
Material	Polystyrene latex	Polystyrene latex
Dispersant	Water	Water
Temperature	$25^\circ\text{C}$	$25^\circ\text{C}$
Equilibration Time	2 min	2 min
Cell Type	Disposable Cuvettes	Dip Cell for Zeta potential
Number of measurements	3	3

### 3.3. Cell Culture

The C6 rat glioma cell line used in this study was cultivated in Ham's F-12K (Kaighn's) medium, supplemented with 15 % of horse serum, 2.5 % of fetal bovine serum, and 1% of penicillin/streptomycin. The cells were always incubated at 37°C in 5 % CO<sub>2</sub> humidified atmosphere. There were different containers which were used to culture the cells in this study, and each of them required different volumes of medium (see Table 3.2).

Table 3.2: The volumes of medium for the different containers used in cell culturing. The bottles were used in subculturing, and the plates were used for the *in vitro* tests.

Container types	Volumes of medium in mL
25cm <sup>2</sup> bottle	5
75cm <sup>2</sup> bottle	10
6-well-plate	2.5
24-well-plate	0.5
96-well-plate	0.2

The subculture procedure was performed on every 3<sup>rd</sup> day. Briefly, the old medium was removed, and the cells were washed with pre-warmed PBS 3 times. Then, 500 µL of Trypsin/EDTA was added to the cells for approximately 15 min of induction for detachment. A pipette was used to gently disperse the cells for about 5-10 times. An appropriate volume of the fresh medium was added into the cell solution. These cells were separated into new culture bottles and incubated at 37 °C. In the case of using a well-plate, the appropriate volume of dispersed cell solution was transferred into each well of the plate.

In the case of cryopreservation, the cells were separated from the cell solution via a 900 rpm, 5 min centrifugation at 4°C. Following, the cells were dispersed in a solution composing of 100 µL of DMSO and 1.9 mL of fresh medium. The cells were transferred to a preservation tube and frozen at -20°C for 2 hrs. Finally, the frozen cells were stored at -80°C.

To recover the cryopreserved cells, the frozen cells were warmed up in a 37°C water bath as quickly as possible, and then centrifuged at 900 rpm for 5 min. After removal of the supernatant, the preservation medium was replaced by the fresh medium. Finally, the cells were pipetted into culture bottle and incubated at 37°C.

### 3.4. Cytotoxicity

200  $\mu\text{L}$  of approximately 20,000/mL C6 cells were seeded in a 96-well plate, as described above, and allowed to attach onto the surface of the plate by 24 hrs of incubation at 37°C and 5 % of  $\text{CO}_2$ . The cells were subsequently exposed to 0.1 %, 0.5 %, 1 %, 5 %, and 10 % of the PBCA NPs for 48 hrs at 37°C in a  $\text{CO}_2$  incubator. After incubation, the medium was refreshed after washing with PBS for 3 times. Then, 10  $\mu\text{L}$  of 5 mg/mL MTT solution was added to the each well. After 4 hrs of incubation, the medium was replaced by 100  $\mu\text{L}$  of DMSO. The plate was shaken for 10 min. Finally, the cell survival rate was measured by a spectrophotometer and calculated according to the absorption at 560 nm of each well. In some assays, 10  $\mu\text{L}$  of 1 mg/mL staurosporine (Stau) was applied to trigger apoptosis. The Stau treatment was scheduled for 24 hrs after seeding C6 cells into the 96-well plate. After 1 hr of incubation with Stau, the cells were exposed in addition to 0.1 %, 0.5 %, 1 %, 5 % and 10 % of blank PBCA NPs and caspase-3 siRNA-PBCA NPs (casp3 PBCA NPs), respectively.

### **3.5. Protein Samples Preparation, SDS-PAGE and Immunoblotting**

Cells were seeded in a 6-well-plate at a concentration of  $2.0 \times 10^5$  cells/well and cultivated for 24 hrs to allow cell attachment. The old medium was refreshed with the culture medium. For the case of Stau treatment, the medium containing 0.5  $\mu\text{g}/\text{mL}$  of Stau was used to replace the old medium. Different types of PBCA NPs, caspase-3 siRNA-calcium particle, and PBS were subsequently added in different wells. After 48 hrs of incubation, the cells were detached by using trypsin/EDTA, and were collected by centrifugation at 900 rpm for 5 min. Then the cells were lysed in 200  $\mu\text{L}$  of cell lysis buffer, pre-mixed with phenylmethanesulfonyl fluoride in an ice bath. After waiting for 30 min, the protein samples were obtained by centrifugation at 12000 rpm for 5 min. The concentrations of the total proteins in lysate were immediately detected by using a Pierce™ BCA Protein Assay Kit. According to the detected concentration, these protein samples were diluted with water resulting in the same concentration for each of the samples and subsequently mixed with one third volume of the 4 times concentrated Laemmli buffer. Then, the protein samples were ready to be researched.

For SDS-PAGE, a 15 % SDS-polyacrylamide gel was produced by mixing the reagents sequentially according to Table 3.3. The separating gel was prepared first and added into a gel module directly. Then, roughly 2 mL of water was gently added on the top of the separating gel as quickly as possible. After 10-15 min, when the separating gel solidified, the water was removed. After 10-15 min of the addition of stacking gel, the polyacrylamide gel was

prepared. A comb was used on stacking gel during the solidification to prepare the space for samples. Before the start of the electrophoresis, 25  $\mu$ g of the protein samples were loaded on the 15 % SDS-polyacrylamide gels. The electrophoresis was performed under the voltages of 80 mV for stacking gel and 100 mV for separating gel. The electrophoresis was completed when the proteins, which were coloured by the Laemmli buffer, almost reached the end of the gel.

Table 3.3: The reagents to prepare a 15 % SDS-polyacrylamide gel for western blot analysis.

The stacking gel and the separating gel are prepared individually. The tetramethylethylenediamine should be the last reagent added.

No.	Reagents	Volumes	
		Stacking Gel	Separating Gel
1	water	3.4 mL	2.3 mL
2	30 % Acr/Bic	0.83 mL	5.0 mL
3	1.5 M tris buffer, pH 8.8	/	2.5 mL
4	1.0 M tris buffer, pH 6.8	0.63 mL	/
5	10 % SDS <sup>1</sup>	0.05 mL	0.1 mL
6	10 % ammonium persulfate <sup>1</sup>	0.05 mL	0.1 mL
7	tetramethylethylenediamine	0.05 mL	0.05 mL

1: SDS and ammonium persulfate were dissolved in double distilled water (w/v).

After the electrophoresis, the gel was carefully taken out and put into a tank containing the transfer buffer, a nitrocellulose membrane, two blotting papers, and two blotting sponge pads. Subsequently, the gel was spread on the nitrocellulose membrane, and then covered by blotting papers and blotting sponge pads on both sides of the gel and membrane. The blotting sandwich was prepared and mounted into the Mini Gel Tank and Blot Module Set for transferring at a constant electric current of 350 mA for 75 min. In this way, the proteins were immobilized onto the nitrocellulose membrane. Afterwards, the membrane was blocked in TBST buffer with 5 % (w/v) of non-fat dry milk for 1hr, and then incubated with the primary antibody at 4°C overnight. Subsequently, The HRP-linked secondary antibody was used to incubate the membrane at room temperature for at least 1 hr. Before visualization, SignalFire™ ECL Reagent was prepared and added onto the membrane. The western blot images were obtained using an enhanced chemical luminescence (ECL) image system. In this

study,  $\alpha$ -tubulin antibody and caspase-3 antibody were used as primary antibodies. All the results were quantified in integrated optic density by the ImageJ software [120].

### 3.6. Optic Nerve Crush Surgery & Intravitreal Injection

The optic nerve crush (ONC) surgery was performed on Charles River Phylum Lister Hooded adult rats (CrI:LIS Stamm: Charles River, 280–390 g, aged 10 weeks). Fifteen rats were divided into 5 groups, and the surgeries were performed on only one eye of each rat, but at least one left and right eye of different rats were operated on each group. Animals were at first anesthetized with Ketanest (Ketamine 10 %, 75 mg/kg) and Medetomidine (0.5 mg/kg), which was injected intraperitoneally to induce a deep narcosis. 30 min after injection, the surgery started. Proparacain-POS 5.0 %, which induced local anaesthesia, was dropped on the eye 1 min before start. A small cut was made at the *Saccus conjunctivalis* of the eyeball, of which the position is shown in Figure 3.2. Close to the surface of the eyeball, two forceps were inserted to reach the optic nerve achieved by blunt dissection of the muscle and fibrous tissue. The forceps were used to clean the nerve from the surrounding tissues carefully without touching the optic nerve. Then, the optic nerve was placed between two tips of a crush forceps, and a moderate crush (distance of tips of forceps 0.2 mm) was applied on the optic nerve for 30 sec. After the crush, the forceps were taken out carefully, and floxal, an antibiotic cream, was added on the wound for the prophylactic antibiotic treatment.



Figure 3.2: A rat eye. The red circle marks out the position of the cut site for the ONC surgery [118].



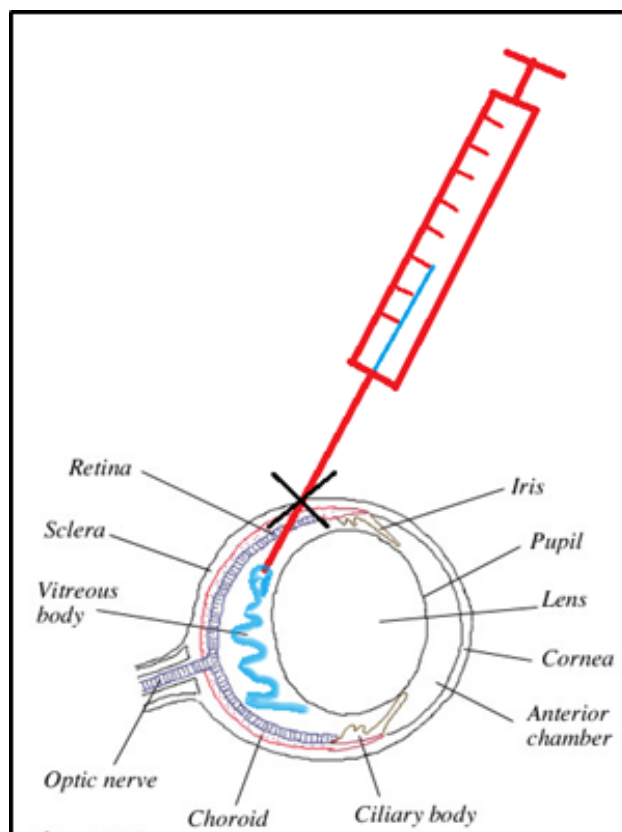


Figure 3.3: The injection point. The needle entered the vitreous body through the sclera. The black cross indicated the point where is the cut into the connective tissue and the insertion point for the needle and Hamilton syringe [119].

Bilateral intravitreal injections were performed immediately after the unilateral ONC. In the beginning, the connective tissue was cut to detach the sclera, while pulling it with the colibri forceps. A sharp needle with a diameter of 0.8 mm then penetrated the sclera at the position shown in Figure 3.3. The injection into the vitreous was performed by a Hamilton syringe with a blunt cannula. 3  $\mu$ L of casp3 PBCA NPs, caspase-3 siRNA-calcium particles, blank PBCA NPs, negative siRNA-PBCA NPs (neg PBCA NPs), and PBS were injected into those 5 groups of rats, respectively.

### 3.7. Paraffin Section & Immuno-Fluorescence

At 48 hrs after the ONC and intravitreal injections, the animals were anesthetized again by intraperitoneal injection of Ketanest (75 mg/kg) and Medetomidine (0.5 mg/kg). After reaching a deep narcosis, both eye balls of the animals were taken out and immersed in 4 % formalin. Then, these eyeballs were washed with 4 % formalin for 4 hrs. Following, the eyeballs were washed successively with 70 %, 85 %, 2  $\times$  96 % and 3  $\times$  100 % ethanol

solution for 1 hr. Subsequently, they were washed 2 times with RotiHistol for 1 hr and 1.5 hrs respectively. After that, the eyeballs were immersed into liquid paraffin wax for 2 hrs. The paraffin wax was refreshed and immersed the eyeballs for another 2 hrs. The eyeballs were taken out from the oil paraffin, quickly put in an embedding module and covered with new paraffin wax, with subsequent cooling at room temperature for a duration of 3 hrs. Finally, the paraffin embedded eyeballs were stored at 4°C until they were sliced. The necessary reagents and required times are listed in Table 3.4.

Table 3.4: The necessary reagents and required times for dehydration of eyeballs. The eyeballs of rats were immersed in these reagents successively.

No.	reagents	time(hrs)	No.	reagents	time(hrs)
1	4 % formalin	4	7	100 % ethanol	1
2	70 % ethanol	1	8	100 % ethanol	1
3	85 % ethanol	1	9	RotiHistol	1
4	96 % ethanol	1	10	RotiHistol	1.5
5	96 % ethanol	1	11	Paraffin	2
6	100 % ethanol	1	12	Paraffin	2

The paraffin cubes were cut into slices of 10 µm thickness by a microtome. Then, the slices were put in a water bath with the temperature of 42°C. The slices were stretched by the the surface tension between water and air, and stuck on the upper surface of Superfrost™ slides. Next, the slides with the slices were dried on a hot plate, at a temperature of 50°C for at least 15 min until all the water from the slices was removed. The paraffin sections were stored at 4°C.

Before hydration, the paraffin sections were taken out of the refrigerator and dried again on the hot plate for 10 min at 50°C. As the next step, hydration was started by washing in a sequence of xylol, 100 % ethanol, 96 % ethanol, 90 % ethanol, 80 % ethanol, 70 % ethanol solutions, and rinsing with water for 5 min each at room temperature. Then, all the slices were immersed in a pre-mixed 0.01 M citrate buffer and heated by steam for 45 min, in order to recover antigens in tissues. When the steaming was completed, the samples were cooled down in the citrate buffer for 30 min at room temperature, and then washed 3 times for 5 min each with PBS. The power block solution was added onto all the samples for 6 min and subsequently washed 3 times for 5 min each with PBS in order to reduce the background from un-specific immunoreactions. The primary antibodies against caspase-3 were added onto the

samples at 4°C overnight. The antibodies were removed by washing with distilled water on the next day. A secondary antibody conjugated with Alex-fluor 647<sup>®</sup> was added on the samples for 2 hrs in the dark at room temperature. After washing down secondary antibody by PBS 3 times for 5 min each, 2 µg/mL of Hoechst 33342 diluted in water was used to stain the nuclei in the retinal tissues for 6 min in the dark. Finally, all the samples on slides were closed by coverslips, using Immu-mount. The slices were ready to be imaged.

Table 3.5: The necessary reagents and times for hydration of paraffin sections. The paraffin sections were washed with these reagents successively.

No.	reagents	time(min)	No.	reagents	time(min)
1	xylol	5	6	90 % ethanol	5
2	xylol	5	7	80 % ethanol	5
3	100 % ethanol	5	8	70 % ethanol	5
4	100 % ethanol	5	9	rinsing water	5
5	96 % ethanol	5	10	distilled water	1

Table 3.6: The reagents to prepare the citrate buffer. The buffer solution, which is prepared only before use, is used to retrieve the denatured protein in a paraffin section..

Reagents	Preparation
Stock solution A	4.8 g citric acid in 250 mL distilled water
Stock solution B	7.35 g citric acid tri-sodium salt di-hydrate in 250 mL distilled water
buffer solution	4.5 mL solution A + 20.5 mL solution B + 225 mL distilled water.

### 3.8. *In Vivo* Confocal Neuroimaging

Animals were anaesthetized with an intraperitoneal injection of 75 mg/kg of Ketanest and 0.5 mg/kg of Medetomidine, which has been described (see Section 3.6.). *In vivo* confocal neuroimaging experiments were performed as described: Neosynephrine-POS 5 % was applied for the dilation of the pupils; Vidisic optical gel was added regularly during the procedure as an immersion medium for the contact lens, and to protect the cornea from drying. Under narcosis, the rats were placed under the objective of a standard confocal laser scanning microscope with a large probe space and a long working distance objective lens. The eye was directed towards the objective lens, and a Hruby style-80 dioptre plan concave lens was

placed directly onto the surface of the cornea, to adjust the path of the laser rays to the rat's retina.

The rhodamine-123 labelled PBCA NPs were injected intravenously from the tail vein with a single dose of 0.1 mL/100 g body weight via a pre-implanted catheter. Confocal images were taken from 5 min to 2 hrs post-injection, for every 2-5 min. Each experimental condition was confirmed in at least three animals.

## 4. Results

### 4.1. Characterization and Optimization of PBCA NPs

The particle size, the Zeta potential, and the polydispersity index (PDI) of PBCA NPs were measured using a Zetasizer. These characteristics are used to evaluate the stability of PBCA NPs and their size for biological applications. Specifically, the stability of PBCA NPs was considered taking into account a variety of surfactants types, water/oil rate, and BCA monomer/oil rate with respect to the median diameter ( $d_{50,3}$ ), the Zeta potential, and the PDI.

#### 4.1.1. Surfactants

The PBCA NPs were initially formed in the oil phase and subsequently re-dispersed in water. Thus, it was necessary to consider the stability of the PBCA NPs in both the oil and water phases. Different mixtures of surfactants, which have a variety of HLB values, were used to stabilize the PBCA NPs. The HLB values of each mixture are shown in Table 4.1. We observed that the lower the HLB value, the more hydrophilic the surfactant [110]. After the measurements, these characteristics of PBCA NPs, such as the particle size, the PDI, and the Zeta potential, were used to compare the stability of the particles between each type of surfactants.

Table 4.1: HLB values of the surfactants. The surfactants used in preparation of the PBCA NPs are composed of Tween® 80 and Span® 80. Their HLB values change depending on the different mixtures of Tween® 80 and Span® 80.

Tween® 80 in total surfactants (Span® 80 and Tween® 80) (wt./wt.)	HLB
0 %	4.30
20 %	6.44
40 %	8.58
60 %	10.72
80 %	12.86
100 %	15.00

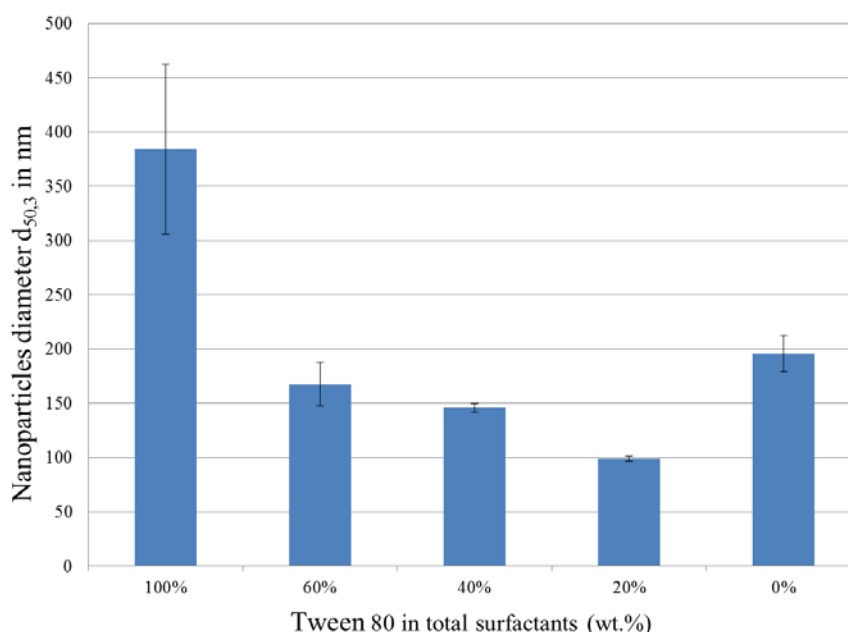


Figure 4.1: The median particle diameter ( $d_{50,3}$ ) in nm with different surfactants mixtures of Tween<sup>®</sup> 80 and Span<sup>®</sup> 80. The median diameter ( $d_{50,3}$ ) of the PBCA NPs was changed corresponding to the types of surfactants. When a pure surfactant Tween<sup>®</sup> 80 or Span<sup>®</sup> 80 was available, large NPs were obtained. The finest NPs were found when 20 % of Tween<sup>®</sup> 80 and 80 % of Span<sup>®</sup> 80 were mixed as the surfactant.

According to the diameters of the PBCA NPs in Figure 4.1, in a mixture of Tween<sup>®</sup> 80 and Span<sup>®</sup> 80, an increasing concentration of Span<sup>®</sup> 80 leads to a decrease in the size of the formed NPs. When the percentage of Span<sup>®</sup> 80 increases from 0 % to 80 %, the diameter of the NPs decreases from  $384.3 \pm 78.2$  nm to  $99.0 \pm 2.3$  nm. However, using only Span<sup>®</sup> 80 as surfactant (no Tween<sup>®</sup> 80) increases the diameter of the produced PBCA NPs (about  $195.9 \pm 16.5$  nm). It is assumed that Span<sup>®</sup> 80, which has a HLB value of 4.30, has an excellent affinity to oil, so it may stabilize the water droplets very well in the oil phase and form small NPs. In contrast, when the NPs are re-dispersed in water, Span<sup>®</sup> 80 does not provide an efficient repulsion which may lead to the aggregation of particles. Comparing with Span<sup>®</sup> 80, Tween<sup>®</sup> 80 is a hydrophilic surfactant, it cannot maintain a stable W/O mini-emulsion which has led to a large  $d_{50,3}$  ( $384.33$  nm) of the NPs and high deviation of diameter ( $78.2$  nm in standard deviation). But if a mixture of Span<sup>®</sup> 80 and Tween<sup>®</sup> 80 is used in a mini-emulsion, the  $d_{50,3}$  declines significantly, to  $167.7 \pm 20.2$  nm,  $145.7 \pm 4.3$  nm, and  $99.0 \pm 2.3$  nm depending on 60 %, 40 %, and 20 % of Tween<sup>®</sup> 80 in the surfactants. It indicates that Tween<sup>®</sup> 80 performs as a stabilizer when NPs are re-dispersed in water, and Span<sup>®</sup> 80 participates in

the formation of the small water droplets. Therefore, a mixture of surfactants provides the best results for the W/O mini-emulsion polymerization. In the experiments, the fine NPs were obtained when both Span® 80 and Tween® 80 were used for production, and the smallest  $d_{50,3}$  was found if the surfactant contained 20 % of Tween® 80 and 80 % of Span® 80 in wt. %.

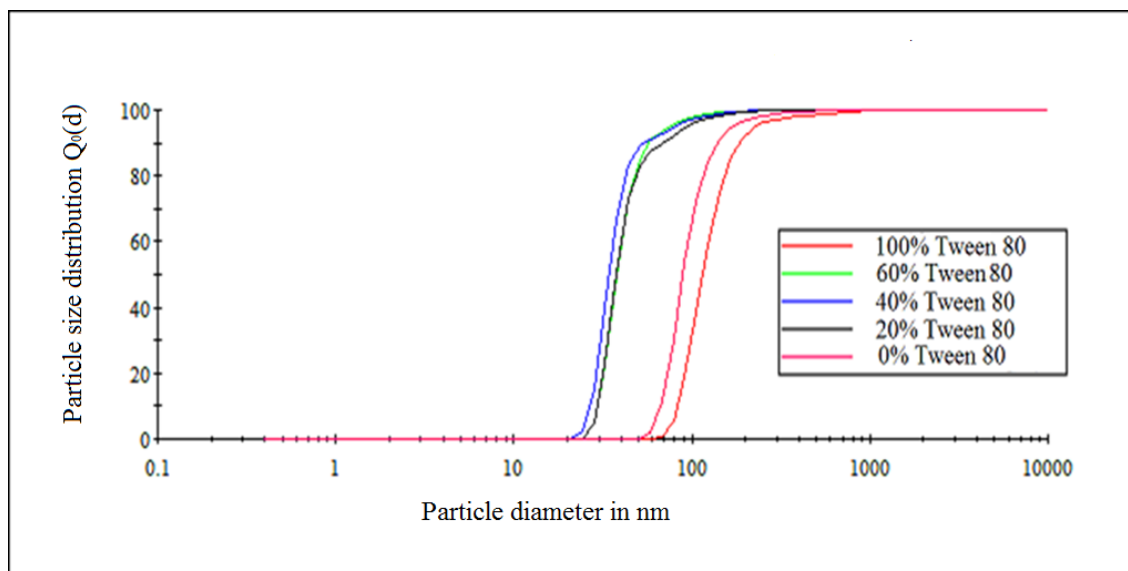


Figure 4.2: The particle size distribution  $Q_0(d)$  by different Tween® 80 / Span® 80 surfactant mixtures. The lines present the percentage of NPs under the corresponding size. Different ratios of Tween® 80 and Span® 80 were used to produce PBCA NPs. The particle size distributions of obtained PBCA NPs are shown in different colours (described in box).

The PDI values as presented in Figure 4.3 are in line with the published literature [111]. The surfactant mixtures composed of both Tween® 80 and Span® 80 were more suitable to produce PBCA NPs in a W/O mini-emulsion compared to pure Tween® 80 or Span® 80 surfactant. The smallest PDI value of  $0.193 \pm 0.023$  was obtained when 20 % Tween® 80 was in the surfactant mixture, as well as, the values of  $0.194 \pm 0.026$  and  $0.231 \pm 0.020$  corresponding to 40 % and 60 % of Tween® 80, respectively. In contrast, the PDI values were significantly higher if only Tween® 80 or Span® 80 was used in mini-emulsions, resulting in  $0.487 \pm 0.014$  for Tween® 80 and  $0.286 \pm 0.043$  for Span® 80.

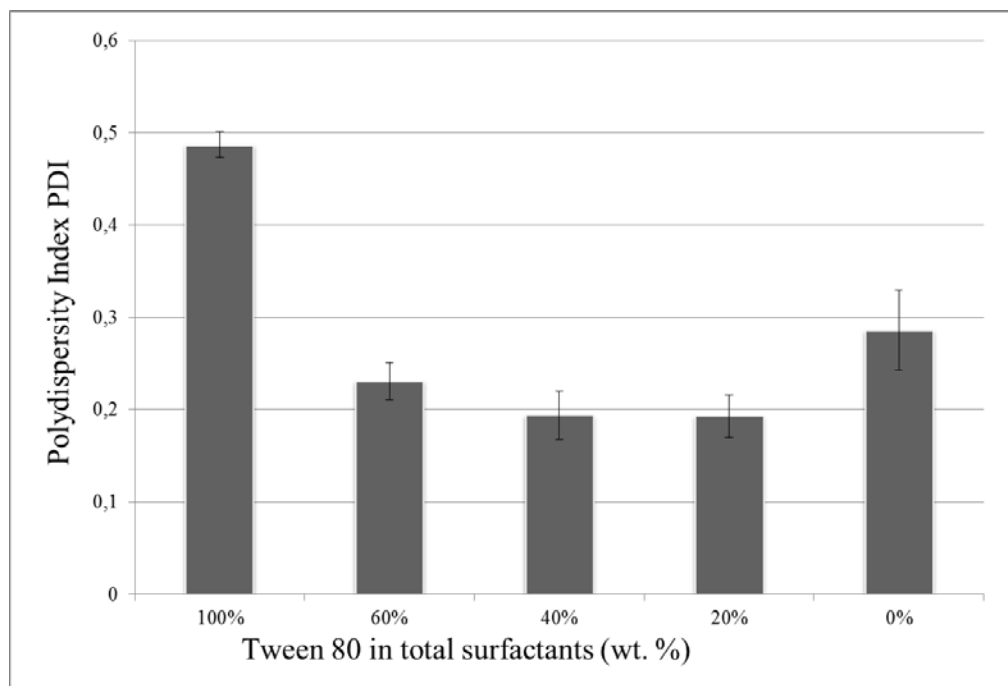


Figure 4.3: The polydispersity index (PDI) of NPs with the different types of Tween<sup>®</sup> 80 / Span<sup>®</sup> 80 surfactants mixtures. The PDI values indicates a similar trend with the results of NP diameter that the pure surfactant, Tween<sup>®</sup> 80 or Span<sup>®</sup> 80, is not suitable to produce fine PBCA NPs in a W/O mini-emulsion compared to the mixture of Tween<sup>®</sup> 80 and Span<sup>®</sup> 80.

However, the Zeta potential seems to suggest a different hypothesis: namely that only Span<sup>®</sup> 80 is enough to stabilize the NPs. The absolute value of the Zeta potential increases with the decrease of Tween<sup>®</sup> 80 concentration (see Figure 4.4.). The strongest Zeta potential of  $-27.1 \pm 0.8$  mV, which induces the electronic repulsion between NPs, was detected from the NPs with only Span<sup>®</sup> 80 in the surfactant. The NPs without Span<sup>®</sup> 80 in the surfactant are very instable, because the Zeta potential is only  $-6.8 \pm 0.8$  mV. According to the literature, a Zeta potential between  $\pm 30$  mV cannot offer an efficient electronic force to push the other NPs apart [112, 113], and the stability of PBCA NPs is mainly supported by a steric repulsion: the long tails of surfactants are sticking out of the particle surface (see Figure 2.6) and prevent particles from aggregating [111]. So, the Zeta potential is not the main factor to stabilize NPs, but, both Tween<sup>®</sup> 80 and Span<sup>®</sup> 80 have the ability to keep NP disperse. As a result, the mixture of 20 % Tween<sup>®</sup> 80 and 80 % Span<sup>®</sup> 80 is the optional choice to produce PBCA NPs containing a water core.



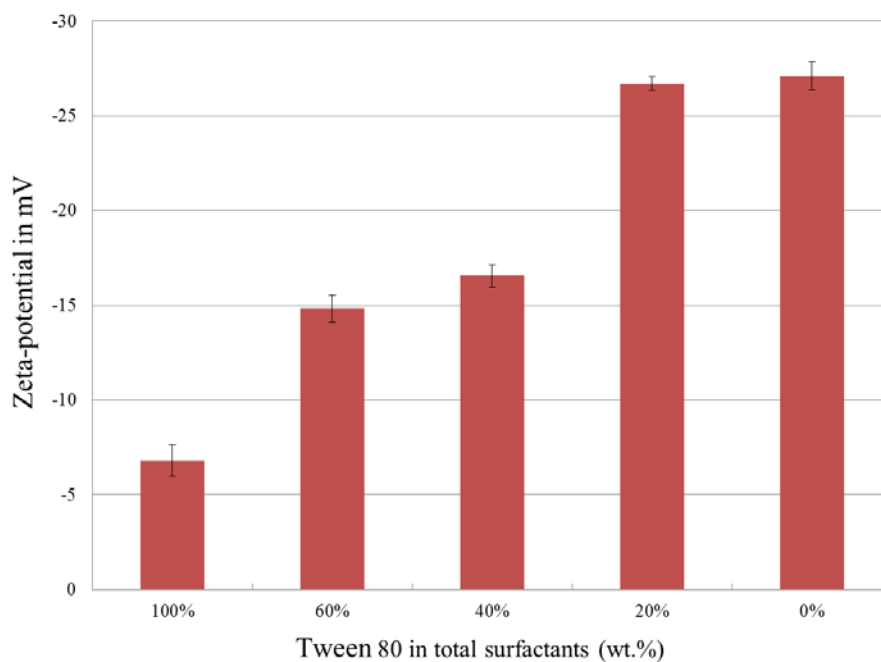


Figure 4.4: The Zeta potential in mV of the PBCA NPs with different types of Tween<sup>®</sup> 80 / Span<sup>®</sup> 80 surfactants mixtures. Span<sup>®</sup> 80 improves the value of Zeta potential of the PBCA NPs, while Tween<sup>®</sup> 80 induces more neutral charged NPs.

Table 4.2: The median diameter ( $d_{50,3}$ ), the Zeta potential and the PDI of the PBCA NPs produced with the different surfactants. The surfactants are the mixtures of Tween<sup>®</sup> 80 and Span<sup>®</sup> 80, as well as the pure Tween<sup>®</sup> 80 or Span<sup>®</sup> 80 surfactants.

Tween <sup>®</sup> 80 in surfactants	$d_{50,3}$ (nm) $\pm$ SD	Zeta potential (mV) $\pm$ SD	PDI $\pm$ SD
100 %	384.3 $\pm$ 78.2	-6.8 $\pm$ 0.8	0.487 $\pm$ 0.014
60 %	167.7 $\pm$ 20.2	-14.8 $\pm$ 0.7	0.231 $\pm$ 0.020
40 %	145.7 $\pm$ 4.3	-16.6 $\pm$ 0.6	0.194 $\pm$ 0.026
20 %	99.0 $\pm$ 2.3	-26.7 $\pm$ 0.4	0.193 $\pm$ 0.023
0 %	195.9 $\pm$ 16.5	-27.1 $\pm$ 0.8	0.286 $\pm$ 0.043

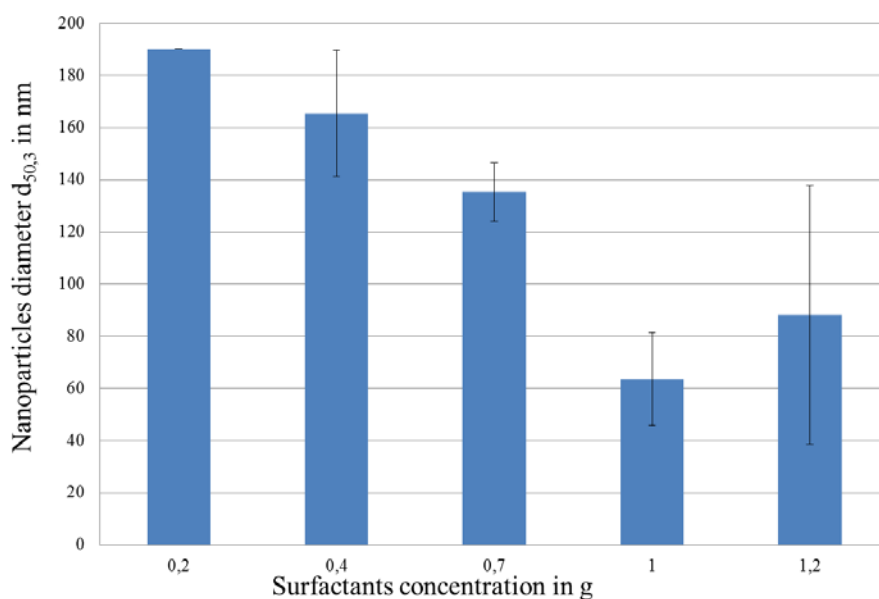


Figure 4.5: The median diameter ( $d_{50,3}$ ) of the NPs produced with different amounts of surfactants (Span<sup>®</sup> 80 : Tween<sup>®</sup> 80 is 4:1 in wt.) and a constant of 4.0 g of Miglyol 812N. A large amount of surfactant leads to a small  $d_{50,3}$  of NPs, which is not good for the loading efficiency.

Besides the types of the surfactants, the concentration of the surfactants (20 % of Tween<sup>®</sup> 80 and 80 % of Span<sup>®</sup> 80, w/w) in a W/O mini-emulsion was investigated with constants of Miglyol 812N (4.0 g), PBS (1.0 g), and the BCA monomer (50  $\mu$ L). As shown in Figure 4.5, the  $d_{50,3}$  of the NPs declines from 190.1  $\pm$ 0.1 nm to 88.2  $\pm$ 49.7 nm, when the amount of surfactants increases from 0.2 g to 1.2 g. But, the PDI values do not change significantly (see Figure 4.6). This means that the quantity of surfactants influences the  $d_{50,3}$  of NPs but not their dispersity. Considering the loading capability, large NPs are better to deliver siRNA into cells and tissue. In this case, the best combination of rather large size and low PDI value, 0.4 g of surfactants, which resulted in the  $d_{50,3}$  of 165.4  $\pm$ 24.2 nm and the PDI value of 0.231  $\pm$ 0.02, was used to produce PBCA NPs.

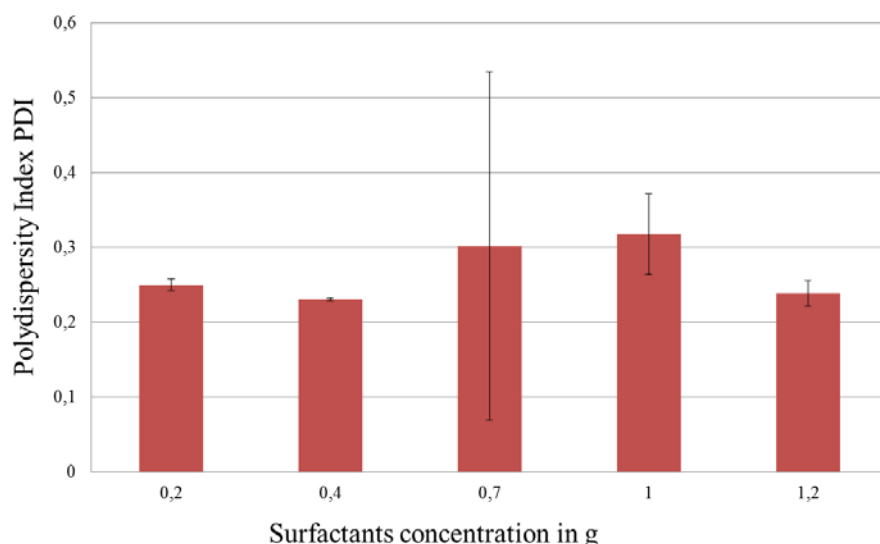


Figure 4.6: The polydispersity index (PDI) of NPs with different amounts of surfactants (Span® 80: Tween® 80 is 4:1 in weight) and a constant of 4.0 g of Miglyol 812N. There is not a direct relationship between the amounts of surfactants and the PDI values of NPs.

Table 4.3: The median diameters ( $d_{50,3}$ ) and the PDI values of the PBCA NPs which were produced in the W/O mini-emulsion containing 4.0 g of oil, 1.0 g of water, and 50  $\mu$ L of BCA monomer. The surfactant was composed of 20 % of Tween® 80 and 80 % of Span® 80.

weight of surfactants (g)	$d_{50,3}$ (nm) $\pm$ SD	PDI $\pm$ SD
0.2	190.1 $\pm$ 0.1	0.25 $\pm$ 0.008
0.4	165.4 $\pm$ 24.2	0.231 $\pm$ 0.002
0.7	135.3 $\pm$ 11.2	0.302 $\pm$ 0.232
1.0	63.6 $\pm$ 17.9	0.318 $\pm$ 0.054
1.2	88.2 $\pm$ 49.7	0.239 $\pm$ 0.017

#### 4.1.2. Water Phase

PBS was used as the water phase to produce PBCA NPs. The PBS, pH 7.4, offers OH<sup>-</sup> ions to initiate the polymerization reaction and maintains the stability of RNA. Therefore, the quantity of PBS not only affects the stability of NPs, but it also determines the loading efficiency. In this study, the different weights of PBS were added to prepare W/O mini-emulsions with constants of Miglyol 812N (4.0 g), surfactants (0.4 g), and BCA monomers (50 $\mu$ L). The results of the particles size distributions, the PDI values, and the Zeta potentials are shown in Table 4.4.

Table 4.4: The quantiles of the particle size distribution, the PDI, and the Zeta potential corresponding to the different weights of the PBS used in the mini-emulsion. The  $d_{10,3}$ ,  $d_{50,3}$ , and  $d_{90,3}$  mean that 10 % , 50 % , and 90 % of NPs have smaller diameters, respectively.

PBS in g	$d_{10,3} \pm SD$	$d_{50,3} \pm SD$	$d_{90,3} \pm SD$	PDI $\pm SD$	Zeta potential $\pm SD$
0.4	$35.9 \pm 10.1$	$66.6 \pm 9.5$	$267.2 \pm 25.1$	$0.253 \pm 0.004$	$-16.3 \pm 0.6$
1.0	$58.8 \pm 23.2$	$167.7 \pm 20.2$	$306.3 \pm 84.0$	$0.231 \pm 0.020$	$-14.8 \pm 0.7$
1.2	$59.9 \pm 25.0$	$135.0 \pm 20.6$	$366.7 \pm 15.7$	$0.192 \pm 0.013$	$-9.9 \pm 1.1$
1.6	$74.6 \pm 3.2$	$152.1 \pm 6.2$	$491.5 \pm 19.6$	$0.208 \pm 0.008$	$-12.0 \pm 1.0$

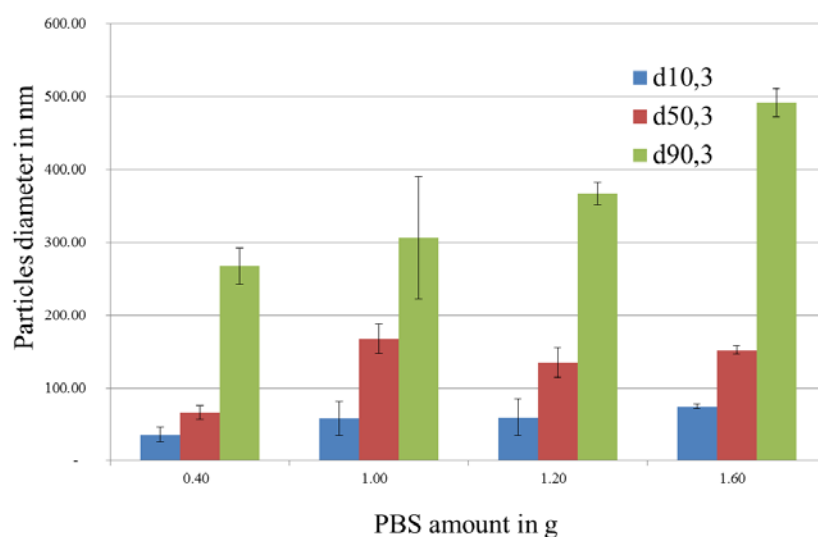


Figure 4.7: The quantiles of the particle size distribution presenting in  $d_{10,3}$ ,  $d_{50,3}$  and  $d_{90,3}$ . The  $d_{10,3}$ , which means 10 % of NPs have a smaller diameter, is represented by the blue bar.

In the same way,  $d_{50,3}$  and  $d_{90,3}$ , that 50 % and 90 % of NPs have smaller diameters, are presented as the red and green bars, respectively. The diameter of NPs increases when the more amount of PBS was used in the mini-emulsions.

The quantity of PBS affects NPs' diameters notably (see Figure 4.7). The diameter in  $d_{90,3}$  rises from  $267.2 \pm 25.1$  nm to  $491.5 \pm 19.6$  nm,  $d_{50,3}$  from  $66.0 \pm 9.6$  nm to  $152.1 \pm 6.2$  nm, and  $d_{10,3}$  from  $35.9 \pm 10.1$  nm to  $74.6 \pm 3.2$  nm, while the increase of the amount of PBS. However, when the weight of PBS is more than 1.0 g, both the  $d_{10,3}$  and  $d_{50,3}$  do not further increase, whereas  $d_{90,3}$  increases a lot. Great enlargement between  $152.1 \pm 6.2$  nm in  $d_{50,3}$  and  $491.5 \pm 19.6$  nm in  $d_{90,3}$  were observed when 1.6 g of PBS were used in the mini-emulsion. This may be caused by the aggregation of the large NPs. So, it is clear that too much PBS weakens the stability of NPs.

As shown in Figure 4.8, the low stability is in line with the fact that the value of the Zeta potential decreases from  $-16.3 \pm 0.6$  mV to  $-12.0 \pm 1.0$  mV. But, this effect is not sufficient to explain the low stability. As described in Section 4.1.1., the Zeta potential between  $\pm 30$  mV is not the main factor for the stability of NPs. So, taking into account the constant of surfactant (0.4 g in weight, containing 80 % of Span<sup>®</sup> 80 and 20 % of Tween<sup>®</sup> 80), it is assumed that the large amount of PBS in the mini-emulsion requires much more surfactants to stabilize the suspension.

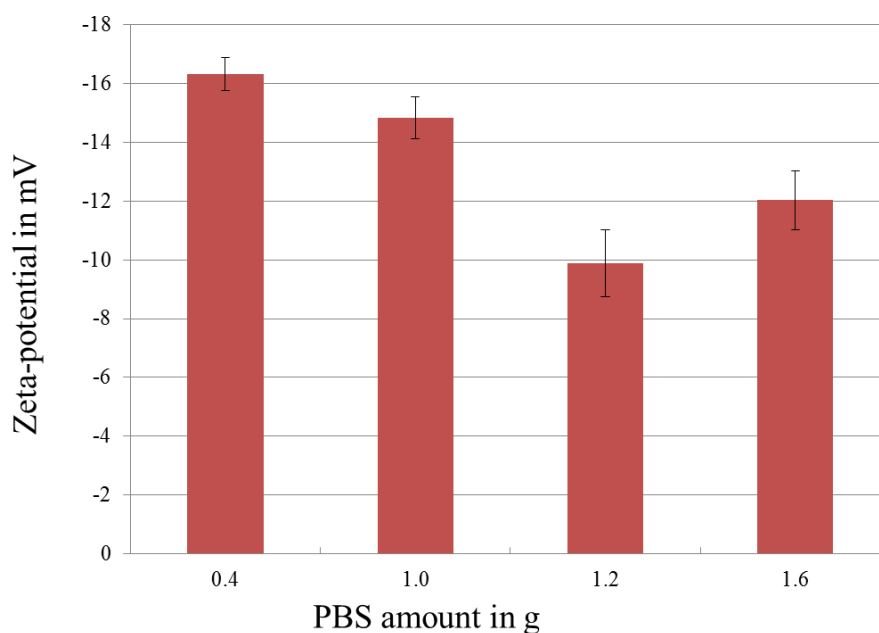


Figure 4.8: The Zeta potentials for different amounts of PBS. From 0.4 to 1.2 g, the increasing of water amount decreases the absolute value of the Zeta potential of NPs.

Regarding the PDI (see Figure 4.9), the quantity change of PBS does not show a significant difference. All the PDI values are under 0.3, which indicates a good dispersion of the NPs. Among them, the lowest PDI value is  $0.192 \pm 0.013$ , when 1.2 g of PBS was used. To consider about the loading efficiency, 1.2 g of PBS was chosen to produce the PBCA NPs loaded with siRNA, because a large amount of PBS is able to dilute plenty of siRNA.

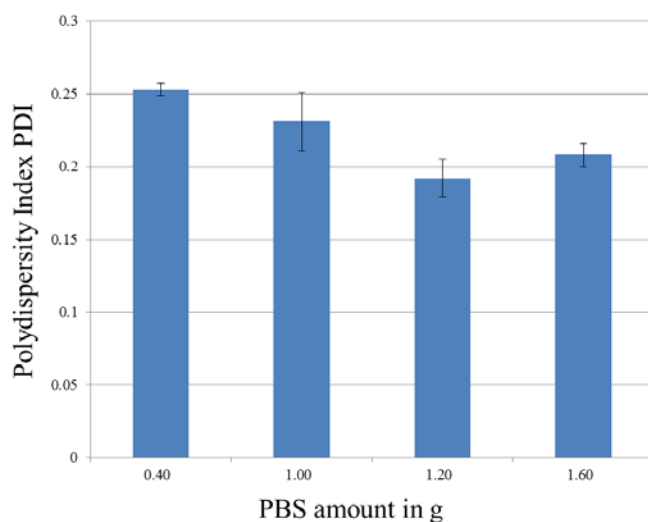


Figure 4.9: The polydispersity index (PDI) of PBCA NPs produced with the different quantities of PBS in the W/O mini-emulsion. All the PDI values are under 0.3, which indicate a good dispersity of NPs.

#### 4.1.3. *n*-Butyl-2-Cyanoacrylate

Different volumes of BCA monomer were used to produce PBCA NPs in the experiments. Their effects on the particle size distribution, the PDI, and the Zeta potential of these PBCA NPs were studied on the W/O mini-emulsions containing constants of Miglyol 812N (4.0 g), surfactants (0.4 g), and PBS (1.2 g). As demonstrated in Figure 4.10, no significant influence on the particle size and size distribution of PBCA NPs was observed with different quantities of PBCA monomer. The different volumes of BCA monomer, from 10  $\mu$ L to 100  $\mu$ L, were added into mini-emulsions, but as shown in Figure 4.10, the  $d_{50,3}$  of the PBCA NPs fluctuates between  $132.1 \pm 1.5$  nm and  $167.7 \pm 1.0$  nm. A similar result is shown in Figure 4.11, which demonstrates that PDI is not significantly influenced via varying the amounts of the BCA monomer. The reason is explained with the characteristics of the W/O mini-emulsion polymerization. As described in Section 2.4.2, the polymerization occurred on the interface between the water and the oil in the mini-emulsion. However, once formed, the shell of BCA polymer did no longer react with the BCA monomer, and also prevented the BCA monomer and the ions in the water core from touching each other. Then, the polymerization was terminated. As a consequence, there is not any significant influence of the amount of the BCA monomer on the particle size distribution (see Figure 4.11), and either is on the Zeta potentials, which is mainly affected by the surfactant (see Figure 4.12).

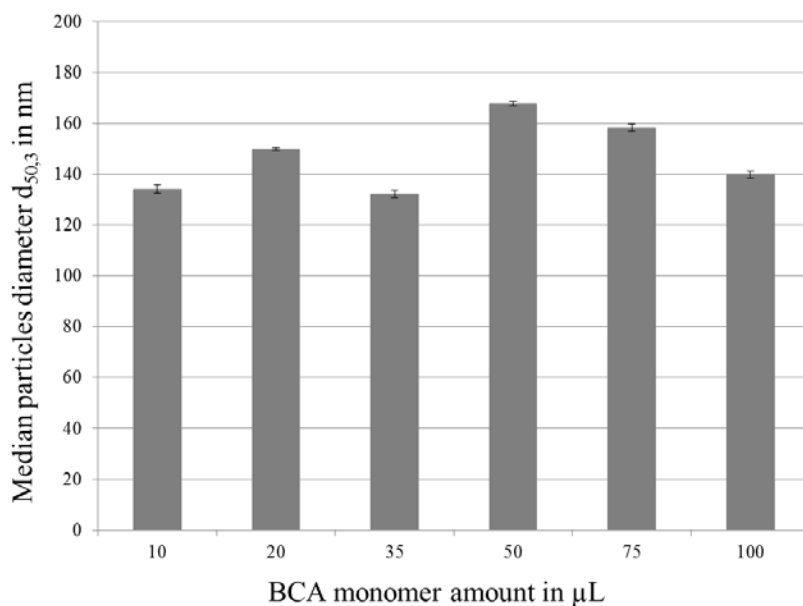


Figure 4.10: The median particles diameter ( $d_{50,3}$ ) in nm corresponding to the volume in  $\mu\text{L}$  of the BCA monomer. The figure shows that there was not a clear relationship between the volume of the BCA monomer and the median diameter ( $d_{50,3}$ ) of NPs.

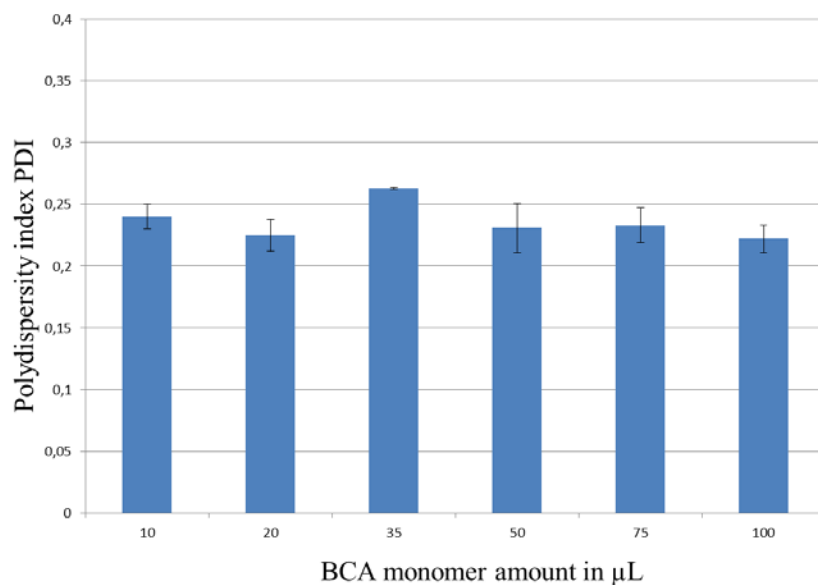


Figure 4.11: The polydispersity index (PDI) values of NPs with different volumes of the BCA monomer. No significant difference was observed when different volumes of the BCA monomer were used to produce the PBCA NPs.

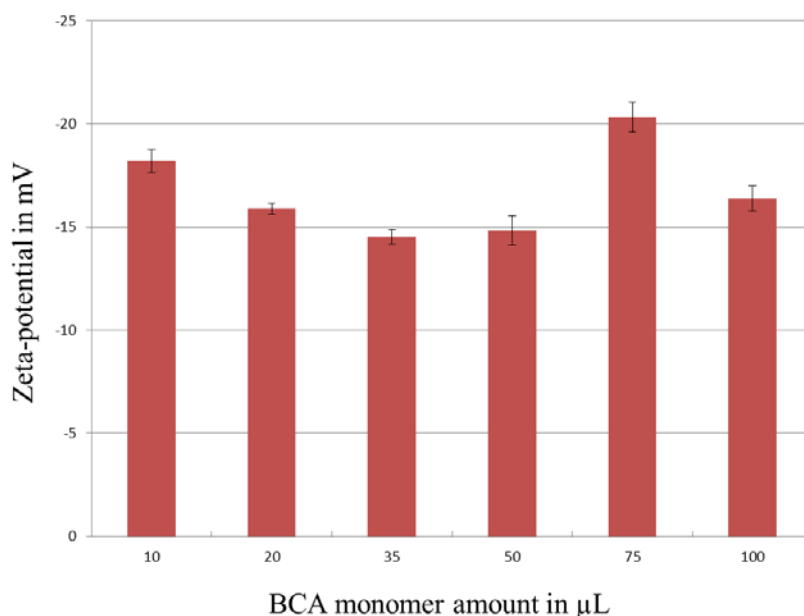


Figure 4.12: The Zeta potential of NPs corresponding to different volumes of the BCA monomer. The figure shows that there is not a clear relationship between the volume of the BCA monomer and the Zeta potential of NPs.

Table 4.5 The median particle diameters ( $d_{50,3}$ ), the PDI, and the Zeta potential of PBCA NPs by varying the amount of the BCA monomer in W/O mini-emulsion.

BCA amount in $\mu\text{L}$	Median diameter ( $d_{50,3}$ ) $\pm$ SD in nm	PDI $\pm$ SD	Zeta potential $\pm$ SD in mV
10	134.1 $\pm$ 1.6	0.240 $\pm$ 0.010	-18.2 $\pm$ 0.6
20	149.8 $\pm$ 0.5	0.225 $\pm$ 0.013	-15.9 $\pm$ 0.3
35	132.1 $\pm$ 1.5	0.263 $\pm$ 0.001	-14.5 $\pm$ 0.4
50	167.7 $\pm$ 1.0	0.231 $\pm$ 0.020	-14.8 $\pm$ 0.7
75	158.2 $\pm$ 1.3	0.233 $\pm$ 0.014	-20.3 $\pm$ 0.7
100	139.8 $\pm$ 1.3	0.222 $\pm$ 0.011	-16.4 $\pm$ 0.6

In summary, the PBCA NPs production in a W/O mini-emulsion was optimized by the mixture of the surfactants with a low HLB value, but not a pure surfactant (Tween<sup>®</sup> 80 or Span<sup>®</sup> 80). The Zeta potential of the NPs which were produced in the mini-emulsions containing the different types of surfactants was always weaker than  $\pm 30$  mV, which did not provide an efficient electronic repulsion. Therefore, the stability of NPs mainly depends on the molecular structure of the surfactants. From the results, the best option of the preparation of the PBCA NPs is to mix 20 % of Tween<sup>®</sup> 80 and 80 % of Span<sup>®</sup> 80 as surfactants and use



in the W/O mini-emulsion. The amount of surfactants determines the  $d_{50,3}$  of the PBCA NPs, but no influence on dispersity is found. As a consequence, 0.4 g of the mixed surfactant was chosen to produce the siRNA loaded PBCA NPs.

The weight of PBS, which is the water phase in the mini-emulsion, had an influence on the particle size distribution of PBCA NPs. A large amount of PBS led to a wide particle size distribution, and reduced the stability of NPs. But according to the requirement of the loading efficiency, a large amount of PBS is benefit to deliver a sufficient amount of siRNA into cells and tissues. So, as a compromise, 1.2 g of PBS was selected to produce the siRNA loaded PBCA NPs.

The effect of the BCA monomer on the particles size distribution, the PDI, and the Zeta potential was investigated. As the results show, no significant influences were detected, which is because of the localisation of the polymerization in the W/O mini-emulsion. So, to ensure an intact shell of BCA monomer, a large amount, 100  $\mu$ L, of BCA monomer is used for the production of the siRNA loaded PBCA NPs.

Using these parameters, the casp3 PBCA NPs were produced. They had an average diameter of 217.5 nm, the  $d_{50,3}$  of 195.2 nm, and the Zeta potential of -24.8 mV. The solid content was 0.199 g/mL.

Table 4.6: The quantiles of PBCA NPs size distribution ( $d_{10,0}$ ,  $d_{50,0}$ , and  $d_{90,0}$ ) for *in vitro* and *in vivo* experiments. These PBCA NPs were produced in the W/O mini-emulsion containing 4.0 g of Miglyol 812N, 1.2 g of PBS, 0.32 g of Span® 80, 0.08 g of Tween® 80. 100  $\mu$ L of BCA was used to initiate the polymerization reaction.

	Blank PBCA NPs	siRNA-PBCA NPs for <i>in vitro</i>	siRNA-PBCA NPs for <i>in vivo</i>
$d_{10,0}$	99.8	114.18	128.00
$d_{50,0}$	195.2	259.80	258.27
$d_{90,0}$	356.2	515.82	522.96

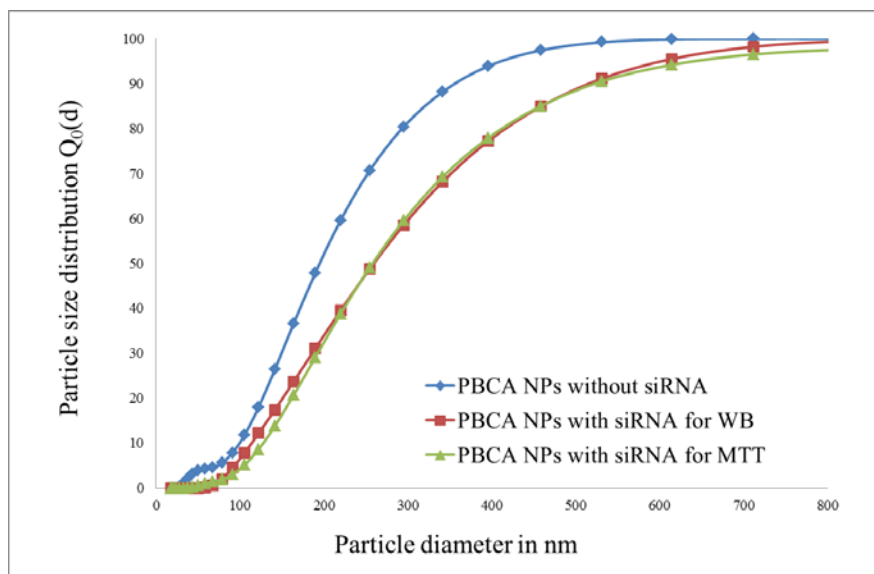


Figure 4.13: The particle size distribution in  $Q_0(d)$ . The lines represent the percentage of NPs under a certain size (nm) of diameter. The size distribution of the blank PBCA NPs (PBCA NPs without siRNA) is represented by the blue line. The distributions of casp3 PBCA NPs used for *in vitro* and *in vivo* applications are quite similar (in red and green line, respectively).

## 4.2. Cytotoxicity of PBCA NPs

As it is our aim to deliver the siRNA into the C6 cells, the cytotoxicity of PBCA NPs was studied by the MTT assay. The principle of the MTT assay has been introduced in Section 2.6. In the *in vitro* experiments, in addition, staurosporine (Stau), which is a type of alkaloid, was used to trigger apoptosis in C6 cells [114]. After 1 hr of the incubation with Stau, the cells were treated with the blank PBCA NPs and the casp3 PBCA NPs, respectively. After a duration of 48 hrs, the cell survival ratio of C6 cells was calculated depending on the absorption of each group according to the formula:

$$\text{Survival ratio} = \frac{\text{absorbance of NPs treated cells}}{\text{absorbance of PBS treated cells}}$$

The PBS is a non-toxic buffer for C6 cells, so the survival ratio of PBS treatment is defined as 100%. The same volume of PBCA NPs and PBS was added into different wells which contained a similar quantity of cells and the same volume of medium. After 48 hrs, the data from the C6 cells treated with PBS were used as the baseline to analyse the survival ratio of PBCA NPs treatment.

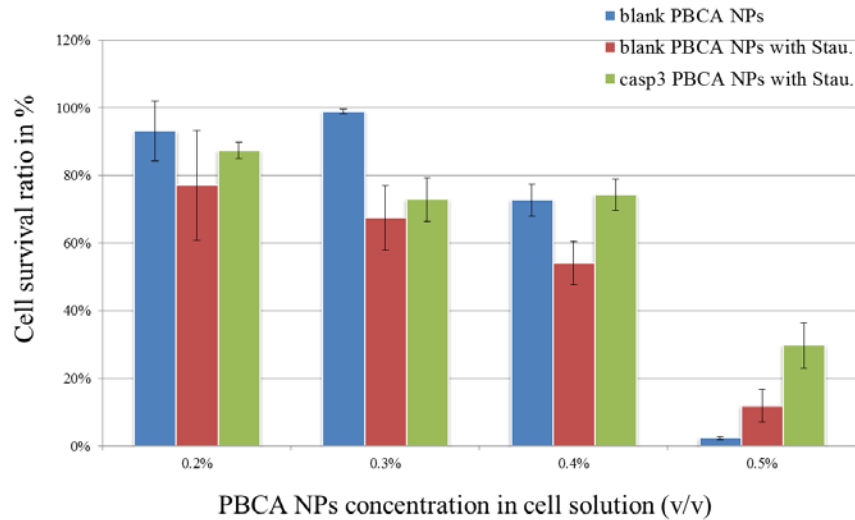


Figure 4.14: The C6 cell survival ratios (%) depend on the different concentrations of the PBCA NPs. Both blank and casp3 PBCA NPs were used to treat C6 cells. In some groups, Stau was added to trigger apoptosis of C6 cells.

From Figure 4.14, it can be concluded that the treatment with a high concentration of blank PBCA NPs as well as with Stau leads to the lower survival ratios than the treatment with siRNA-PBCA NPs. Compared to the incubation with blank PBCA NPs, the Stau has a clear deleterious effect, and much more cells died because of apoptosis. However, for the treatment of casp3 PBCA NPs with Stau, a larger number of living cells was observed as compared to the treatment of blank PBCA NPs with Stau. This indicates that caspase-3 siRNA indeed has an anti-apoptotic effect. Besides this, the proper concentration range of PBCA NPs for the cell test is determined by the median lethal dose (LD50), in which concentration more than 50 % of cells are alive. For the C6 cells, the LD50 is 0.4 % (v/v) of blank PBCA NPs in PBS (see Figure 4.14). With that concentration, at least 54.17 % of living cells survived when they were treated with blank PBCA NPs and Stau, as well as 72.80 % of living cells incubated with blank PBCA NPs and Stau, as well as 74.32 % of living cells incubated with casp3 PBCA NPs and Stau. However, a higher concentration of 0.5 % PBCA NPs killed most of the cells, and left only 2.34 % living cells after the incubation with blank PBCA NPs. Slight increases of the survival ratios of C6 cells were detected after the treatment of blank PBCA NPs with Stau (11.95 %) and casp3 PBCA NPs with Stau (29.77 %), but both of the ratios are far lower than 50 %. So, the concentrations under 0.4 % of PBCA NPs ensure sufficient number of living cell for RNA interference.

The differences in cell survival ratios between blank and casp3 PBCA NPs is worth to be analysed under the same Stau treatment. The aim of this study is to save more cells by casp3

PBCA NPs because of their anti-apoptosis effect. In Figure 4.15, more living cells were detected after the treatment with casp3 PBCA NPs rather than the treatment with blank PBCA NPs. Furthermore, the increasing differences from 10.34 % to 17.82 % were observed with the increasing concentrations of PBCA NPs from 0.2 % to 0.5 %. The peak of the differences, 20.15 %, appears at 0.4 % of the PBCA NPs treatment. This indicates an anti-apoptosis effect of casp3 PBCA NPs, which is caused by the caspase-3 siRNA in the NPs.

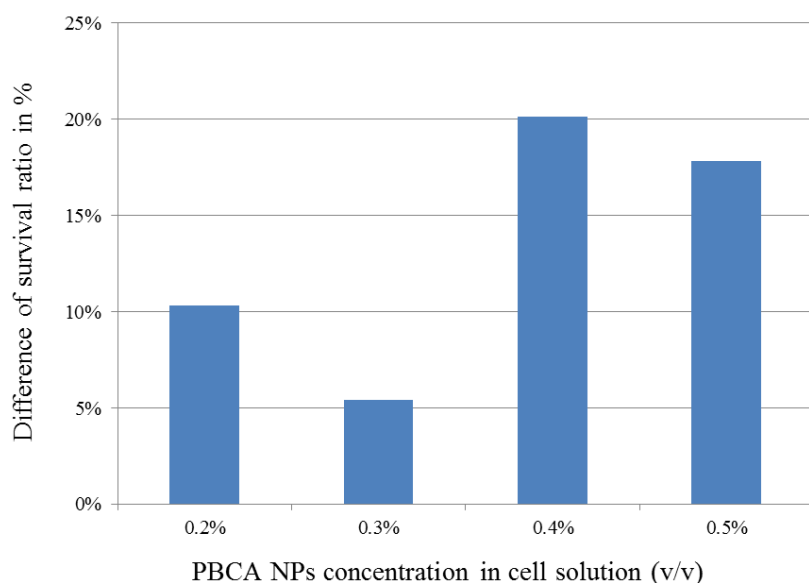


Figure 4.15: The differences of C6 cell survival ratios (%) between blank PBCA NPs and casp3 PBCA NPs treatments. All the groups were treated with the same volume of PBCA NPs, and were exposed to Stau. The survival ratios of the treatment with blank PBCA NPs are always lower than casp3 PBCA NPs. When a high concentration of blank PBCA NPs and casp3 PBCA NPs was used, a great difference of survival ratio was observed. This indicates that the casp3 PBCA NPs prevent C6 cells to dead in general.

In summary, the proper concentration range for the test in C6 cells is defined under 0.4 % of PBCA NPs as indicated by MTT test. Therefore, the decision is to apply these concentrations for RNA interference. Moreover, due to the function of caspase-3 siRNA, an anti-apoptosis effect was observed when using casp3 PBCA NPs. Comparing a variety of concentrations of PBCA NPs, it becomes clear that a high concentration of casp3 PBCA NPs saves more cells rather than blank PBCA NPs under the same treatment with Stau.

Table 4.7: The survival ratios of C6 cells after the treatments with blank PBCA NPs, blank PBCA NPs and Stau, and casp3 PBCA NPs and Stau of the concentrations of 0.2 %, 0.3 %, 0.4 %, and 0.5 %.

Treatment	NPs concentration			
	0.20 %	0.30 %	0.40 %	0.50 %
Blank PBCA NPs	93.13 %	98.96 %	72.80 %	2.35 %
Blank PBCA NPs with Stau	77.02 %	67.44 %	54.17 %	11.95 %
Casp3 PBCA NPs with Stau	87.36 %	72.86 %	74.32 %	29.77 %

### 4.3. Immunoblotting of Caspase-3 expression

The PBCA NPs used for the immunoblotting experiments were produced according to the optimized protocol, using 4.0 g of Miglyol 812N, 0.32 g of Span<sup>®</sup> 80, 0.08 g of Tween<sup>®</sup> 80, 1.2 g of PBS, and 100  $\mu$ L of BCA monomer. For the treatment of siRNA, 5 nmol of caspase-3 siRNA or negative siRNA were applied in PBS, respectively. After the re-dispersion of the PBCA NPs in water, the concentration of siRNA in PBCA NPs was 3.3  $\mu$ M, and the final concentration of siRNA applied in the cell solution was 6.6 nM, 9.9 nM, and 13.2 nM corresponding to 0.2 %, 0.3 %, and 0.4 % of PBCA NPs.

#### 4.3.1. Caspase-3 Silencing by siRNA-PBCA NPs

The PBCA NPs mediated caspase-3 siRNA silencing was investigated in the C6 cells. The method and theory have been described (see Section 2.7.). The caspase-3 siRNA used in the current study is designed to specifically knock down the caspase-3 protein expression in rats. The negative siRNA, which have no significant sequence similarity to mouse, rat, or human gene as a negative control, were loaded into PBCA NPs. The C6 cells were treated under the same conditions and schedule.

The silencing of caspase-3 gene was observed from the western blot results (see Figure 4.16). There are two layers of bands, an upper layer and a lower layer, which indicate caspase-3 and cleaved-caspase-3, respectively. Caspase-3, which is 32 kDa, participates in the initiation of apoptosis, after that, caspase-3 is cut into two pieces. One of them is the cleaved-caspase-3, which is 17 kDa and keeps the same epitopes of caspase-3 and is able to react with the caspase-3 antibody. Hence, the amount of cleaved-caspase-3 represents the degree of apoptosis in the cells. After 48 hrs of treatment, a lot of cells were dying (see Figure 4.16),

because the bands representing the cleaved-caspase-3 are much darker than caspase-3. This means that plenty of caspase-3 is activated and becomes cleaved-caspase-3. Meanwhile, the bands representing caspase-3 were detectable in both the groups which were treated with PBS and neg PBCA NPs respectively. However, the bands of caspase-3 are almost invisible after the treatment with casp3 PBCA NPs. This indicates that the expression of caspase-3 is blocked after the treatment with casp3 PBCA NPs, so less or no caspase-3 exists in the C6 cells. Furthermore, this demonstrates that the caspase-3 siRNA is delivered by PBCA NPs into C6 cells and silences their caspase-3 gene expression.

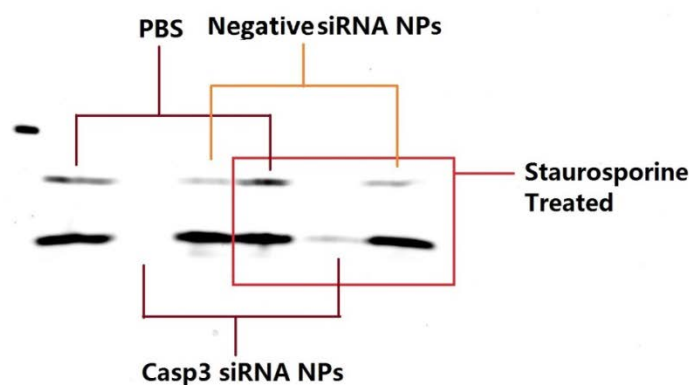


Figure 4.16: The western blot result of the caspase-3 expression in C6 cells. As marked in figure, the cells were treated with PBS, casp3 PBCA NPs, and neg PBCA NPs. All the treatments were repeated under the exposure of the Stau. Caspase-3 is visible in the upper layer of bands and the cleaved-caspase-3 is in the lower layer.

In addition, the treatment with Stau was included in the silencing experiment. The same amount of casp3 PBCA NPs, neg PBCA NPs, and PBS were added to C6 cells which were exposed to Stau previously, for the duration of 1 hr. The band from the cells treated with casp3 PBCA NPs appears very light in colour, most likely due to the Stau, which stimulates cell apoptosis; but once casp3 PBCA NPs were added, the caspase-3 expression was blocked immediately. As a result, only a light band of caspase-3 was detected (see Figure 4.16).

#### 4.3.2. siRNA Transfection by Different Delivery Strategies

To demonstrate the silencing function of casp3 PBCA NPs, the cells were treated by using casp3 PBCA NPs, blank PBCA NPs, mixture of blank PBCA NPs and caspase-3 siRNA (casp3 & NPs), caspase-3 siRNA-calcium particles, and PBS, respectively. Their extracts were subsequently detected by western blot analysis. The blank PBCA NPs, which have only PBS incorporated, could show the influence of PBCA NPs on caspase-3 expression in the C6 cells. Furthermore, Blank PBCA NPs were pre-mixed with caspase-3 siRNA and available to C6 cells, to investigate whether the loading methods affected the transfection or not. Moreover, the C6 cells treated with caspase-3 siRNA-calcium particles were also measured by using western blot analysis, which could reveal RNA interference targeting caspase-3 in the treatment without any PBCA NPs. Finally, the same volume of PBS was applied to identify the normal concentration of caspase-3 in C6 cells. The western blot results of these treatments are shown in Figure 4.17.

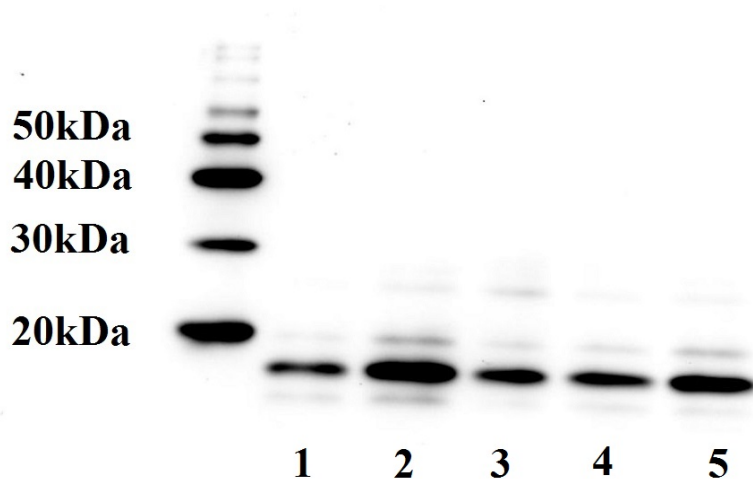


Figure 4.17: The blots of caspase-3. Each band presents the cleaved-caspase-3, which has 17 kDa. The treatments in lane 1 to 5 are 1) casp3 PBCA NPs, 2) blank PBCA NPs, 3) casp3 & NPs, 4) caspase-3 siRNA-calcium particles, and 5) PBS, respectively. All the cells were pre-treated by the same amount of Stau

The Figure 4.17 shows that only the cleaved-caspase-3 has been detected, which was caused by the Stau treatment, and most of the cells were in the apoptosis process, especially in the cells treated with blank PBCA NPs, which induced deleterious conditions for C6 cells.

Besides this, the  $\alpha$ -tubulin expression was imaged as a loading control, shown in Figure 4.18. The  $\alpha$ -tubulin, 55 kDa, is the basic unit of cell structure. Its quantity corresponds highly to the amount of C6 cells. Hence, it was used as the loading control to indicate the difference of the cell quantity in each group.

These blotting pictures were analysed by the ImageJ [120]. With this software, the images data is transformed to integrated optical density (IOD) values, which is determined by multiplying the pixel mean grey value of the area by the area of the region of the band. At first, the quantity correlation is calculated from  $\alpha$ -tubulin according to

$$\text{Correlation} = \frac{\text{IOD value for each group}}{\text{highest IOD value}}$$

The IOD values of caspase-3 blots were calculated by the corresponding correlations of the  $\alpha$ -tubulin (see Table 4.8), and shown in Figure 4.19. The treatment of casp3 PBCA NPs resulted in the lowest IOD value ( $1038.2 \pm 183.7$ ) as compared to blank PBCA NPs ( $3381.2 \pm 204.0$ ) and PBS ( $2171.4 \pm 247.1$ ). The cells after the treatment with casp3 PBCA NPs had only approximately half the amount of caspase-3 compared to the cells treated with PBS. This is evidence that the casp3 PBCA NPs silences the caspase-3 gene in C6 cells. Besides this, the treatment with blank PBCA NPs led to an extremely high amount of caspase-3 in C6 cells, which suggests that apoptosis is stimulated by the presence of PBCA NPs. On the other hand, the low concentration of caspase-3 demonstrates the reduction of the apoptotic cell death when cells were treated with casp3 PBCA NPs, although the cells were exposed to PBCA NPs as well. So, this confirmed that casp3 PBCA NPs have the ability to silence the caspase-3 gene.

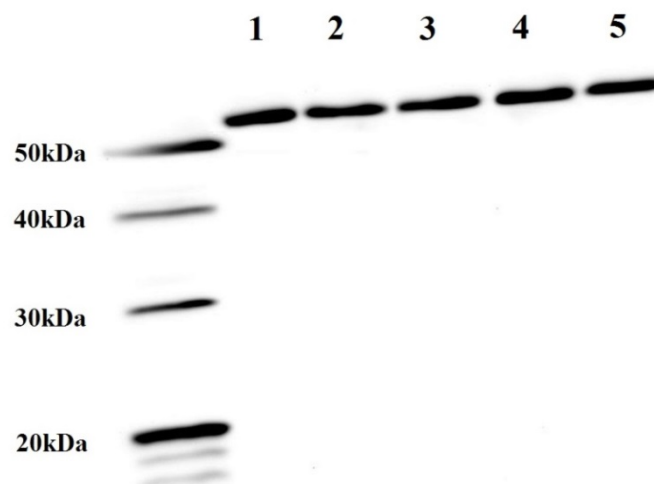


Figure 4.18: The bands presenting the 55 kDa  $\alpha$ -tubulin in C6 cells. This protein is used as the loading control to show the correlation between cell quantities under different treatment conditions. From lane 1 to 5, the following conditions were tested: 1) casp3 PBCA NPs, 2) blank PBCA NPs, 3) casp3 & NPs, 4) caspase-3 siRNA-calcium particles, and 5) PBS.



Table 4.8: The quantity correlations of C6 cells between each treatment. The correlation values are calculated according to the IOD value of the  $\alpha$ -tubulin in Figure 4.18, and used to correct the IOD value of caspase-3 in Figure 4.17.

Treatment	casp3 PBCA NPs	blank PBCA NPs	casp3 & NPs	caspase-3 siRNA	PBS
correlation	96.00 %	75.07 %	79.72 %	100.00 %	79.00 %

In addition, the treatment with casp3 & NPs, which had 13.2 nM of caspase-3 siRNA in the cell solution, reflects a down-regulation of caspase-3 expression. Its IOD value of caspase-3 is  $1310.4 \pm 479.7$ , which is lower than the value from the cells treated with PBS, but still higher than the cells treated with casp3 PBCA NPs. Due to the charge and surface activity of NPs, siRNA adhered onto the surface of NPs. When the cell membrane was penetrated by these NPs, the siRNA was transported into the cell as well. But, a large deviation of the IOD value was detected when repeating the treatment three times, which means that the adhesion of siRNA and NPs is not stable. Therefore, the adhesion method cannot guarantee a similar amount of siRNA being delivered in each transfection.

Moreover, the caspase-3 siRNA without any PBCA NPs was used to treat C6 cells. Normally, siRNA cannot go through the cell membrane. So, 2 mol/L  $\text{CaCl}_2$  in Tris-buffer were used to deliver the caspase-3 siRNA into the cells. At first, the siRNA was diluted in 1 mL of double distilled water, and then 12.5 % (v/v) of 2 mol/L  $\text{CaCl}_2$  in Tris-buffer were added, droplet-wise, into the siRNA solution. The final concentration of siRNA in the C6 cell solution was 13.2 nM. Because the reaction between calcium ion and phosphate group of siRNA, siRNA-Calcium particles were assembled and insoluble in water. These particles have the ability to adhere to the cell membrane and then penetrate it [115]. Similar IOD values of caspase-3 siRNA ( $1286.0 \pm 14.7$ ) and blank PBCA NPs mixed with caspase-3 siRNA ( $1310.4 \pm 479.7$ ) indicate a similar concentration of caspase-3 in C6 cells (see Figure 4.19). Considering the influence of PBCA NPs on C6 cells, the transport of PBCA NPs is more efficient than siRNA-calcium particles, because it reduced the toxic effect of PBCA NPs and limited the concentration of caspase-3 to a level similar to siRNA-Calcium particles. On the other hand, siRNA-calcium particles are much more stable than blank PBCA NPs mixed with caspase-3 siRNA because of the tiny deviation of the IOD values ( $1286.0 \pm 14.7$ ).

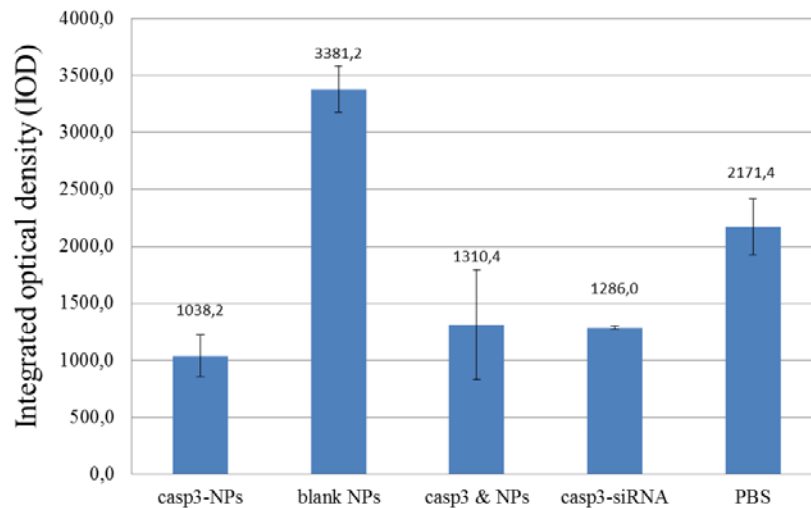


Figure 4.19: The integrated optic density (IOD) value of caspase-3 in C6 cells. Each column represents the IOD value from the cells treated with casp3 PBCA NPs, blank PBCA NPs, casp3 & NPs, caspase-3 siRNA-calcium particles as well as PBS, from left to right. All groups were pre-treated by Stau.

### 4.3.3. Transfection Efficiency of Caspase-3 siRNA-PBCA NPs

To investigate the transfection efficiency, varying concentrations of casp3 PBCA NPs were used to treat C6 cells. The same concentrations were used for the cells which were exposed to Stau. In Figure 4.20, the blots corresponding to the different concentrations of casp3 PBCA NPs was visualized. No signal was discovered at the position of 32 kDa, which indicates that most of caspase-3 is cleaved and the apoptosis process in these cells is activated completely. The Stau and PBCA NPs are the culprits causing the apoptosis, which has been described in Section 4.2. and 4.3.2. The cleaved-caspase-3, which is 17 kDa, was detected clearly by using western blot analysis. It also indicates that the apoptosis has taken place in these C6 cells. Besides that, from the western blot imaging, the cells treated with Stau (right 3 bands in Figure 4.20) produced less caspase-3 and cleaved-caspase-3, compared to the cells in which Stau was not present (lane 1 to 3 in Figure 4.20). But, considering the decomposition of proteins in the cells which treated with PBCA NPs and Stau, at the late stage of apoptosis, the peptides, which are obtained from the decomposition of protein, were still detectable by the BCA reagent, which is used to measure the concentration of total protein contents. But, these peptides are not available to the antibody. So, if the extract samples were diluted into the same concentration of protein, which was detected by using BCA reagent, it is reasonable that less amounts of caspase-3 are detected in the cells treated with Stau. Incidentally, the bands

which were visualized at the size position around 28 kDa are ignored as meaningless bands according to the manufacturer of the antibody.

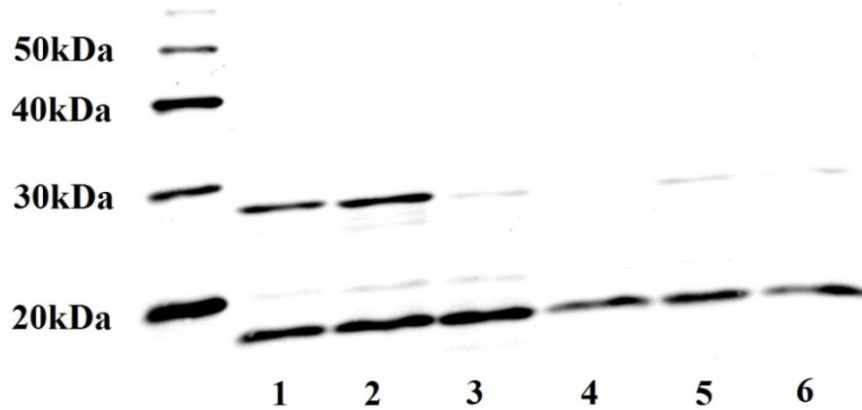


Figure 4.20: The blots of caspase-3 in C6 cells. The cells were treated with 0.4 %, 0.3 % and 0.2 % of casp3 PBCA NPs without Stau (lane 1 to 3) and with Stau (lane 4 to 6).

The degradation of proteins was confirmed by the  $\alpha$ -tubulin, as can be seen in Figure 4.21. As introduced in Section 4.3.2., the  $\alpha$ -tubulin is a basic unit of cytoskeleton. In Figure 4.21, the blots of  $\alpha$ -tubulin show the bands at the size position of 55 kDa. It can be distinguished by the naked eye that the blots from the cells treated with Stau (lane 4 to 6) are much lighter than from non-Stau treated cells (lane 1 to 3). Therefore, both the concentrations of the cleaved-caspase-3 (see Figure 4.20) and the  $\alpha$ -tubulin declined in the cells exposed to Stau. It demonstrates that the apoptosis induced protein degradation in C6 cells leads to a low concentration of these two kinds of target protein. But, the cells whose  $\alpha$ -tubulin is decomposed are considered as dead. Therefore, the living cells which still have  $\alpha$ -tubulin are worth to be analysed. Then, in order to reduce the influence of dead cells, the correlation values in Table 4.9 were used to correct the IOD values of blots of cleaved-caspase-3. Therefore, the quantities of cleaved-caspase-3 are able to be compared under the same baseline of living cells. The bands at 40 kDa are meaningless, which may come from the decomposition of  $\alpha$ -tubulin.

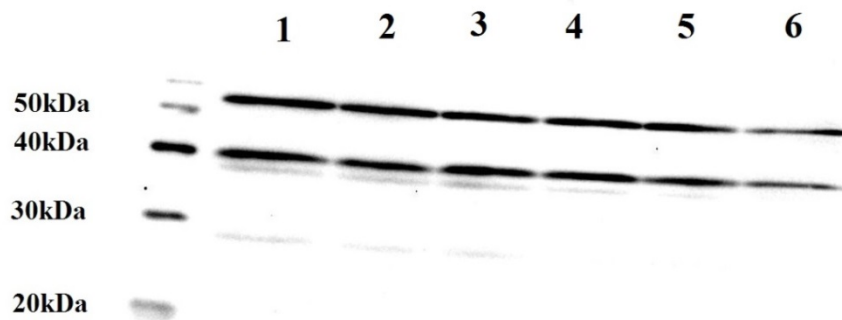


Figure 4.21: The bands present  $\alpha$ -tubulin, which is 55 kDa, in C6 cells. This protein is used as a loading control to show the correlation of cell quantities between each treatment. The cells were treated with 0.4 %, 0.3 % and 0.2 % of casp3 PBCA NPs without Stau (lane 1 to 3) and the same concentrations of casp3 PBCA NPs with Stau (lane 4 to 6).

The IOD values from the blots of cleaved-caspase-3 are shown in Figure 4.22. The main trend of the IOD is that their values increase with the decreasing concentrations of casp3 PBCA NPs. But, in the non-Stau treated cells, the IOD values do not increase when the concentration of PBCA NPs is 0.2 % (552.46) compared to the treatment with 0.3 % of PBCA NPs (658.39). It declares that the caspase-3 expression is influenced by the presence of the PBCA NPs. No more caspase-3 was produced in the cells treated with 0.3 % of PBCA NPs. However, this effect was overridden when Stau was applied. The IOD value from the cells treated with Stau achieves an extremely high value (1053.17) when 0.2 % of casp3 PBCA NPs have been used to treat the cells. An increasing trend from 222.78 to 1053.17 is revealed while the concentrations of casp3 PBCA NPs decrease from 0.4 % to 0.2 %. On the other hand, the IOD results indicate that the casp3 PBCA NPs are effective to RNA interference in C6 cells. The caspase-3 expression is blocked in the C6 cells treated with casp3 PBCA NPs, especially in 0.4 % of PBCA NPs.

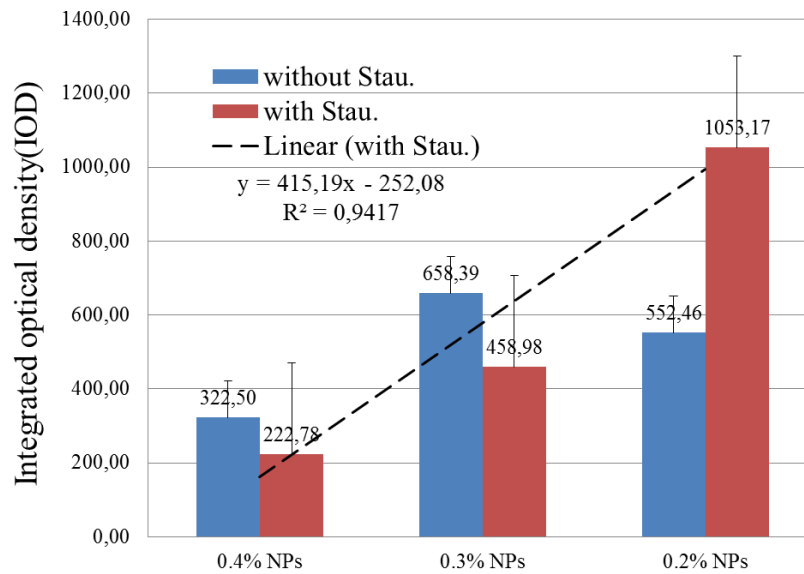


Figure 4.22 The integrated optic density (IOD) values of cleaved-caspase-3. The columns represent the IOD values from the cells treated with different concentrations of casp3 PBCA NPs with/without Stau. The line relation of the IOD values from the cells treated with varying concentrations of casp3 PBCA NPs and Stau is indicated by the dotted line.

Table 4.9: The quantities correlation of the C6 cells between the treatments of different concentrations of casp3 PBCA NPs. The correlation is determined by the IOD values of blots of  $\alpha$ -tubulin, and used to correct the IOD values of the blots of caspase-3.

Treatment	without Stau			with Stau		
	0.4 % NPs	0.3 % NPs	0.2 % NPs	0.4 % NPs	0.3 % NPs	0.2 % NPs
correlation	100.00 %	70.04 %	88.77 %	80.65 %	54.02 %	17.99 %

In summary, I was able to demonstrate the casp3 PBCA NPs-induced RNA interference using western blot analysis. The IOD values, which are evaluated by the ImageJ from the blots, demonstrate quantitatively the effects of different treatments in C6 cells. The caspase-3 siRNA and the negative siRNA were encapsulated, respectively, into the PBCA NPs to investigate the caspase-3 silencing. The block of caspase-3 was observed from the C6 cells treated with casp3 PBCA NPs. The delivery and silencing function of casp3 PBCA NPs has been confirmed comparing to the C6 cells treated with neg PBCA NPs.

The different delivery strategies, such as casp3 & NPs, caspase-3 siRNA-calcium particles, were compared to casp3 PBCA NPs, and blank PBCA NPs and PBS were used as control

treatments. All the treatments were performed in the presence of Stau. As a result, casp3 PBCA NPs have the best efficiency of RNA interference, which led to the lowest concentration of caspase-3 in C6 cells. The treatments of casp3 & NPs and caspase-3 siRNA-calcium particles showed similar amounts of caspase-3, which are, however, higher than the treatment of casp3 PBCA NPs, but lower than the treatment of PBS. The highest caspase-3 expression among these treatments was found in the cells treated with blank PBCA NPs, probably due to the cytotoxicity of PBCA NPs to C6 cells.

Finally, the transfection efficiency of casp3 PBCA NPs was studied by using different concentrations of PBCA NPs. A high concentration of casp3 PBCA NPs maintained caspase-3 at a low concentration in C6 cells, whether Stau was available or not. The concentration of caspase-3, however, did not increase when the concentration of casp3 PBCA NPs declined from 0.3 % to 0.2 %, which is probably due to the reduction of the NPs in C6 cells. In the presence of the Stau, though, the adverse effect of the NPs was negligible and an extremely high IOD value of caspase-3 blotting was obtained at the lowest concentration (0.2 %, v/v) of casp3 PBCA NPs.

#### **4.4. Immunofluorescence of Retina**

The *in vivo* research of casp3 PBCA NPs was performed using the immunofluorescence technique. The paraffin sections were used for the location and the semi-quantitative detection of caspase-3 in the rat retina. In the experiment, an ONC surgery was applied on each animal to trigger a damage-induced apoptosis in its retina. After that, caspase-3 in the retina was detected by the caspase-3 primary antibody and the Alexa Fluor<sup>®</sup> 647 conjugate secondary antibody. In parallel, the Hoechst 33342, which stained nuclei, illustrated the location of retinal cells. The PBCA NPs used *in vivo* were produced in the W/O mini-emulsion containing 4.0 g of oil, 0.32 g of Span<sup>®</sup> 80, 0.08 g of Tween<sup>®</sup> 80, and 1.2 g of PBS. 100  $\mu$ L of BCA monomer was added in the mini-emulsion to initiate the polymerization reaction. For the treatments with siRNA-PBCA NPs, 5 nmol caspase-3 siRNA or negative siRNA was diluted in PBS and then loaded into the PBCA NPs. The concentration of these siRNA in the PBCA NPs was 3.3  $\mu$ M. 3  $\mu$ L of each type of PBCA NPs was injected intravitreally in all the rat eyes.

##### **4.4.1. Caspase-3 siRNA-PBCA NPs**

The aim of this study is to silence caspase-3 expression in the retina of a rat. Therefore, a negative or weak detectable signal was expected in respective experiments. In order to understand the results easily, an imaging of caspase-3 from post-ONC retina is first shown (see Figure 4.23). Caspase-3 is depicted in red colour after immunohistological staining. As described in Section 2.10., a retina is subdivided in the following layers: an inner plexiform layer, an inner nuclear layer, an outer plexiform layer, an outer nuclear layer, and an outer & inner segment layer. From the Figure 4.23, the fluorescent signal appeared mainly in the outer plexiform layer and the outer & inner segment layer, but rarely in the area of both the nuclei layers. The outer & inner segment layer is full of the cytoplasm from rod and cone cells. It is reasonable to find a lot of caspase-3 in this layer. But normally, a healthy cell maintains its caspase-3 in an extremely low amount, which is hardly observed via immunofluorescence. Therefore, the discovery of caspase-3 in the cytoplasm of rods and cones indicates a relatively high ratio of cells which are at risk of undergoing apoptosis. For the same reason, outer plexiform layer, which is consisted of neuronal synapses, had more caspase-3 than other layers of this retina.

The Hoechst 33342 labelling of the retina is also shown in Figure 4.23. By the staining, the inner nuclear layer and outer nuclear layer can be recognized easily. A merged figure which combines the signal of caspase-3 and Hoechst 33342 is also presented in Figure 4.23. In the merged picture, the blue circles indicate the nuclei of cells, which were stained by Hoechst 33342. There are two layers of blue circles in the figure: a wide layer presenting the nuclei of rod and cone cells, which are very densely packed and defined as the outer nuclear layer; and the other layer presenting the inner nuclear layer, where is the nuclei of horizontal cells, bipolar cells, and amacrine cells. So, the layer with red dots, the signal of caspase-3, between the outer and inner nuclear layer is recognized as the outer plexiform layer, and the other red layer posterior to the outer nuclear layer is outer & inner segment layer.

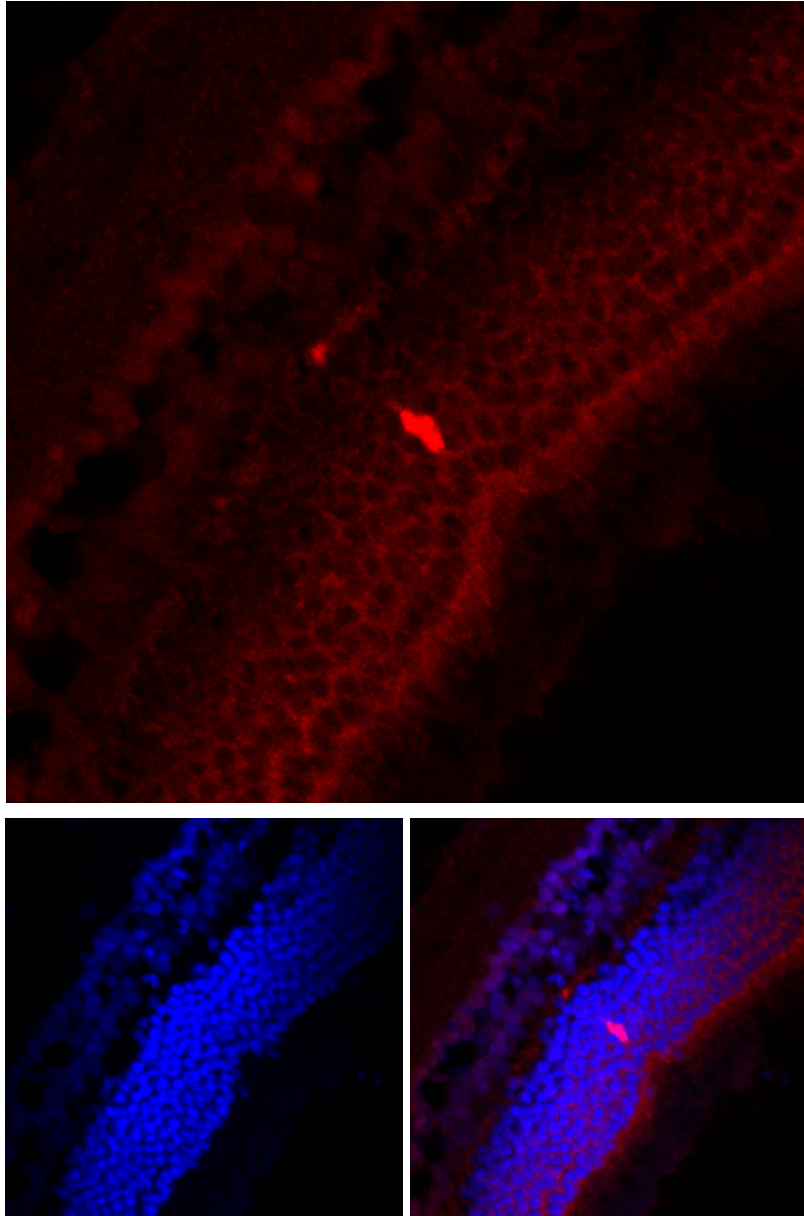


Figure 4.23: The ONC retina treated with PBS. The signal from caspase-3 was labelled in red, and Hoechst 33342 in blue in a cross-section of the retina.

The casp3 PBCA NPs were injected into vitreous body of an eye to prevent apoptosis in the injured retina. Compared the red dots in the respective image (see Figure 4.24) with the control treatment in Figure 4.23, the signal of caspase-3 was quite weak after the treatment of casp3 PBCA NPs. So, an assumption can be made that apoptosis is initiated in the retina after ONC but restricted by casp3 PBCA NPs. In order to demonstrate this assumption, some comparative experiments are participated.



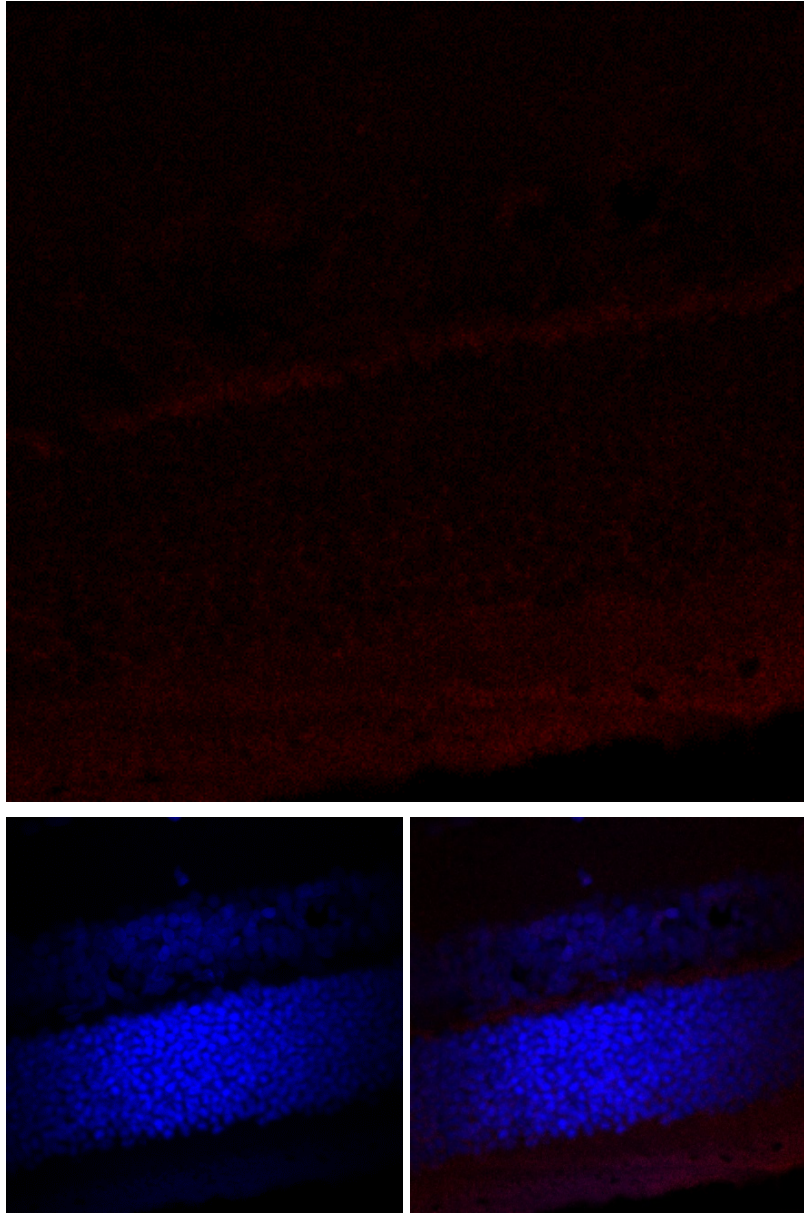


Figure 4.24: The retina treated with casp3 PBCA NPs after ONC. The signal of caspase-3 is labelled in red, and nuclei staining with Hoechst 33342 in blue. In the picture, the signal of caspase-3 is quite difficult to be detected. It indicates that the caspase-3 expression is shut down by casp3 PBCA NPs, although ONC triggers apoptosis in the retina.

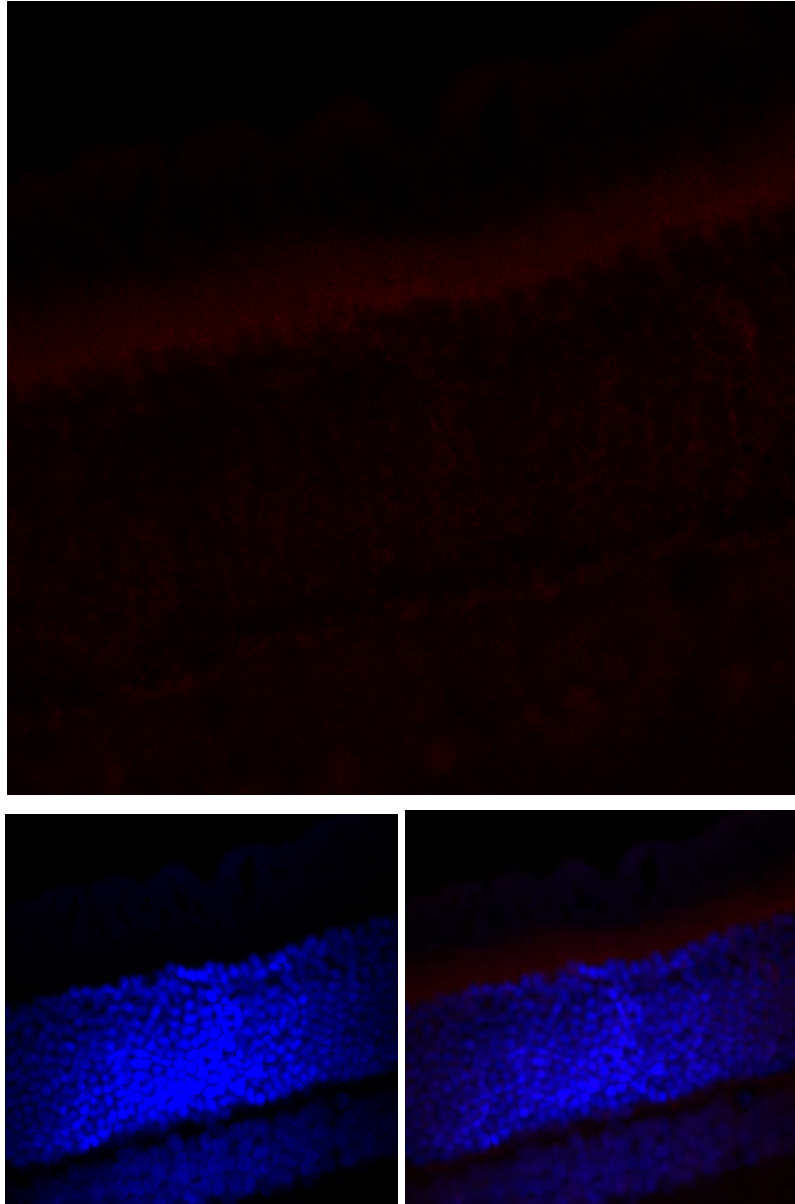


Figure: 4.25: Normal retina, non-ONC retina treated with PBS. The signal of caspase-3 is labelled in red, and nuclei stained with Hoechst 33342 in blue. No ONC surgery and only PBS was injected. The red dots in the picture represent a normal concentration of caspase-3 in a naive retina.

In order to demonstrate the effect of the casp3 PBCA NPs, the retina tissues from rats without lesion were stained with the same method as a baseline, and the respective immunofluorescent images are shown in Figure 4.25. The same volume of PBS as *in verum* experiments was injected into vitreous, and no ONC performed. So, this retina represents the naive conditions which allow the investigation of caspase-3 in a normal retina tissue. As the figure shows, the signal of caspase-3 was very weak. Only a few red dots can be found in the outer & inner segment layer. So, it points out that the caspase-3 protein expression is very low in a healthy

retina tissue. Compared to Figure 4.23, the signal of caspase-3 is quite weak, which indicates a lower concentration of caspase-3 in the healthy retina tissue than in the damaged retina tissue.

#### **4.4.2. Control Treatments**

The neg PBCA NPs, which were one of the control treatments, were also applied to transfect the cells in the retina. The Figure 4.26 reveals that caspase-3 is detected not only in the outer & inner segment layer, but also surrounding nuclei in the outer and inner nuclear layer. Different from the retina treated with casp3 PBCA NPs, the signal of caspase-3 was very prominent in the retinal cells after the injection of neg PBCA NPs. It means that a lot of caspase-3 is produced in this retina, but the neg PBCA NPs cannot block it. Then, a substantial cell death can be expected. In other words, this control treatment is evidence that the caspase-3 siRNA in the PBCA NPs is the essential factor of this nanocarrier system to silence the caspase-3 expression in the retinal cells of the rat.

The influence of PBCA NPs on the retina tissue was also studied. The blank PBCA NPs were used to treat eyes which had ONC. The influence on the retina is shown in Figure 4.27. Compared to Figure 4.26, which reveals the function of neg PBCA NPs, no significant difference was found. The signal of caspase-3 was also widely distributed in the retina. It confirms that blank PBCA NPs do not have the ability to knock down caspase-3 gene.

To investigate whether the PBCA NPs were necessary for the transfection of the retinal cells, the caspase-3 siRNA-calcium particles were injected into the vitreous body immediately after the standard process of ONC. The result is shown in Figure 4.28. Caspase-3 was detectable in the entire retina tissue. Similar to the treatments with neg PBCA NPs and blank PBCA NPs, the signal of caspase-3 indicates a failure of RNA interference. So, it means that the caspase-3 expression is blocked by only caspase-3 siRNA. In summary, the PBCA NPs are useful nanocarriers to achieve RNA interference *in vivo*.

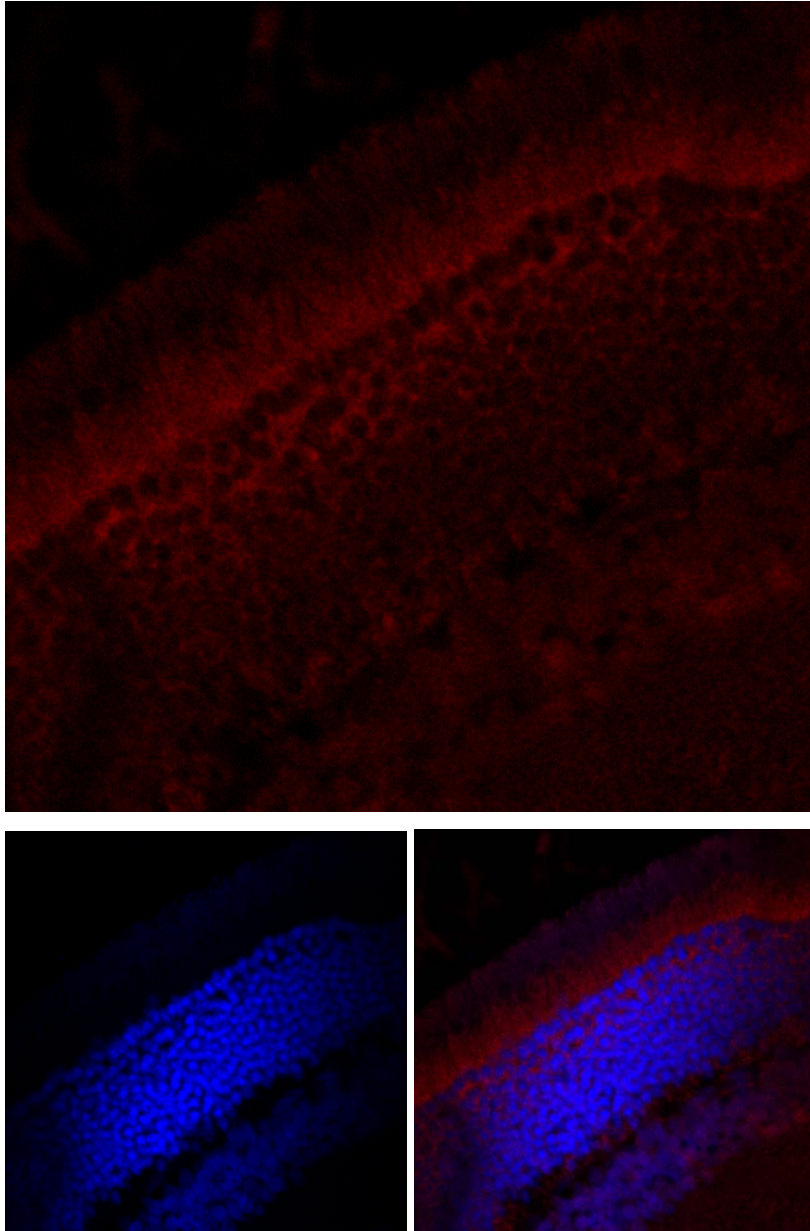


Figure 4.26: The retina treated with neg PBCA NPs after ONC. The signal of caspase-3 is labelled in red, and nuclei stained with Hoechst 33342 in blue. The figure reveals that a lot of caspase-3 is produced in the retina, but neg PBCA NPs cannot block the caspase-3 protein expression.

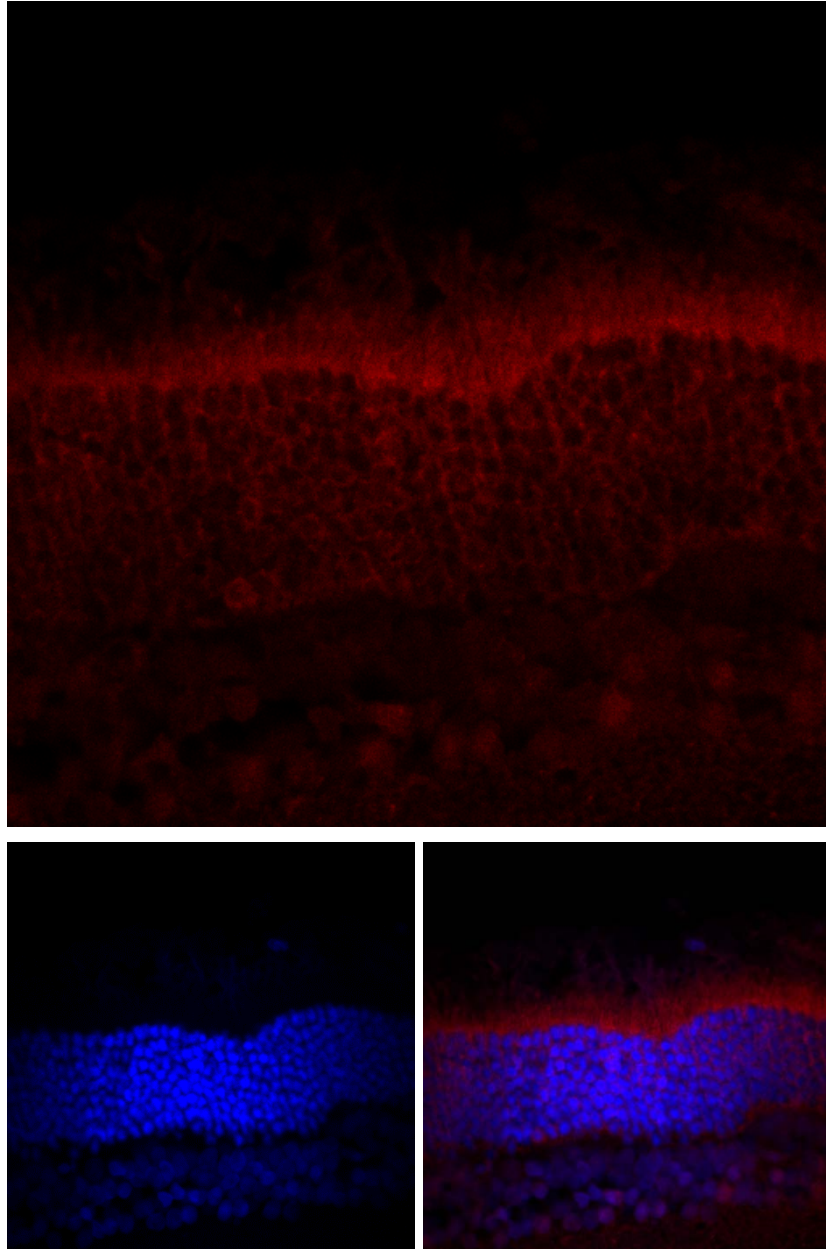


Figure 4.27: The retina treated with blank PBCA NPs after ONC. The signal of caspase-3 is labelled in red, and nuclei stained with Hoechst 33342 in blue. The signal of caspase-3 is widely distributed in the entire retina. It means that the blank PBCA NPs have no influence on knocking down the caspase-3 gene.

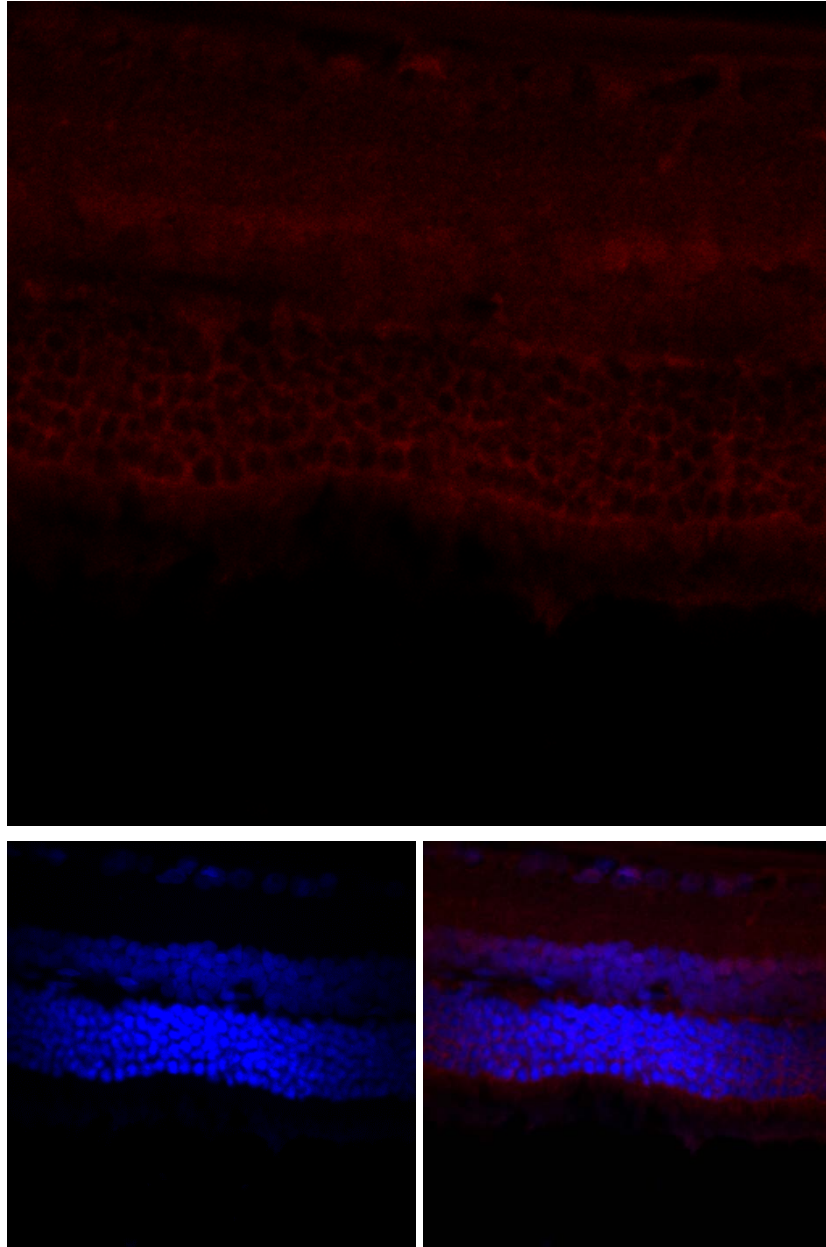


Figure 4.28: The retina treated with caspase-3 siRNA-calcium particles after ONC. The signal of caspase-3 is labelled in red, and nuclei stained with Hoechst 33342 in blue. Caspase-3 is detected in the entire retina tissue. It indicates a failure of transfection by calcium phosphate method for the retina. The PBCA NPs are necessary to complete RNA interference.

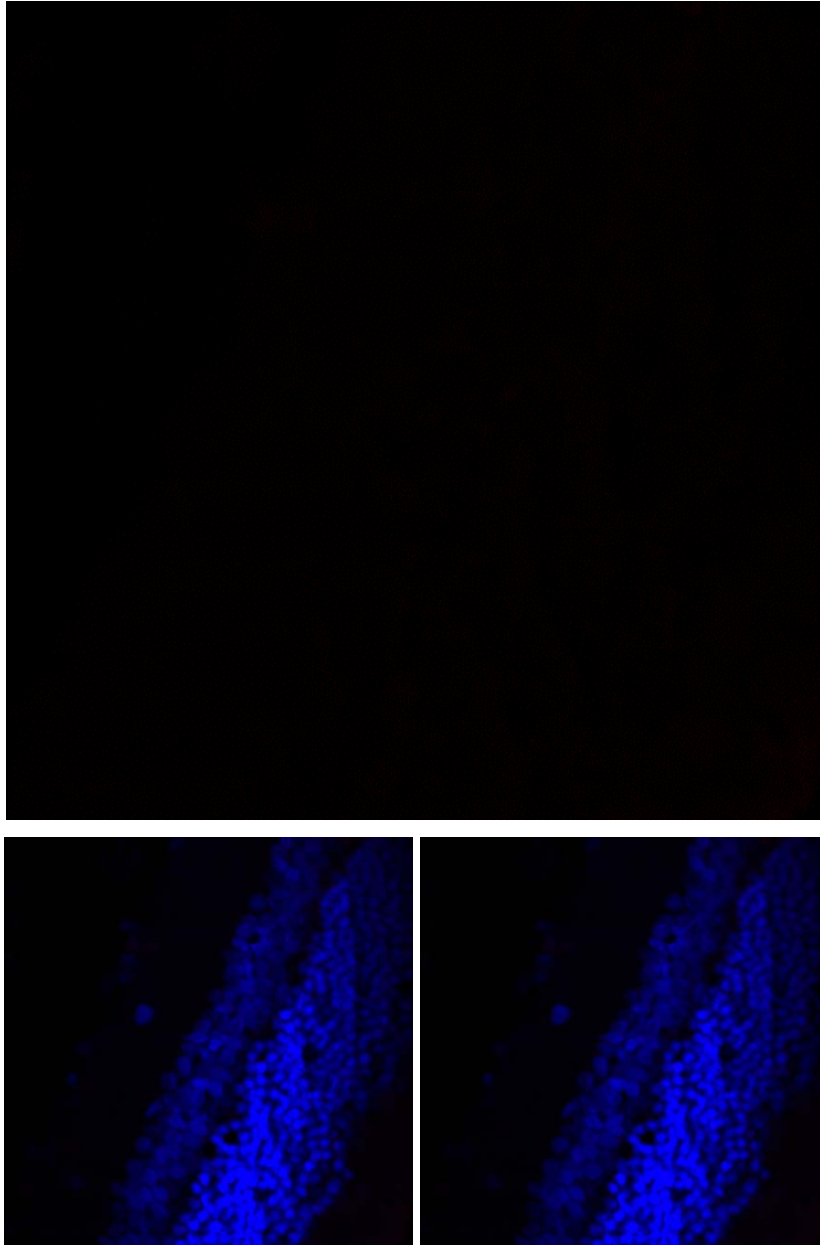


Figure 4.29: the negative control images of the retina. No caspase-3 antibody was used. Only the Alexa Fluor<sup>®</sup> 647 conjugate secondary antibody was used in this figure. It excludes the possibility of a false positive signal which is caused by a direct binding of secondary antibody and retina.

In the immunofluorescent detection, caspase-3 was firstly connected to the caspase-3 primary antibody. Then, the primary antibody was labelled by Alexa Fluor<sup>®</sup> 647 conjugate secondary antibody. If any epitope could react with the secondary antibody directly, a false positive signal would disturb the detection of the real signal. So, a control imaging, which had only the secondary antibody, was made to exclude the false positive signal. As a result, no signal is seen in Figure 4.29. It means that the secondary antibody does not bind unspecifically to the

retina. So, the signal of caspase-3 observed above reflects the real distribution of caspase-3 in the retinae.

#### **4.4.3. Mean IOD Analysis**

Like the western blot analysis, a quantitative analysis of the signal gives more reliable results. So, it is necessary to transform the image data to the IOD values. The mean IOD represents the average IOD per unit of area in the picture. For the signal of caspase-3, the IOD is an evaluation value of the fluorescent intensity. Therefore, a semi-quantitative result is presented in Figure 4.30. From this picture, the effect of ONC on caspase-3 expression is confirmed by the high values of IOD representing a high concentration of caspase-3 in the retina. The retina which suffered from the ONC and the PBS injection had a mean IOD value of 449.12, which is much higher than the value of 161.82 from the normal retina. So, ONC surgery initiates the apoptosis process in the retina. As a consequence, a lot of caspase-3 was detected by immunofluorescence in the cytoplasm of retinal cells. This effect was also found in the ONC retinae which were treated by caspase-3 siRNA, neg PBCA NPs, and blank PBCA NPs. Their mean IOD values reach 505.42, 429.51, and 485.21 respectively.

But, a significant decrease regarding the mean IOD values resulted from the analysis of the retina which was treated by casp3 PBCA NPs after ONC surgery. Figure 4.30 shows an IOD value of 204.17, which is very close to the IOD value of 161.82 from normal retina tissue. In other words, a low concentration of caspase-3 was found in the retina treated with casp3 PBCA NPs after ONC, and this concentration almost meets the normal concentration of caspase-3 in a healthy retina. So, it is demonstrated that the casp3 PBCA NPs transfect the cells in the retina and silence the caspase-3 gene expression. The relevance of PBCA NPs for the RNA delivery is also demonstrated by the fact that an injection of only caspase-3 siRNA cannot reduce the expression of caspase-3. The influence of PBCA NPs on retinal cells are also evidenced by the poor effect of the blank PBCA NPs and neg PBCA NPs.



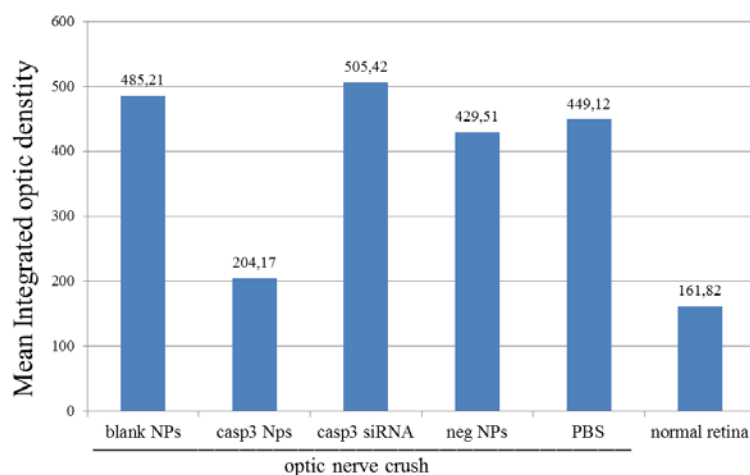


Figure 4.30: The mean integrated optic density (IOD) from the figures of immunofluorescence. The columns represent the mean IOD values of caspase-3. The lowest IOD value is found in the normal retina, which did not suffer from ONC and was treated with PBS. A down-regulation of the caspase-3 expression in the post-ONC retina was observed after the treatment with the casp3 PBCA NPs (casp3 NPs in figure).

In summary, the caspase-3 gene was silenced by casp3 PBCA NPs *in vivo*. First, the ONC surgery was performed on each animal to trigger apoptosis in the retina. Then, the rats were intravitreally injected with casp3 PBCA NPs. Finally, the caspase-3 silencing was confirmed by using the immunofluorescence imaging. The concentration of caspase-3 in the retina with ONC almost returned to the normal level of a healthy retina after the treatment with casp3 PBCA NPs. In contrast, any of blank PBCA NPs, caspase-3 siRNA, and neg PBCA NPs cannot knock down the caspase-3 expression in any rat retina.

#### 4.5. *In Vivo* Confocal Neuroimaging of PBCA NPs

For further applications of the nanoparticulate carrier systems, their ability to cross the blood-brain barrier is an important point to consider. Therefore, first experiments were performed to test in principle whether the NPs used in this project were able to cross the blood-brain barrier. To this end, the blood-retinal barrier was used as a model, and the blood-retinal barrier passage with PBCA NPs was demonstrated in rats after *i.v.* injection. The blood-retinal barrier, which has the highly similar functions as the blood brain-barrier, is a natural obstacle for CNS treatment. To test the potential of PBCA NPs to deliver compounds into the brain, the rhodamine 123 labelled PBCA NPs, which were produced according to the same protocol described in Section 3.1., were intravenously injected in the tail vein of a rat. An *in vivo* confocal neuroimaging technique was used to track the PBCA NPs in the retina.

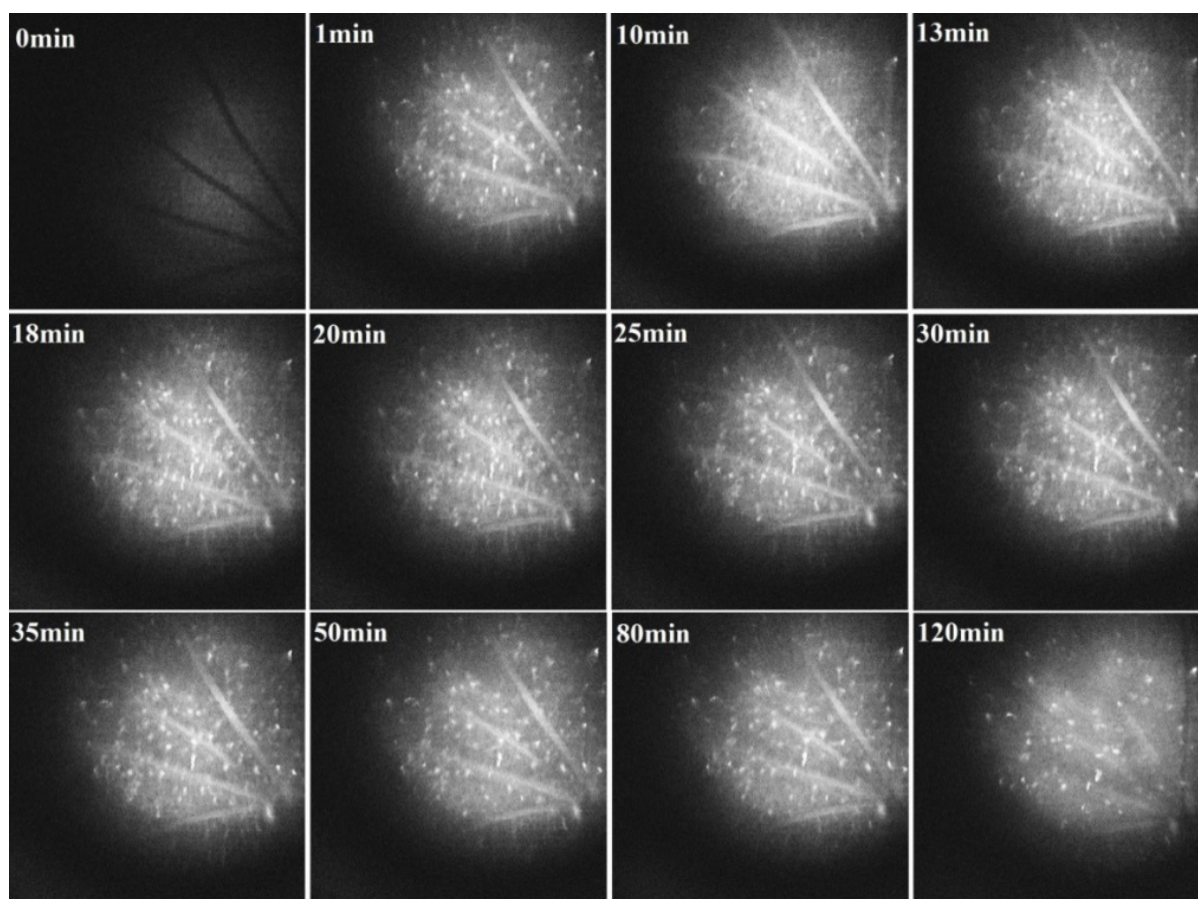


Figure 4.31: The rhodamine 123 labelled PBCA NPs track *in vivo* in the retina after the *i.v.* injection. The shining dots are the rhodamine 123 labelled PBCA NPs. the bright tubulars are considered as the blood vessel. From the figure, it is confirmed that PBCA NPs have the ability to penetrate the blood-brain barrier, because that they are detected in retina tissue for more than 2 hrs.

As shown in Figure 4.31, the bright dots represent the location of the fluorescent PBCA NPs in the retina. The blood vessels are also visible due to rhodamine 123. The PBCA NPs were detectable within 1 min after *i.v.* injection from the tail. The images indicate clearly that the light dots, which represent the PBCA NPs, are outside of the blood vessels. It means that the blood-retinal barriers were penetrated by PBCA NPs. Besides this, the PBCA NPs stayed in the retina for a long time. From 1 min to 80 min, the quantity of the light dots in the retina was not significantly different. Until 120 min, the fluorescent signal in the blood vessel started to fade and part of the light dots disappear. As a result, the experiments demonstrate that PBCA NPs have the ability to cross the blood-retinal barrier, and their fluorescent signal can be detected for at least 2 hrs after the *i.v.* injection.

However, there are still a number of challenges regarding *i.v.* injection of the PBCA nano-carriers for the retina treatment. First of all, approximately 1 mL of PBCA NPs solution is necessary for *i.v.* injection to get a substantial amount of NPs in the retina parenchyma. But, only 3  $\mu$ L of the PBCA NPs are enough to induce clear pharmacological effects after the intravitreal injection. Moreover, after *i.v.* injection, the systemic distribution of NPs may affect other organs; especially an accumulation in the organs of the reticulo-endothelial system can be expected. In addition, it is more difficult to ensure a similar volume of the PBCA NPs in the retina for each rat after *i.v.* injection, which is due to the different bodyweights and the health conditions. Therefore, currently, the intravitreal injection is preferred to the treatment of the retinal damage and diseases.

## 5. Conclusions

In this study, the caspase-3 siRNA was delivered by poly (butylcyanoacrylate) nanoparticles (PBCA NPs) into C6 cells and retinal tissues of rats. The efficiency of RNA interference was investigated via the quantification of caspase-3, which was imaged by western blot analysis for C6 cells and by the immunofluorescence for retina. The image data were transformed to numerical values by the ImageJ as integrated optical density (IOD). Finally, this work demonstrates that the PBCA NPs loaded with caspase-3 siRNA (casp3 PBCA NPs) have the ability to silence the caspase-3 expression in C6 cells and the rat retinae, whereas neither caspase-3 siRNA nor PBCA NPs alone can achieve a substantial transfection.

The PBCA NPs were synthesized in a water-in-oil mini-emulsion, which was prepared by homogenizing an oil phase, a water phase, and surfactants. After that, the polymerization was initiated when the BCA monomer accumulated at the interface of water drops. Due to a lack of OH<sup>-</sup> ions in water, the polymerization took approximately 4 hrs. The PBCA NPs were finally separated from the oil and re-dispersed in water. The particle size distribution and the Zeta potential were measured using the Zetasizer. Furthermore, the optimization of the production of the PBCA NPs was performed with varying amounts of surfactants, water, and BCA monomer, as well as different types of surfactants. According to their size distribution and Zeta potential, the best protocol for siRNA loaded PBCA NPs is confirmed to be 0.4 g of surfactants (Tween<sup>®</sup> 80: Span<sup>®</sup> 80 = 1:4 w/w), 4.0 g of Miglyol 812N, 1.2 g of PBS, and 100  $\mu$ L of BCA monomer. The  $d_{50,3}$  of casp3 PBCA NPs is 217.5 nm, and the value of their Zeta potential is -24.8 mV. Then, the NPs were ready to be used in the biological experiments.

The cytotoxicity of PBCA NPs to C6 cells was tested *in vitro*. The blank PBCA NPs were used to define the median lethal dose of PBCA NPs, which is the limit for incubation with C6 cells. Because of casp3 PBCA NPs, the anti-apoptotic effect was investigated in parallel to checking the toxicity of the NPs. For comparison, blank PBCA NPs and casp3 PBCA NPs were applied to C6 cells for 48 hrs, and extra groups, which were incubated with staurosporine (Stau), were used in part of the C6 cells. After reacting with the MTT solution, the survival ratio of the C6 cells was evaluated and compared to each treatment. As a result,

0.4 % (v/v) of PBCA NPs in the C6 cell solution is the limit of the concentration that lead to more than 50 % of survival of C6 cells. Comparing blank PBCA NPs with casp3 PBCA NPs, an anti-apoptosis effect was detected. There were substantially more cells alive after the treatment with the casp3 PBCA NPs as compared to the blank PBCA NPs. Therefore, it is worth to follow this approach further to demonstrate the gene silencing in the C6 cells.

Caspase-3 and cleaved-caspase-3 are the targets in western blot analysis. After the treatments for a duration of 48 hrs, the C6 cells were lysed and then used in western blot analysis. From the blots, it was confirmed that the casp3 PBCA NPs knock down the caspase-3 expression in the C6 cells, because the bands representing caspase-3 from the cells treated with casp3 PBCA NPs are missing. Furthermore, blank PBCA NPs, neg PBCA NPs, and caspase-3 siRNA-calcium particles were incubated with C6 cells. Their extracts were detected using western blot analysis, and the results of the western blot analysis were transformed to IOD values by the ImageJ. According to these IOD values, I was able to demonstrate that the casp3 PBCA NPs have induced gene silencing. In conclusion, neither the casp3 & NPs, nor caspase-3 siRNA, nor the caspase-3 siRNA-calcium particles have the ability to induce RNA interference at a level of efficiency that is as good as casp3 PBCA NPs. Besides, the transfection efficiency is demonstrated by varying the concentrations of the casp3 PBCA NPs in the cell solution, and there was a linear relationship between casp3 PBCA NPs and caspase-3 expression.

Having confirmed the effect of the casp3 PBCA NPs *in vitro*, their characterization was further advanced using *in vivo* tests. Optic nerve crush (ONC) surgery was performed on adult rats in which the optic nerve triggered apoptosis in the retina. Then, the casp3 PBCA NPs were injected into the vitreous body of the rats, and after 48 hrs, the eyeballs were taken out and sliced for immunofluorescent staining and imaging. From the images, the gene silencing effect was clearly observed. Despite the retinal damage, the fluorescent signal of caspase-3 from the cells treated with casp3 PBCA NPs was hardly detected, *i.e.* it was similar to a healthy rat retina. In addition, blank PBCA NPs, neg PBCA NPs (the PBCA NPs loaded with negative silencing siRNA), caspase-3 siRNA-calcium particles, and PBS were used, respectively, to treat the retinae of rats. In all of these groups, the strong and widely distributed fluorescent signal representing caspase-3 was detected in the retinae. It indicates the high concentrations of caspase-3. Furthermore, the fluorescent images are transformed to the IOD values. According to the difference in these IOD values, the pronounced gene silencing effect induced by the casp3 PBCA NPs was confirmed. The IOD value from the

post-ONC retina treated with casp3 PBCA NPs has a similar value to a normal, healthy retina, and the value is much lower than the other treatments.

In addition, the rhodamine 123 PBCA NPs were prepared to evaluate the possibility of the blood-brain barrier passage after *i.v.* injection for the retina treatment. The *in vivo* confocal neuroimaging system provided to track the NPs in the retina. The fluorescent PBCA NPs were shown to cross the blood-retinal barrier, which is virtually identical to the blood-brain barrier, within 1 min after the injection, and the NPs were detectable in retina tissue for more than 2 hrs. So, the PBCA NPs can be successfully applied systemically to transport siRNA into retina tissue. However, local intravitreal injection is superior to *i.v.* injection, because no systemic side effects are expected and significantly less siRNA is needed for a substantially smaller volume, which is sufficient for the local application.

Based on this study, PBCA NPs could be further modified to specifically bind to the cells in retina and enhance the transfection efficiency on retina tissues, as well as reduce side effects. By using PBCA NPs delivery system, caspase-3 siRNA or other short nucleic acids can be delivered not only into retina but also some other brain structures for different purposes in the future, for example the treatment of Alzheimer's disease. Besides this, PBCA NPs modified with PEG or lactose can control the speed of their biodegradation to meet different requirements for the complex environment in animals or humans. On the other hand, these casp3 siRNA PBCA NPs should be tested further. For example, the behaviors of the rats that suffer from the ONC before and after the treatments with casp3 siRNA PBCA NPs are worth to be investigated. Further, casp3 siRNA PBCA NPs will be possible to contribute on human eyes' protection by reducing the deterioration of vision loss.

## 6. Acknowledgments

The production and characterization of PBCA NPs are mainly completed at the laboratory of Institut für Verfahrenstechnik (IVT), Otto-von-Guericke Universität Magdeburg. The biology experiments are performed mainly at the laboratory of Institut für Medizinische Psychologie (IMP), Otto-von-Guericke Universität Magdeburg. I would like to thank my supervisors Prof. Berend van Wachem, Dr. Werner Hintz (IVT), and my colleague Talea Hopf (IVT) for their kindly guidance of PBCA NPs preparation. I also would like to thank Prof. Bernhard Sabel (IMP) and Dr. Petra Henrich-Noack (IMP) for their advices of biology experiments. I wish to thank technician Lisa Grigartzik (IMP) for her efforts of the preparation and guidance in all the biology experiments, and Enqi Zhang (IMP) for her technical help to complete the ICON imaging. I am grateful to Susanne Bonifatius and her colleagues (Universitätsklinik Magdeburg) for their knowledge and imaging instrument for western blot analysis. I also want to express my gratitude to Dr. Peter Heiduschka and his colleagues (Klinik für Augenheilkunde, Universitätsklinikum Münster) for their knowledge and experience in paraffin section and immunofluorescence. Cremer Oleo GmbH & Co. KG is thanked for the chemical they provided, and I am thankful to Max Delbrück Center for Molecular Medicine in Berlin for their gift of C6 cell line.

## 7. Bibliography

- [1] R. C. Rao; D. N. Zacks, Cell and gene therapy. In *Cell-Based Therapy for Retinal Degenerative Disease*, Karger Publishers: 2014; Vol. 53, pp 167-177.
- [2] A. Aiuti; M. G. Roncarolo; L. Naldini, „Gene therapy for ADA - SCID, the first marketing approval of an <em>ex vivo</em> gene therapy in Europe: paving the road for the next generation of advanced therapy medicinal products“. *EMBO Molecular Medicine*, vol., pp. 2017.
- [3] W. V. Graham; A. Bonito-Oliva; T. P. Sakmar, „Update on Alzheimer's Disease Therapy and Prevention Strategies“. *Annual Review of Medicine*, vol. 68, pp. 413-430 2017.
- [4] G. Shim; D. Kim; Q.-V. Le; G. T. Park; T. Kwon; Y.-K. Oh, „Nonviral Delivery Systems For Cancer Gene Therapy: Strategies And Challenges“. *Curr Gene Ther*, vol., pp. 2018.
- [5] C. Hardee; L. Arévalo-Soliz; B. Hornstein; L. Zechiedrich, „Advances in Non-Viral DNA Vectors for Gene Therapy“. *Genes*, vol. 8, pp. 65 2017.
- [6] J. Zhang; X. Li; L. Huang, „Non-viral nanocarriers for siRNA delivery in breast cancer“. *Journal of controlled release : official journal of the Controlled Release Society*, vol. 190, pp. 440-50 2014.
- [7] J. Li; L. Feng; L. Fan; Y. Zha; L. Guo; Q. Zhang; J. Chen; Z. Pang; Y. Wang; X. Jiang; V. C. Yang; L. Wen, „Targeting the brain with PEG-PLGA nanoparticles modified with phage-displayed peptides“. *Biomaterials*, vol. 32, pp. 4943-50 2011.
- [8] J. Guo; X. Gao; L. Su; H. Xia; G. Gu; Z. Pang; X. Jiang; L. Yao; J. Chen; H. Chen, „Aptamer-functionalized PEG-PLGA nanoparticles for enhanced anti-glioma drug delivery“. *Biomaterials*, vol. 32, pp. 8010-20 2011.
- [9] A. Musyanovych; K. Landfester, „Synthesis of Poly(butylcyanoacrylate) Nanocapsules by Interfacial Polymerization in Miniemulsions for the Delivery of DNA Molecules“. *Progress in Colloid and Polymer Science*, vol. 134, pp. 120-127 2008.
- [10] H. de Martimprey; C. Vauthier; C. Malvy; P. Couvreur, „Polymer nanocarriers for the delivery of small fragments of nucleic acids: oligonucleotides and siRNA“. *European*



- journal of pharmaceutics and biopharmaceutics : official journal of Arbeitsgemeinschaft fur Pharmazeutische Verfahrenstechnik e.V.*, vol. 71, pp. 490-504 2009.
- [11] M. V. Balashanmugam; S. Nagarethinam; H. Jagani; V. R. Josyula; A. Alrohaimi; N. Udupa, „Preparation and characterization of novel PBAE/PLGA polymer blend microparticles for DNA vaccine delivery“. *TheScientificWorldJournal*, vol. 2014, pp. 385135 2014.
- [12] M. Kolter; M. Ott; C. Hauer; I. Reimold; G. Fricker, „Nanotoxicity of poly(n-butylcyanoacrylate) nanoparticles at the blood-brain barrier, in human whole blood and in vivo“. *Journal of controlled release : official journal of the Controlled Release Society*, vol. 197, pp. 165-79 2015.
- [13] A. M. Hall; R. Hemmer; R. Spaulding; H. N. Wetzel; J. Curcio; B. A. Sabel; P. Henrich-Noack; S. Pixley; T. Hopkins; R. L. Boyce; P. J. Schultheis; K. L. Haik, „Cytotoxicity and apoptotic gene expression in an in vitro model of the blood-brain barrier following exposure to poly(butylcyanoacrylate) nanoparticles“. *Journal of drug targeting*, vol. 24, pp. 635-44 2016.
- [14] N. Voigt; P. Henrich-Noack; S. Kockentiedt; W. Hintz; J. Tomas; B. A. Sabel, „Surfactants, not size or zeta-potential influence blood-brain barrier passage of polymeric nanoparticles“. *European journal of pharmaceutics and biopharmaceutics : official journal of Arbeitsgemeinschaft fur Pharmazeutische Verfahrenstechnik e.V.*, vol. 87, pp. 19-29 2014.
- [15] E. Sulheim; H. Baghirov; E. von Haartman; A. Boe; A. K. Aslund; Y. Morch; L. Davies Cde, „Cellular uptake and intracellular degradation of poly(alkyl cyanoacrylate) nanoparticles“. *Journal of nanobiotechnology*, vol. 14, pp. 1 2016.
- [16] G. Tiwari; R. Tiwari; B. Sriwastawa; L. Bhati; S. Pandey; P. Pandey; S. K. Bannerjee, „Drug delivery systems: An updated review“. *International Journal of Pharmaceutical Investigation*, vol. 2, pp. 2-11 2012.
- [17] N. Anton; J. P. Benoit; P. Saulnier, „Design and production of nanoparticles formulated from nano-emulsion templates-a review“. *Journal of controlled release : official journal of the Controlled Release Society*, vol. 128, pp. 185-99 2008.
- [18] S. Prilloff; J. Fan; P. Henrich-Noack; B. A. Sabel, „In vivo confocal neuroimaging (ICON): non-invasive, functional imaging of the mammalian CNS with cellular resolution“. *The European journal of neuroscience*, vol. 31, pp. 521-8 2010.

- [19] S. Tomcin; G. Baier; K. Landfester; V. Mailander, „Pharmacokinetics on a microscale: visualizing Cy5-labeled oligonucleotide release from poly(n-butylcyanoacrylate) nanocapsules in cells“. *International journal of nanomedicine*, vol. 9, pp. 5471-89 2014.
- [20] C. Y. Chung; J. T. Yang; Y. C. Kuo, „Polybutylcyanoacrylate nanoparticle-mediated neurotrophin-3 gene delivery for differentiating iPS cells into neurons“. *Biomaterials*, vol. 34, pp. 5562-70 2013.
- [21] D. Reischl; A. Zimmer, „Drug delivery of siRNA therapeutics: potentials and limits of nanosystems“. *Nanomedicine : nanotechnology, biology, and medicine*, vol. 5, pp. 8-20 2009.
- [22] Y. Zhang; Y. Zhang; J. Chen; B. Zhang; Y. Pan; L. Ren; J. Zhao; Y. Luo; D. Zhai; S. Wang; J. Wang, „Polybutylcyanoacrylate nanoparticles as novel vectors in cancer gene therapy“. *Nanomedicine : nanotechnology, biology, and medicine*, vol. 3, pp. 144-53 2007.
- [23] S. Elmore, „Apoptosis: a review of programmed cell death“. *Toxicologic pathology*, vol. 35, pp. 495-516 2007.
- [24] H. Wajant, „The Fas signaling pathway: more than a paradigm“. *Science*, vol. 296, pp. 1635-1636 2002.
- [25] S. Fulda; K.-M. Debatin, „Extrinsic versus intrinsic apoptosis pathways in anticancer chemotherapy“. *Oncogene*, vol. 25, pp. 4798 2006.
- [26] E. Gramage; J. Li; P. Hitchcock, „The expression and function of midkine in the vertebrate retina“. *British journal of pharmacology*, vol. 171, pp. 913-923 2014.
- [27] R. J. Bold; P. M. Termuhlen; D. J. McConkey, „Apoptosis, cancer and cancer therapy“. *Surgical oncology*, vol. 6, pp. 133-142 1997.
- [28] L. E. Munoz; C. v. Bavel; S. Franz; J. Berden; M. Herrmann; J. v. d. Vlag, „Apoptosis in the pathogenesis of systemic lupus erythematosus“. *Lupus*, vol. 17, pp. 371-375 2008.
- [29] K. A. Roth, „Caspases, apoptosis, and Alzheimer disease: causation, correlation, and confusion“. *Journal of Neuropathology & Experimental Neurology*, vol. 60, pp. 829-838 2001.
- [30] S. Gupta, „Molecular signaling in death receptor and mitochondrial pathways of apoptosis (Review)“. *International journal of oncology*, vol. 22, pp. 15-20 2003.
- [31] L. I. Benowitz; Z. He; J. L. Goldberg, „Reaching the brain: Advances in optic nerve regeneration“. *Experimental neurology*, vol. 287, pp. 365-373 2017.
- [32] C. C. Mello; D. Conte Jr, „Revealing the world of RNA interference“. *Nature*, vol. 431, pp. 338 2004.

- [33] Y. Deng; C. C. Wang; K. W. Choy; Q. Du; J. Chen; Q. Wang; L. Li; T. K. H. Chung; T. Tang, „Therapeutic potentials of gene silencing by RNA interference: Principles, challenges, and new strategies“. *Gene*, vol. 538, pp. 217-227 2014.
- [34] A. Reynolds; D. Leake; Q. Boese; S. Scaringe; W. S. Marshall; A. Khvorova, „Rational siRNA design for RNA interference“. *Nature biotechnology*, vol. 22, pp. 326 2004.
- [35] Y. C. Tseng; S. Mozumdar; L. Huang, „Lipid-based systemic delivery of siRNA“. *Advanced drug delivery reviews*, vol. 61, pp. 721-31 2009.
- [36] J. Wang; Z. Lu; M. G. Wientjes; J. L. Au, „Delivery of siRNA therapeutics: barriers and carriers“. *The AAPS journal*, vol. 12, pp. 492-503 2010.
- [37] Y. Zhao; E. B. Butler; M. Tan, „Targeting cellular metabolism to improve cancer therapeutics“. *Cell death & disease*, vol. 4, pp. e532 2013.
- [38] A. Fire; S. Xu; M. K. Montgomery; S. A. Kostas; S. E. Driver; C. C. Mello, „Potent and specific genetic interference by double-stranded RNA in *Caenorhabditis elegans*“. *Nature*, vol. 391, pp. 806-811 1998.
- [39] S. M. Elbashir; J. Harborth; W. Lendeckel; A. Yalcin; K. Weber; T. Tuschl, „Duplexes of 21-nucleotide RNAs mediate RNA interference in cultured mammalian cells“. *Nature*, vol. 411, pp. 494 2001.
- [40] P. D. Zamore; T. Tuschl; P. A. Sharp; D. P. Bartel, „RNAi: Double-Stranded RNA Directs the ATP-Dependent Cleavage of mRNA at 21 to 23 Nucleotide Intervals“. *Cell*, vol. 101, pp. 25-33 2000.
- [41] A. Vermeulen; L. Behlen; A. Reynolds; A. Wolfson; W. S. Marshall; J. O. N. Karpilow; A. Khvorova, „The contributions of dsRNA structure to Dicer specificity and efficiency“. *RNA*, vol. 11, pp. 674-682 2005.
- [42] H. Siomi; M. C. Siomi, „On the road to reading the RNA-interference code“. *Nature*, vol. 457, pp. 396 2009.
- [43] E. Bernstein; A. A. Caudy; S. M. Hammond; G. J. Hannon, „Role for a bidentate ribonuclease in the initiation step of RNA interference“. *Nature*, vol. 409, pp. 363 2001.
- [44] RNA-Interferenz. <https://de.wikipedia.org/wiki/RNA-Interferenz>.
- [45] J. F. Kerr, „History of the events leading to the formulation of the apoptosis concept“. *Toxicology*, vol. 181, pp. 471-474 2002.
- [46] J. F. Kerr; A. H. Wyllie; A. R. Currie, „Apoptosis: a basic biological phenomenon with wideranging implications in tissue kinetics“. *British journal of cancer*, vol. 26, pp. 239 1972.

- [47] C. J. Norbury; I. D. Hickson, „Cellular responses to DNA damage“. *Annual review of pharmacology and toxicology*, vol. 41, pp. 367-401 2001.
- [48] M. a. T. Valenzuela; M. a. I. Núñez; M. a. R. Guerrero; M. Villalobos; J. M. R. de Almodovar, „Capillary electrophoresis of DNA damage after irradiation: apoptosis and necrosis“. *Journal of Chromatography A*, vol. 871, pp. 321-330 2000.
- [49] R. W. Johnstone; A. A. Ruefli; S. W. Lowe, „Apoptosis: a link between cancer genetics and chemotherapy“. *Cell*, vol. 108, pp. 153-164 2002.
- [50] E. B. Thompson, „Apoptosis and steroid hormones“. *Molecular Endocrinology*, vol. 8, pp. 665-673 1994.
- [51] A. Ashkenazi; V. M. Dixit, „Death receptors: signaling and modulation“. *Science*, vol., pp. 1305-1308 1998.
- [52] F. Kischkel; S. Hellbardt; I. Behrmann; M. Germer; M. Pawlita; P. Krammer; M. Peter, „Cytotoxicity - dependent APO - 1 (Fas/CD95) - associated proteins form a death - inducing signaling complex (DISC) with the receptor “. *The EMBO journal*, vol. 14, pp. 5579-5588 1995.
- [53] C. Fumarola; G. Guidotti, „Stress-induced apoptosis: toward a symmetry with receptor-mediated cell death“. *Apoptosis*, vol. 9, pp. 77-82 2004.
- [54] K. Cain; S. B. Bratton; G. M. Cohen, „The Apaf-1 apoptosome: a large caspase-activating complex“. *Biochimie*, vol. 84, pp. 203-214 2002.
- [55] X. Jiang; X. Wang, „Cytochrome c promotes caspase-9 activation by inducing nucleotide binding to Apaf-1“. *Journal of Biological Chemistry*, vol. 275, pp. 31199-31203 2000.
- [56] H.-E. Kim; F. Du; M. Fang; X. Wang, „Formation of apoptosome is initiated by cytochrome c-induced dATP hydrolysis and subsequent nucleotide exchange on Apaf-1“. *Proceedings of the National Academy of Sciences of the United States of America*, vol. 102, pp. 17545-17550 2005.
- [57] S. M. Srinivasula; P. Datta; X.-J. Fan; T. Fernandes-Alnemri; Z. Huang; E. S. Alnemri, „Molecular determinants of the caspase-promoting activity of Smac/DIABLO and its role in the death receptor pathway“. *Journal of Biological Chemistry*, vol. 275, pp. 36152-36157 2000.
- [58] C. Du; M. Fang; Y. Li; L. Li; X. Wang, „Smac, a mitochondrial protein that promotes cytochrome c-dependent caspase activation by eliminating IAP inhibition“. *Cell*, vol. 102, pp. 33-42 2000.

- [59] M. Madesh; B. Antonsson; S. M. Srinivasula; E. S. Alnemri; G. Hajnóczy, „Rapid kinetics of tBid-induced cytochrome c and Smac/DIABLO release and mitochondrial depolarization“. *Journal of Biological Chemistry*, vol. 277, pp. 5651-5659 2002.
- [60] L. Li; R. M. Thomas; H. Suzuki; J. K. De Brabander; X. Wang; P. G. Harran, „A small molecule Smac mimic potentiates TRAIL-and TNF $\alpha$ -mediated cell death“. *Science*, vol. 305, pp. 1471-1474 2004.
- [61] H. Hillaireau; P. Couvreur, „Nanocarriers' entry into the cell: relevance to drug delivery“. *Cellular and molecular life sciences : CMLS*, vol. 66, pp. 2873-96 2009.
- [62] P. Kumar; H. Wu; J. L. McBride; K. E. Jung; M. H. Kim; B. L. Davidson; S. K. Lee; P. Shankar; N. Manjunath, „Transvascular delivery of small interfering RNA to the central nervous system“. *Nature*, vol. 448, pp. 39-43 2007.
- [63] L. Sercombe; T. Veerati; F. Moheimani; S. Y. Wu; A. K. Sood; S. Hua, „Advances and challenges of liposome assisted drug delivery“. *Frontiers in pharmacology*, vol. 6, pp. 286 2015.
- [64] G. A. Koning; G. Storm, „Targeted drug delivery systems for the intracellular delivery of macromolecular drugs“. *Drug discovery today*, vol. 8, pp. 482-483 2003.
- [65] J. Li; X. Wang; T. Zhang; C. Wang; Z. Huang; X. Luo; Y. Deng, „A review on phospholipids and their main applications in drug delivery systems“. *Asian journal of pharmaceutical sciences*, vol. 10, pp. 81-98 2015.
- [66] P. Mukerjee; K. J. Mysels *Critical micelle concentrations of aqueous surfactant systems*; National Standard reference data system: 1971.
- [67] R. J. Hunter, *Zeta potential in colloid science: principles and applications*. Academic press: 2013; Vol. 2.
- [68] Q. He; J. Shi, „Mesoporous silica nanoparticle based nano drug delivery systems: synthesis, controlled drug release and delivery, pharmacokinetics and biocompatibility“. *Journal of Materials Chemistry*, vol. 21, pp. 5845-5855 2011.
- [69] Y. S. Siu; L. Li; M. F. Leung; K. L. D. Lee; P. Li, „Polyethylenimine-based amphiphilic core-shell nanoparticles: study of gene delivery and intracellular trafficking“. *Biointerphases*, vol. 7, pp. 16 2012.
- [70] J. D. Clogston; A. K. Patri, Zeta potential measurement. In *Characterization of nanoparticles intended for drug delivery*, Springer: 2011; pp 63-70.
- [71] H. C. Huang; S. Barua; G. Sharma; S. K. Dey; K. Rege, „Inorganic nanoparticles for cancer imaging and therapy“. *Journal of controlled release : official journal of the Controlled Release Society*, vol. 155, pp. 344-57 2011.

- [72] J. Li; C. Sabliov, „PLA/PLGA nanoparticles for delivery of drugs across the blood-brain barrier“. *Nanotechnology Reviews*, vol. 2, pp. 2013.
- [73] V. Mudgal; N. Madaan; A. Mudgal, „Biochemical mechanisms of salt tolerance in plants: a review“. *International Journal of Botany*, vol. 6, pp. 136-143 2010.
- [74] T. Yoshikawa; N. Okada; A. Oda; K. Matsuo; K. Matsuo; Y. Mukai; Y. Yoshioka; T. Akagi; M. Akashi; S. Nakagawa, „Development of amphiphilic  $\gamma$ -PGA-nanoparticle based tumor vaccine: potential of the nanoparticulate cytosolic protein delivery carrier“. *Biochemical and biophysical research communications*, vol. 366, pp. 408-413 2008.
- [75] A. Evangelatov; R. Skrobanska; N. Mladenov; M. Petkova; G. Yordanov; R. Pankov, „Epirubicin loading in poly(butyl cyanoacrylate) nanoparticles manifests via altered intracellular localization and cellular response in cervical carcinoma (HeLa) cells“. *Drug delivery*, vol., pp. 1-10 2015.
- [76] J. Nguyen; T. W. Steele; O. Merkel; R. Reul; T. Kissel, „Fast degrading polyesters as siRNA nano-carriers for pulmonary gene therapy“. *Journal of controlled release : official journal of the Controlled Release Society*, vol. 132, pp. 243-51 2008.
- [77] G. Mittal; H. Carswell; R. Brett; S. Currie; M. N. Kumar, „Development and evaluation of polymer nanoparticles for oral delivery of estradiol to rat brain in a model of Alzheimer's pathology“. *Journal of controlled release : official journal of the Controlled Release Society*, vol. 150, pp. 220-8 2011.
- [78] N. Segovia; M. Pont; N. Oliva; V. Ramos; S. Borrós; N. Artzi, „Hydrogel doped with nanoparticles for local sustained release of siRNA in breast cancer“. *Advanced healthcare materials*, vol. 4, pp. 271-280 2015.
- [79] B. Xie; Y. Liu; Y. Guo; E. Zhang; C. Pu; H. He; T. Yin; X. Tang, „Progesterone PLGA/mPEG-PLGA Hybrid Nanoparticle Sustained-Release System by Intramuscular Injection“. *Pharmaceutical research*, vol. 35, pp. 62 2018.
- [80] C. K. Weiss; M. R. Lorenz; K. Landfester; V. Mailander, „Cellular uptake behavior of unfunctionalized and functionalized PBCA particles prepared in a miniemulsion“. *Macromolecular bioscience*, vol. 7, pp. 883-96 2007.
- [81] Z. Liu; P. Koczera; D. Doleschel; F. Kiessling; J. Gatjens, „Versatile synthetic strategies for PBCA-based hybrid fluorescent microbubbles and their potential theranostic applications to cell labelling and imaging“. *Chemical communications*, vol. 48, pp. 5142-4 2012.
- [82] S. Fokong; B. Theek; Z. Wu; P. Koczera; L. Appold; S. Jorge; U. Resch-Genger; M. van Zandvoort; G. Storm; F. Kiessling; T. Lammers, „Image-guided, targeted and triggered

- drug delivery to tumors using polymer-based microbubbles“. *Journal of controlled release : official journal of the Controlled Release Society*, vol. 163, pp. 75-81 2012.
- [83] E. F. Gregory Lambert, Huguette Pinto-Alphandary, Annette Gulik, and Patrick Couvreur, „Polyisobutylcyanoacrylate Nanocapsules Containing an Aqueous Core as a Novel Colloidal Carrier for the Delivery of Oligonucleotides“. *Pharmaceutical research*, vol. 17, pp. 8 2000.
- [84] R. Rempe; S. Cramer; S. Huwel; H. J. Galla, „Transport of Poly(n-butylcyano-acrylate) nanoparticles across the blood-brain barrier in vitro and their influence on barrier integrity“. *Biochemical and biophysical research communications*, vol. 406, pp. 64-9 2011.
- [85] M. Ryou; C. C. Thompson, „Tissue Adhesives: A Review“. *Techniques in Gastrointestinal Endoscopy*, vol. 8, pp. 33-37 2006.
- [86] C. Limouzin; A. Caviggia; F. Ganachaud; P. Hémary, „Anionic polymerization of n-butyl cyanoacrylate in emulsion and miniemulsion“. *Macromolecules*, vol. 36, pp. 667-674 2003.
- [87] P. Couvreur; B. Kante; M. Roland; P. Guiot; P. Bauduin; P. Speiser, „Polycyanoacrylate nanocapsules as potential lysosomotropic carriers: preparation, morphological and sorptive properties“. *Journal of pharmacy and pharmacology*, vol. 31, pp. 331-332 1979.
- [88] K. Landfester; J. Eisenblätter; R. Rothe, „Preparation of polymerizable miniemulsions by ultrasonication“. *JCT research*, vol. 1, pp. 65-68 2004.
- [89] K. Landfester; N. Bechthold; F. Tiarks; M. Antonietti, „Formulation and stability mechanisms of polymerizable miniemulsions“. *Macromolecules*, vol. 32, pp. 5222-5228 1999.
- [90] J. M. Williams, „High internal phase water-in-oil emulsions: influence of surfactants and cosurfactants on emulsion stability and foam quality“. *Langmuir*, vol. 7, pp. 1370-1377 1991.
- [91] H. Hillaireau; T. Le Doan; H. Chacun; J. Janin; P. Couvreur, „Encapsulation of mono- and oligo-nucleotides into aqueous-core nanocapsules in presence of various water-soluble polymers“. *International journal of pharmaceutics*, vol. 331, pp. 148-52 2007.
- [92] S. C. M. Po C Chen , Adegboyega K Oyelere, „Gold nanoparticles: From nanomedicine to nanosensing“. *Nanotechnology, Science and Applications*, vol. 1, pp. 45-66 2008.
- [93] J. S. Mattick, „RNA regulation: a new genetics?“. *Nature Reviews Genetics*, vol. 5, pp. 316 2004.

- [94] A. Bootz; V. Vogel; D. Schubert; J. Kreuter, „Comparison of scanning electron microscopy, dynamic light scattering and analytical ultracentrifugation for the sizing of poly (butyl cyanoacrylate) nanoparticles“. *European Journal of Pharmaceutics and Biopharmaceutics*, vol. 57, pp. 369-375 2004.
- [95] M. Instruments, „Zetasizer nano series user manual“. *MAN0317*, vol. 1, pp. 2004.
- [96] J.-T. Lue, „A review of characterization and physical property studies of metallic nanoparticles“. *Journal of physics and chemistry of solids*, vol. 62, pp. 1599-1612 2001.
- [97] Q. A. Pankhurst; J. Connolly; S. Jones; J. Dobson, „Applications of magnetic nanoparticles in biomedicine“. *Journal of physics D: Applied physics*, vol. 36, pp. R167 2003.
- [98] R. Pecora, „Dynamic light scattering measurement of nanometer particles in liquids“. *Journal of nanoparticle research*, vol. 2, pp. 123-131 2000.
- [99] T. Mosmann, „Rapid colorimetric assay for cellular growth and survival: Application to proliferation and cytotoxicity assays“. *Journal of Immunological Methods*, vol. 65, pp. 55-63 1983.
- [100] H. Towbin; T. Staehelin; J. Gordon, „Electrophoretic transfer of proteins from polyacrylamide gels to nitrocellulose sheets: procedure and some applications“. *Proceedings of the National Academy of Sciences of the United States of America*, vol. 76, pp. 4350-4354 1979.
- [101] W. N. Burnette, „“Western Blotting”: Electrophoretic transfer of proteins from sodium dodecyl sulfate-polyacrylamide gels to unmodified nitrocellulose and radiographic detection with antibody and radioiodinated protein A“. *Analytical Biochemistry*, vol. 112, pp. 195-203 1981.
- [102] J. A. Reynolds; C. Tanford, „Binding of Dodecyl Sulfate to Proteins at High Binding Ratios. Possible Implications for the State of Proteins in Biological Membranes“. *Proceedings of the National Academy of Sciences of the United States of America*, vol. 66, pp. 1002-1007 1970.
- [103] S. Asoh; I. Ohsawa; T. Mori; K.-i. Katsura; T. Hiraide; Y. Katayama; M. Kimura; D. Ozaki; K. Yamagata; S. Ohta, „Protection against ischemic brain injury by protein therapeutics“. *Proceedings of the National Academy of Sciences*, vol. 99, pp. 17107-17112 2002.
- [104] S. M. Attard; M. Coutts; O. Devaja; J. Summers; R. Jyothirmayi; A. Papadopoulos, „Accuracy of frozen section diagnosis at surgery in pre-malignant and malignant lesions



- of the endometrium“. *European journal of gynaecological oncology*, vol. 29, pp. 435-440 2008.
- [105] N. S. Goldstein; M. Ferkowicz; E. Odish; A. Mani; F. Hastah, „Minimum Formalin Fixation Time for Consistent Estrogen Receptor Immunohistochemical Staining of Invasive Breast Carcinoma“. *American Journal of Clinical Pathology*, vol. 120, pp. 86-92 2003.
- [106] R. T. Miller; P. E. Swanson; M. R. Wick, „Fixation and epitope retrieval in diagnostic immunohistochemistry: a concise review with practical considerations“. *Applied Immunohistochemistry & Molecular Morphology*, vol. 8, pp. 228-235 2000.
- [107] P. Henrich-Noack; S. Prilloff; N. Voigt; J. Jin; W. Hintz; J. Tomas; B. A. Sabel, „In vivo visualisation of nanoparticle entry into central nervous system tissue“. *Archives of toxicology*, vol. 86, pp. 1099-105 2012.
- [108] R. F. Guthoff; A. Zhivov; O. Stachs, „In vivo confocal microscopy, an inner vision of the cornea—a major review“. *Clinical & experimental ophthalmology*, vol. 37, pp. 100-117 2009.
- [109] E. C. Dreaden; A. M. Alkilany; X. Huang; C. J. Murphy; M. A. El-Sayed, „The golden age: gold nanoparticles for biomedicine“. *Chemical Society reviews*, vol. 41, pp. 2740-79 2012.
- [110] M.-G. Song; S.-H. Jho; J.-Y. Kim; J.-D. Kim, „Rapid evaluation of water-in-oil (W/O) emulsion stability by turbidity ratio measurements“. *Journal of colloid and interface science*, vol. 230, pp. 213-215 2000.
- [111] W. Yu; H. Xie, „A review on nanofluids: preparation, stability mechanisms, and applications“. *Journal of nanomaterials*, vol. 2012, pp. 1 2012.
- [112] V. Mohanraj; Y. Chen, „Nanoparticles-a review“. *Tropical journal of pharmaceutical research*, vol. 5, pp. 561-573 2006.
- [113] S. Honary; F. Zahir, „Effect of zeta potential on the properties of nano-drug delivery systems-a review (Part 1)“. *Tropical Journal of Pharmaceutical Research*, vol. 12, pp. 255-264 2013.
- [114] R. Bertrand; E. Solary; P. O'Connor; K. W. Kohn; Y. Pommier, „Induction of a common pathway of apoptosis by staurosporine“. *Experimental cell research*, vol. 211, pp. 314-321 1994.
- [115] B. Goetze; B. Grunewald; S. Baldassa; M. Kiebler, „Chemically controlled formation of a DNA/calcium phosphate coprecipitate: application for transfection of mature hippocampal neurons“. *Developmental Neurobiology*, vol. 60, pp. 517-525 2004.

- [116] X. Zhang; E. Zhang; L. Grigartzik; P. Henrich - Noack; W. Hintz; B. A. Sabel, „  
Anti - apoptosis Function of PBCA Nanoparticles Containing Caspase - 3 siRNA for  
Neuronal Protection “. *Chemie Ingenieur Technik*, vol. 90(4), pp.451-455 2018.
- [117] Lecture „Nanoparticle Technology “, Chair of Mechanical Process Engineering, Otto  
von Guericke University.
- [118] Standard Operation Protocol „SOP-Optic Nerve Crush “, Institute of Medical  
Psychology, Otto von Guericke University.
- [119] Standard Operation Protocol „SOP-Intravitreal Injection “, Institute of Medical  
Psychology, Otto von Guericke University.
- [120] M. Gassmann, B. Grenacher, B. Rohde, J. Vogel, „Quantifying Western blots: pitfalls  
of densitometry “. *Electrophoresis*, vol. 30(11), pp. 1845-1855 2009.
- [121] J. Sanchez-Ramos, S. Song, X. Kong, P. Foroutan, G. Martinez, W. Dominguez-  
Viqueria, S. Mohapatra, R. A. Haraszti, A. Khvorova, N. Aronin, V. Sava, „ Chitosan-  
Mangafodipir nanoparticles designed for intranasal delivery of siRNA and DNA to brain  
“. *Journal of Drug Delivery Science and Technology*, vol. 43, pp. 453-460 2018.

## 8. Appendix

### 8.1. Support Information: Instruments

Name	Type version	Company
Analytical Balance	LC2200	Sartorius
Centrifuge (For Cell Culture)	5804 R	Eppendorf
Centrifuge (For Nanoparticle)	UNIVERSAL 320	Hettich
Centrifuge (For Westernblot)	1K15	Sigma
Confocal Laser Scanning Microscope	LSM 5 PASCAL	Carl Zeiss
ECL Image System	CHEMOSTAR ECL & Fluorescence Imager	INTAS Science Imaging Instruments
Heating Plate	/	Omnilab
Incubator	HERACELL 150	Heraeus
Magnetic Stirrer	VARIOMAG MONO	Thermofisher
Microscope (For Cell Culture)	CK30	Olympus
Microtome	JUNG RM 2055	Leica
Mini Blot Module	B1000	Thermofisher
Mini Gel Tank	A25977	Thermofisher
Optics Reader	Opsys MR <sup>TM</sup> Reader Specifications	DYNEX Technologies
Steamer	HD9140/91	Philips
Sterile Workbench	ANTARES 48	Biohit
Temperature Furnace	WST 5010	WLM

Ultrasonic Homogenizer	UW 2070	Bandelin
Waterbath	WNE45	Memmert
Zetasizer	ZETASIZER NANO ZS	Malvern

## 8.2. Support Information: Materials

Name	abbreviation	source	remark
Acrylamide/Bis-acrylamide	Acr/Bic	Sigma-Aldrich	30 %, 37.5:1
Anti-rabbit IgG (H+L), F(ab') <sub>2</sub> Fragment (Alexa Fluor® 647 Conjugate)	/	Cell Signaling	
Anti-rabbit IgG, HRP- linked Antibody	/	Cell Signaling	
Ammonium persulfate	AP	Sigma-Aldrich	
$\alpha$ -tubulin antibody	/	Cell Signaling	
Rat glioma cell	C6	ATCC	gift from Max Delbrück Center for Molecular Medicine
Caspase-3 antibody	/	Cell Signaling	
Cell lysis buffer	/	Cell Signaling	
Citric acid	/	Sigma-Aldrich	
Citric acid tri-sodium di- hydrate	/	Sigma-Aldrich	
Dimethylsulfoxide	DMSO	Sigma-Aldrich	
Ethanol	/	Sigma-Aldrich	
Ham's F-12K (Kaighn's) medium	F-12K medium	Life Technologies	
Fetal bovine serum	/	ATCC	
Floxal	/	Bausch & Lomb	
Hoechst33342	/	Thermofisher	
Horse serum	/	ATCC	
Ketamine 10 %	/	Pfizer	100mg/mL
Laemmli buffer	/	Life Technologies	
Medetomidin	/	Vetoquinol GmbH	1mg/mL
Migyol® 812N		Cremer Oleo GmbH & Co. KG	a gift from Cremer Oleo GmbH

3-(4,5-dimethylthiazol-2-yl)-2,5-diphenyltetrazolium bromide	MTT	Sigma-Aldrich	
N-butyl-2-cyanoacrylate	BCA	Henkel AG & Co. KGaA	
Nitrocellulose membrane	NC	Cell Signaling	
Non-fat dry milk	/	Cell Signaling	
Paraffin	/		
Penicillin/streptomycin	/	Biochrom AG	
Pierce™ BCA protein assay kit	/	Thermo Fisher	
Phenylmethanesulfonyl fluoride	PMSF	Life Technologies	
Neosynephrine-POS	/	URSAPHARM GmbH	5 %
Rhodamine-123	/	Sigma-Aldrich	
RNase-free water	/	Sigma-Aldrich	
Sodium dodecyl sulfate	SDS	Sigma-Aldrich	
Caspase-3 siRNA	casp3 siRNA	Thermo fisher	
Shandon Immu-mount	Immu-mount	Thermo fisher	
silencing negative control siRNA	neg siRNA	Thermo fisher	
Sorbitane monooleate	Span® 80	Carl Roth	
Staurosporine	/	Sigma-Aldrich	
Tris Buffered Saline with Tween® 20	TBST	Cell Signaling	
N,N,N',N'-tetramethylethylenediamine	TEMED	Carl Roth	
2-Amino-2-(hydroxymethyl)-1,3-propanediol	Tris base	Sigma-Aldrich	
Trypsin/EDTA	/	Biochrom AG	0.25 %
Tris-Glycine Transfer	/	Cell Signaling	

Buffer			
Tris-Glycine SDS Running Buffer	/	Cell Signaling	
Polysorbat 80	Tween <sup>®</sup> 80	Sigma-Aldrich	
Xylol	/	Sigma-Aldrich	
Vidisc optical gel	/	Bausch & Lomb	

### 8.3. Ingredient List of the Cell Medium

The ingredients in 100mL of cell medium

Components	Molecular Weight	Content in mg
Amino Acids		
Glycine	75	1.5
L-Alanine	89	1.8
L-Arginine hydrochloride	211	42.2
L-Asparagine-H <sub>2</sub> O	150	3
L-Aspartic acid	133	2.66
L-Cysteine hydrochloride-H <sub>2</sub> O	176	7
L-Glutamic Acid	147	2.9
L-Glutamine	146	29.2
L-Histidine hydrochloride-H <sub>2</sub> O	210	4.58
L-Isoleucine	131	0.788
L-Leucine	131	2.62
L-Lysine hydrochloride	183	7.3
L-Methionine	149	0.896
L-Phenylalanine	165	0.992
L-Proline	115	6.9
L-Serine	105	2.1
L-Threonine	119	2.3
L-Tryptophan	204	0.41
L-Tyrosine disodium salt dihydrate	262	1.35
L-Valine	117	2.3
Vitamins		
Biotin	244	0.007
Choline chloride	140	1.4
D-Calcium pantothenate	477	0.05
Folic Acid	441	0.13
Niacinamide	122	0.0037



Pyridoxine hydrochloride	206	0.006
Riboflavin	376	0.004
Thiamine hydrochloride	337	0.03
Vitamin B12	1355	0.14
i-Inositol	180	1.8
Inorganic Salts		
Calcium Chloride (CaCl <sub>2</sub> ) (anhyd.)	111	10.2
Cupric sulfate (CuSO <sub>4</sub> ·5H <sub>2</sub> O)	250	0.0002
Ferric sulfate (FeSO <sub>4</sub> ·7H <sub>2</sub> O)	278	0.08
Magnesium Chloride (anhydrous)	95	4.97
Magnesium Sulfate (MgSO <sub>4</sub> ) (anhyd.)	120	19.2
Potassium Chloride (KCl)	75	28.5
Sodium Bicarbonate (NaHCO <sub>3</sub> )	84	250
Sodium Chloride (NaCl)	58	753
Sodium Phosphate dibasic (Na <sub>2</sub> HPO <sub>4</sub> ) anhydrous	142	11.55
Sodium Phosphate monobasic (NaH <sub>2</sub> PO <sub>4</sub> ) anhydrous	139	5.9
Zinc sulfate (ZnSO <sub>4</sub> ·7H <sub>2</sub> O)	288	0.0144
Other Components		
D-Glucose (Dextrose)	180	126
Hypoxanthine Na	131	0.4
Lipoic Acid	206	0.021
Phenol Red	376.4	0.3
Putrescine 2HCl	161	0.032
Sodium Pyruvate	110	22
Thymidine	242	0.07
Serum		
Horse Serum	/	15mL
Bovine Fetal Serum	/	2.5mL

# Curriculum Vitae

## Personal Detail

Xiwei Zhang, Male,

Walther-rathenau straÙe 58

39104 Magdeburg

Email: [xiwei.zhang@med.ovgu.de](mailto:xiwei.zhang@med.ovgu.de)

## Academic qualifications

### ***Pursuing doctor degree***

Otto-von-Guericke Universität Magdeburg, Germany      2014-

### ***Master of Science***

Sichuan Agricultural University, China      2011-2014

### ***Bachelor of Science***

Henan Normal University, China      2007-2011

## Research activity

Topic: *Nanoparticles Crossing the Blood-Brain Barrier for Neuroprotection*      2014-2018

Paper: ‘*Anti-apoptosis Function of PBCA Nanoparticles Containing Caspase-3 siRNA for Neuronal Protection*’      2018

Topic: *Application of gold nanoparticles in biology*      2011-2014

Paper: ‘*Applications of DNA-Functionalized Gold Nanoparticles in Small Biomolecules Detection*’      2014